

L. SHAW
PERSONAL FILE

AFFDL-TM-74-19-FYA

**AIR FORCE FLIGHT DYNAMICS LABORATORY
DIRECTOR OF SCIENCE & TECHNOLOGY
AIR FORCE SYSTEMS COMMAND
WRIGHT-PATTERSON AIR FORCE BASE OHIO**



AERO-ACOUSTIC ENVIRONMENT OF A RECTANGULAR CAVITY
WITH A LENGTH TO DEPTH RATIO OF FOUR

L. L. SHAW
D. L. SMITH
R. D. TALMADGE
D. E. SEELY

**Reproduced From
Best Available Copy**

January 1974

20000404 036

Approved for public release; distribution unlimited

NOTICES

When Government drawings, specifications, or other data are used for any purpose other than in connection with a definitely related Government procurement operation, the United States Government thereby incurs no responsibility nor any obligation whatsoever; and the fact that the Government may have formulated, furnished, or in any way supplied the said drawings, specifications, or other data, is not to be regarded by implication or otherwise as in any manner licensing the holder or any other person or corporation, or conveying any rights or permission to manufacture, use, or sell any patented invention that may in any way be related thereto.

Copies of this report should not be returned unless return is required by security considerations, contractual obligations, or notice on a specific document.

REPORT DOCUMENTATION PAGE			Form Approved OMB No. 0704-0188	
<small>Public reporting burden for this collection of information is estimated to average 1 hour per response, including the time for reviewing instructions, searching existing data sources, gathering and maintaining the data needed, and completing and reviewing the collection of information. Send comments regarding this burden estimate or any other aspect of this collection of information, including suggestions for reducing this burden, to Washington Headquarters Services, Directorate for Information Operations and Reports, 1215 Jefferson Davis Highway, Suite 1204, Arlington, VA 22202-4302, and to the Office of Management and Budget, Paperwork Reduction Project (0704-0188), Washington, DC 20503.</small>				
1. AGENCY USE ONLY (Leave blank)		2. REPORT DATE January 1974		3. REPORT TYPE AND DATES COVERED Final October 1971 - January 1974
4. TITLE AND SUBTITLE AERO-ACOUSTIC ENVIRONMENT OF RECTANGULAR CAVITY WITH A LENGTH TO DEPTH RATIO OF FOUR				5. FUNDING NUMBERS
6. AUTHOR(S) L.L. SHAW, D.L. SMITH, R.D. TALMADGE, D. E. SEELY				
7. PERFORMING ORGANIZATION NAME(S) AND ADDRESS(ES) Vehicle Dynamics Division Air Force Flight Dynamics Laboratory Dir of Science & Technology Air Force Systems Command Wright-Patterson AFB OH 45433				8. PERFORMING ORGANIZATION REPORT NUMBER
9. SPONSORING/MONITORING AGENCY NAME(S) AND ADDRESS(ES) Air Force Flight Dynamics Laboratory Dir of Science & Technology Air Force Systems Command Wright-Patterson AFB OH 45433 POC: LEONARD L. SHAW, AFRL/VASS, 937-255-5200				10. SPONSORING/MONITORING AGENCY REPORT NUMBER AFFDL-TM-74-19-FYA
11. SUPPLEMENTARY NOTES				
12a. DISTRIBUTION AVAILABILITY STATEMENT APPROVED FOR PUBLIC RELEASE, DISTRIBUTION UNLIMITED				12b. DISTRIBUTION CODE
13. ABSTRACT (Maximum 200 words) <p>The complete program included the flight testing of 5 cavity configurations; three empty cavities, one with an ogive store, and a closed cavity configuration to determine the existing boundary layer characteristics. All flight tests have been completed. Only the results for the 10 -inch cavity and the closed cavity are presented in this report.</p> <p>Each of the 5 configurations were tested at constant pressure altitudes of 3,000 ft, 20,000 ft, and 30,000 ft. The range of Mach numbers tested were 0.61 - 0.93 at 3,000 ft and 0.61 - 1.30 for 20,000 ft and 30,000 ft. Continuous data were recorded as the aircraft slowly accelerated from the lowest Mach number to the highest Mach number. For each flight condition, with the open cavity, fluctuating pressures were measured at nine locations in the cavity and static pressures were measured at three cavity locations. In addition vibration levels were measured with an accelerometer. For the closed cavity instrumentation was provided to define the boundary layer characteristics prior to opening the cavity which included a microphone, thermocouple, static pressure port and pressure rake.</p> <p>Data were recorded on an FM magnetic tape recorder and data reduction and analysis were performed in the laboratory. Details of the test procedures, instrumentation, data reduction and analysis are given in Appendix A.</p>				
14. SUBJECT TERMS				15. NUMBER OF PAGES 83
				16. PRICE CODE
17. SECURITY CLASSIFICATION OF REPORT UNCLASSIFIED	18. SECURITY CLASSIFICATION OF THIS PAGE UNCLASSIFIED	19. SECURITY CLASSIFICATION OF ABSTRACT UNCLASSIFIED	20. LIMITATION OF ABSTRACT SAR	

FOREWORD

This research was performed by the Aero-Acoustics Branch, Vehicle Dynamics Division, Air Force Flight Dynamics Laboratory, Wright-Patterson Air Force Base, Ohio. This effort was initiated under Project 1471 "Aero-Acoustic Problems in Flight Vehicles", Task 147102, "Aero-Acoustics".

The work was performed by Messrs. L. L. Shaw, D. L. Smith, and R. D. Talmadge of the Aero-Acoustics Branch and Mr. D. E. Seely of the Aerospace Dynamics Branch, during the period of October 1971 to the present. This memorandum covers only the results of two of five configurations tested.

The manuscript was released by the authors in January 1974 as a technical memorandum.

This technical memorandum has been reviewed and is approved.



AXEL W. KOLB
Chief, Aero-Acoustics Branch
Vehicle Dynamics Division

TABLE OF CONTENTS

Section		Page
I	Introduction.....	1
II	Test Program Summary.....	2
III	Results.....	3
IV	Conclusions.....	5
	Appendix A - Description of Test Article and Instrumentation.....	6
	Appendix B - Experimental Procedures and Results.....	8
	Appendix C - Table and Figures.....	22
	References.....	75

LIST OF ILLUSTRATIONS

		Page
Table	I Pressure Reference Data	23
Figure	1 Standard SUU-41 Munitions Dispenser Pod	24
Figure	2 Modifications to the Standard SUU-41 Dispenser Pod	25
Figure	3 Ten Inch Cavity ($L/D=4$) Mounted in Modified SUU-41 Pod	26
Figure	4 Modified SUU-41 Pod Mounted on RF-4C Test Aircraft	27
Figure	5 Open Cavity Instrumentation Location	28
Figure	6 Closed Cavity Instrumentation Location	29
Figure	7 Block Diagram of Data Acquisition Instrumentation	30
Figure	8 Data Reduction System	31
Figure	9 Boundary Layer Profiles from the Modified SUU-41 Pod	32
Figure	10 One-Third Octave Band Spectra from the 10 Inch Deep Modified SUU-41 Pod for 3,000 Foot Altitude and Mach 0.82	33
Figure	11 One-Third Octave Band Spectra from the 10 Inch Deep Modified SUU-41 Pod for 20,000 Foot Altitude and Mach 0.82	34
Figure	12 One-Third Octave Band Spectra from the 10 Inch Deep Modified SUU-41 Pod for 30,000 Foot Altitude and Mach Number 0.82	35
Figure	13 One-Third Octave Band Spectra from Microphone A of the Closed Cavity for 20,000 Foot Altitude	36
Figure	14 Longitudinal Variation of Static Pressure Along Cavity Floor for the Modified SUU-41 Pod	37
Figure	15 Mach Number Variation of the Normalized Static Pressure	38
Figure	16 Overall Fluctuating Pressure Time Histories from Microphone C for the 10 Inch Deep Modified SUU-41 Pod	39
Figure	17 One-Third Octave Band Spectra from Microphone A for a Mach Number of 0.82	40
Figure	18 One-Third Octave Band Spectra from Microphone B for a Mach Number of 0.82	41
Figure	19 One-Third Octave Band Spectra from Microphone C for a Mach Number of 0.82	42
Figure	20 One-Third Octave Band Spectra from Microphone D for a Mach Number of 0.82	43
Figure	21 One-Third Octave Band Spectra from Microphone E for a Mach Number of 0.82	44
Figure	22 One-Third Octave Band Spectra from Microphone F for a Mach Number of 0.82	45

	Page
Figure 23 One-Third Octave Band Spectra from Microphone G for a Mach Number of 0.82	46
Figure 24 One-Third Octave Band Spectra from Microphone H for a Mach Number of 0.82	47
Figure 25 One-Third Octave Band Spectra from Microphone I for a Mach Number of 0.82	48
Figure 26 One-Third Octave Band Spectra for Mach Number 0.82 Depicting Failure of Dynamic Pressure Scaling	49
Figure 27 Longitudinal Variation of Peak One-Third Octave Band Referenced to Free-Stream Dynamic Pressure Depicting Mode Shapes for Mach Number 0.82	50
Figure 28 Longitudinal Variation of Peak One-Third Octave Band Referenced to Free-Stream Dynamic Pressure Depicting Mode Shapes for Mach Number 0.82	51
Figure 29 Longitudinal Variation of Peak One-Third Octave Band Referenced to Free-Stream Dynamic Pressure Depicting Mode Shapes for Mach Number 0.82	52
Figure 30 Suggested Shape for First, Second and Third Order Modes from Reference 2	53
Figure 31 Longitudinal Variation of Peak One-Third Octave Band Depicting Mode Shapes for an Altitude of 3,000 Feet and Mach Number 0.82	54
Figure 32 One-Third Octave Band Spectra from Microphone C for an Altitude of 3,000 Ft	55
Figure 33 One-Third Octave Band Spectra from Microphone C for an Altitude of 20,000 Ft	56
Figure 34 One-Third Octave Band Spectra from Microphone C for an Altitude of 30,000 Ft	57
Figure 35 One-Third Octave Band Peaks from Microphone C for the 10 Inch Deep Modified SUU-41 Pod at 20,000 Foot Altitude	58
Figure 36 Peak One-Third Octave Band SPL as a Function of Mach Number for all Microphone Locations and Altitudes	59
Figure 37 One-Third Octave Band Spectra from the Front of the Cavity at 30,000 Foot Altitude	60
Figure 38 One-Third Octave Spectra for 3,000 Foot Altitude at Mach 0.82 Displaying Longitudinal Effect on Broadband Level	61
Figure 39 Broadband Level Versus Strouhal Number	62
Figure 40 2 Hz Narrowband Spectrum from Microphone C for the 10 Inch Deep Modified SUU-41 Pod at 3000 Foot Altitude and at Mach=0.82	63

	Page
Figure 41 2 Hz Narrowband Spectrum from Microphone C for the 10 Inch Deep Modified SUU-41 Pod at 20,000 Foot Altitude and at Mach=0.61	64
Figure 42 2 Hz Narrowband Spectrum from Microphone C for the 10 Inch Deep Modified SUU-41 Pod at 20,000 Foot Altitude and at Mach=0.82	65
Figure 43 2 Hz Narrowband Spectrum from Microphone C for the 10 Inch Deep Modified SUU-41 Pod at 20,000 Foot Altitude and at Mach=1.05	66
Figure 44 2 Hz Narrowband Spectrum from Microphone C for the 10 Inch Deep Modified SUU-41 Pod at 20,000 Foot Altitude and at Mach=1.30	67
Figure 45 2 Hz Narrowband Spectrum from Microphone C for the 10 Inch Deep Modified SUU-41 Pod at 30,000 Foot Altitude and at Mach=0.82	68
Figure 46 Nondimensional Resonant Frequencies from the Modified SUU-41 Pod as a Function of Mach Number with Rossiter Formula	69
Figure 47 Nondimensional Resonant Frequencies from the Modified SUU-41 Pod as a Function of Mach Number with Modified Rossiter Formula	70
Figure 48 One-Third Octave Band Spectra from Accelerometer J for the 10 Inch Deep Modified SUU-41 Pod at Mach 0.82	71
Figure 49 One-Third Octave Band Spectra from Accelerometer J for the 10 Inch Deep Modified SUU-41 Pod for 3,000 Foot Altitude	72
Figure 50 One-Third Octave Band Spectrum for Measured and Vibration Induced SPL from Microphone E for the 10 Inch Deep Modified SUU-41 Pod at Mach 0.82 and 3,000 Foot Altitude	73
Figure 51 Comparison of Spectra from the Working Example for the Current Prediction Scheme and the Prediction Scheme from Reference 2	74

LIST OF SYMBOLS

P_{rms}, P	Root mean square fluctuating pressure
q	Free stream dynamic pressure
M	Free stream Mach number
P_c	Cavity static pressure
P_∞	Free stream static pressure
L	Cavity length
X/L	Nondimensional cavity location
SPL	Sound pressure level
C, A, K, α	Constants
S	Strouhal number (fL/V)
f	Frequency
V	Free stream velocity
D	Cavity depth
K	Ratio of the specific heats (C_p/C_v)

SUBSCRIPTS

n, m	Integers that define mode number
max	Maximum value
X/L	Nondimensional cavity location

I. INTRODUCTION

Cavities, or rectangular cutouts, exposed to fluid flow can produce an intense aero-acoustic environment. Past experience has shown that severe fluctuating pressures exist in aircraft weapons bays under certain flight conditions. The amplitude of the fluctuating pressures can be sufficiently high to cause structural damage, malfunction of equipment, and problems with store separation and trajectories.

The aero-acoustic phenomena associated with pressure oscillations excited by flow over open cavities have been studied during the past twenty years by several investigators (References 1 - 7). Some knowledge has been gained about the phenomena but due to the complex nature of the problem, it is not completely understood. Methods to predict the pressure oscillations in shallow cavities have been reported in Reference 2. These methods are empirical and are based on wind tunnel results. A test program was established in the Air Force Flight Dynamics Laboratory to verify and/or refine these data from flight tests. Five cavity configurations were tested. This report presents the results obtained for the cavity with a length to depth ratio (L/D) of 4 and for the closed cavity configuration. The measured data were correlated with the empirical wind tunnel aero-acoustic predictions and a modified prediction method resulted. A brief description of the flight test program is given in Section II and the modified prediction method is presented in Section III. Section IV presents the major conclusions determined from this effort. A detailed description of the cavities, instrumentation and data reduction methods is given in Appendix A. Appendix B presents the test procedure and results and Appendix C contains all of the Tables and Figures.

II. TEST PROGRAM SUMMARY

The complete program included the flight testing of 5 cavity configurations; three empty cavities, one with an ogive store, and a closed cavity configuration to determine the existing boundary layer characteristics. All flight tests have been completed. Only the results for the 10 inch cavity and the closed cavity are presented in this report.

Each of the 5 configurations were tested at constant pressure altitudes of 3,000 ft, 20,000 ft, and 30,000 ft. The range of Mach numbers tested were 0.61 - 0.93 at 3,000 ft and 0.61 - 1.30 for 20,000 ft and 30,000 ft. Continuous data were recorded as the aircraft slowly accelerated from the lowest Mach number to the highest Mach number. For each flight condition, with the open cavity, fluctuating pressures were measured at nine locations in the cavity and static pressures were measured at three cavity locations. In addition vibration levels were measured with an accelerometer. For the closed cavity instrumentation was provided to define the boundary layer characteristics prior to opening the cavity which included a microphone, thermocouple, static pressure port and pressure rake.

Data were recorded on a FM magnetic tape recorder and data reduction and analysis were performed in the laboratory. Details of the test procedures, instrumentation, data reduction and analysis are given in Appendix A.

III. RESULTS

The principal result of this effort is the aero-acoustic environment prediction method. The method is presented in five steps.

STEP I - Determine the resonant frequencies with the modified Rossiter expression (Reference 2):

$$f_m = \frac{V}{L} \frac{m - 0.25}{M} + 1.75 \quad m = 1, 2, 3 \quad (11)$$

$$\left(1 + \frac{K-1}{2} M^2\right)^{1/2}$$

where V is the free-stream velocity, L is the cavity length and M is the free stream Mach number.

STEP II - Determine the peak one-third octave normalized SPL for f_1 , f_2 , and f_3 with:

$$20 \log (P_{2\max}/q) = -4 + 20 \log (-M^2 + 2M - 0.7) \quad (8)$$

$$20 \log (P_{1\max}/q) = 20 \log (P_{2\max}/q) - 14 \quad (6)$$

$$20 \log (P_{3\max}/q) = \begin{cases} 20 \log (P_{2\max}/q) - 11 & \text{for } M > 0.7 \\ 20 \log (P_{2\max}/q) & \text{for } M \leq 0.7 \end{cases} \quad (7)$$

where $P_{n\max}$ are the maximum fluctuating pressures for each mode frequency f_n and q is the free-stream dynamic pressure.

STEP III - Determine the peak one-third octave band amplitude at the desired longitudinal position for each resonant frequency with the following equation:

$$20 \log \left(\frac{P_n}{q}\right)_{X/L} = 20 \log \left(\frac{P_{n\max}}{q}\right) - 10 (1.7 - 0.7 X/L - |\cos^n X/L|) \quad (4)$$

$$n = 1, 2, 3$$

where

$$\alpha_1 = 3.5$$

$$\alpha_2 = 6.3$$

$$\alpha_3 = 10.0$$

STEP IV - Determine the peak normalized one-third octave band level of the broadband spectrum at the location in the cavity from:

$$20 \log \left(\frac{P_b}{q} \right)_{X/L} = 20 \log \left(\frac{P_{2max}}{q} \right) - 15 - 10 \left(1 - \frac{X}{L} \right) \quad (9)$$

STEP V - Determine the normalized broadband spectrum from Figure 39.

Another significant finding from the flight test was that dynamic pressure (q) scaling did not account for the total variation in the SPL with altitude for certain cavity locations; however, at two cavity locations scaling with q did account for the complete change in the SPL with a change in the altitude, i.e., the SPL referenced to q was the same for any altitude. Previous investigators have shown that for a fixed Mach number q scaling accounted for any significant change in the SPL for various pressure altitudes. The reason they did not observe this phenomena could be due to the cavity positions analyzed. The position selected could be one at which q scaling accounts for all pressure altitude variations.

The prediction method presented above is based on empirical results which were selected to give the highest sound pressure levels in the cavity. Although scaling with q failed at some points in the cavity the predicted levels will be conservative at these locations.

IV. CONCLUSIONS

The experimental investigation reported herein indicates the following conclusions:

1. The cavity resonant frequencies can be accurately predicted by the modified Rossiter formula.

2. The amplitude prediction methods in Reference 2 were conservative in predicting both the resonant and broadband SPL observed in actual flight tests.

The method described in the results section is recommended for predicting more realistic SPLs for an L/D near 4 and a Mach number range of .6 to 1.3.

3. The longitudinal variation of the rms amplitude associated with each resonant frequency can be described as ordered modes.

4. The maximum broadband levels increased towards the aft end of the cavity by approximately 10 dB.

APPENDIX A

Description of Test Article and Instrumentation

CAVITY MODEL

The cavity was 40 inches long, 10 inches deep and 9 inches wide and was constructed with 0.250 inch thick aluminum (6061-T6). Two 1.50 inch X 1.50 inch X 0.25 inch aluminum (6061-T6) angles were welded to the bottom for additional support. The additional support raised the natural frequency of the structure, and thus it was hoped that the resonant frequencies of the structure and the acoustic resonant frequencies were far enough apart to prevent significant coupling of the two. An accelerometer was mounted in the floor of the cavity about three-fourths of the distance from the leading edge to measure the structural vibration amplitudes and frequencies to determine whether or not they would interfere with the microphone measurements.

The cavity was mounted in a modified SUU-41 munitions dispenser pod. A picture of a standard pod is shown in Figure 1* and the necessary modifications are shown in Figure 2. Figure 3 shows the modified pod mounted on a RF-4C test aircraft which was employed for the tests. The SUU-41 pod was carried on the triple ejection rack (TER) of the left pylon of the aircraft. Figure 4 schematically illustrates the mounting.

A closed cavity configuration was also tested to determine the boundary-layer characteristics. A flat plate was smoothly fit over the cavity so that a boundary-layer rake could be installed just behind the leading edge of the cavity. The velocity profiles were determined from the rake data, thus, indicating whether the boundary-layer was laminar or turbulent. The boundary layer noise was also determined by a microphone located just ahead of the cavity.

* All Tables and Figures referenced are in Appendix C

INSTRUMENTATION

The open cavity was instrumented with nine microphones, one accelerometer, a thermocouple and three static pressure ports. The closed cavity was instrumented with a microphone, thermocouple, static pressure port, and a pressure rake. The location of the instrumentation is shown in Figure 5 and Figure 6 with a typical microphone mounting also shown in Figure 5. The type and models of all instrumentation are presented in Figure 7.

The overall system response for the Model 902H crystal accelerometer was flat within ± 5 percent from 2 to 6000 Hz. The system response for the Model MVA 2100 microphones was flat within 2 dB from 5 to 6000 Hz while the Model MVA 2400 was flat within 2 dB from 2 to 6000 Hz.

The accelerometer was calibrated in the laboratory using a Bruel and Kjaer Type 1606 vibration preamplifier (± 1 g calibrator). The microphones were calibrated in the laboratory with a General Radio Type 1552-B sound level calibrator. The measurement system, once installed in the aircraft, was calibrated with an insert voltage to account for signal loss through the cables.

DATA REDUCTION PROCEDURES

All data were continuously recorded on two fourteen channel tape recorders. The magnetic tapes recorded in-flight were played back in the laboratory on a Honeywell 7400 record-reproduce system. Overall time histories and one-third octave band analysis were performed over the frequency range of 12.5 Hz to 10,000 Hz using a General Radio 1926 multi-channel rms detector interfaced with a 2116 Hewlett-Packard digital computer. The time histories were correlated with the specific flight conditions which were recorded on a voice channel.

For selected microphone and accelerometer data, narrowband (2 Hz) analyses were performed using a 9300 power spectral density analyzer. The system linearity is ± 0.5 dB for a discrete frequency input. Narrowband analyses were also obtained using a Hewlett-Packard 5450 Fourier analyzer. The data reduction system used is schematically shown in Figure 8.

APPENDIX B

Experimental Procedures and Results

TEST PROCEDURES

The three altitudes at which the flight tests were flown are 3,000 ft, 20,000 ft, and 30,000 ft. The tests include flights for the Mach number ranges 0.61 to 0.93 for 3,000 ft and 0.61 to 1.30 for 20,000 ft, and 30,000 ft. Data were obtained at all Mach numbers between the two extremes since the aircraft was slowly accelerated from the lowest to the highest Mach number (approximately 2 to 3 minutes) with data being recorded continuously. The majority of the flight requiring speeds in excess of $M = 0.9$ below 30,000 ft were flown over Lake Huron with the remaining flights being flown over Washington Courthouse, Ohio.

TEST RESULTS

Boundary Layer Characteristics

a. Velocity Profiles

In order to define the flow conditions for which subsequent data were taken, boundary layer profiles were obtained for each altitude and representative Mach numbers. A boundary layer profile rake, thermocouple, and a static pressure transducer were mounted on the flat plate covering the cavity as shown in Figure 6. The resulting normalized velocity profiles are presented in Figure 9 along with the conventional $1/7$ th power law for fully-developed turbulent boundary layers. The data indicate that the profiles existing at the leading edge of the cavity agree reasonably well with those for fully developed turbulent flow.

b. Aerodynamic Noise

The microphone located upstream of the cavity (Figure 6) enabled the boundary layer noise to be determined. Data were recorded continuously as with the open cavity runs. One-third octave band spectra were obtained for each altitude and for approximately every 0.1 Mach number with representative results presented in Figures 10 through 13. Figures 10 through 12 show the closed cavity boundary layer spectra along with the spectra for

Location C of the open cavity at the same conditions. The results show that the boundary layer noise has no appreciable affect on the open cavity analysis. The data also display a lack of scaling between the boundary layer spectra and the open cavity spectra, i.e., the shape of the spectra are entirely different. This observation was also noted in Reference 2. The peak that occurs at 400 Hz in the boundary layer spectra is due to the aircraft power supply used with the instrumentation. Figure 13 depicts the variation of the normalized boundary layer noise with respect to Mach number. The normalized boundary layer noise is seen to decrease with increasing Mach number as was expected since it has been shown (Reference 8) that the normalized boundary layer noise follows the expression:

$$\frac{P_{rms}}{q} = \frac{C_1}{1 + C_2 M^2} \quad (1)$$

with constants C_1 and C_2 depending upon the type of boundary layer. The dynamic pressure (q) may be defined as $0.7 P_o M^2$ where P_o is the local static pressure and Equation 1 may then be written as:

$$P_{rms} = \frac{C_3 P_o}{\frac{1}{M^2} + C_2} \quad (1.a)$$

It is easily noted in Equation 1.a that for a constant pressure altitude the rms pressure will increase with an increase in Mach number

Static Pressures

Static pressures were measured at 3 locations in the cavity. Two pressure transducers were located in the rear half of the floor and one in the aft wall (See Figure 5). The data are presented as the difference between the cavity static pressure P_c and the free-stream static pressure P_∞ normalized with the free-stream static pressure. The data shown in Figure 14 are typical of that for the entire test. It is seen that the

cavity static pressure increases towards the rear of the cavity as earlier investigators (References 2, 5, and 7) observed. As the Mach number is increased the static pressure increases reaching its maximum at the maximum speed. It must be pointed out that one cannot extrapolate this observation very far beyond the range of the test because it was found in Reference 2 (for wind tunnel tests) that the static pressure at the rear of the cavity starts to decrease around $M = 2$. This trend was also noted in Reference 5.

In Figure 15 the average of the static pressure measured at each location is plotted as a function of Mach number and compared to previously obtained wind tunnel data as taken from Reference 2. This figure clearly shows an increase in cavity static pressure with Mach number. The flight data tend to be above the wind tunnel results which can be explained from the fact that from the flight data only pressures in the rear half of the cavity were available, whereas, in the wind tunnel static pressures were measured over the entire cavity length. Consequently, since the static pressure increased at the rear of the cavity the average flight test static pressure would be greater than the average static pressure determined from the wind tunnel tests.

Fluctuating Pressures

Fluctuating pressures were measured at the nine locations shown in Figure 5 for all three test altitudes. The data were obtained from microphones at these locations and were recorded continuously as the aircraft slowly accelerated from the lowest to the highest Mach number. The recorded data were analyzed at approximately every 0.1 Mach number using a two second sample time. For the frequencies of interest this insures a good statistical representation of the data. Throughout the report the fluctuating pressures are either presented as sound pressure levels referenced to $20 \mu\text{N/m}^2$ or are normalized to free stream dynamic pressure and presented logarithmically. The dynamic pressures were computed from the free stream Mach numbers and free stream static pressures. These are presented in Table I

for each pressure altitude and Mach number. In addition Table I includes the quantity required to convert the logarithmic normalized fluctuating pressures to sound pressure levels, i.e., add the last columns of Table I to $20 \log P/q$ to obtain the sound pressure level referenced to $20 \mu\text{N/m}^2$.

The overall fluctuating pressure time histories from Microphone C for all three altitudes are presented in Figure 16. These time histories are representative of all the data observed except the spread between the data at each altitude differs at different positions along the cavity. This variation will be discussed in greater detail below when the third-octave data are presented. The overall levels approximately follow the same trends as the third-octave levels since the strong resonances essentially control the overall levels.

Figures 17 through 25 present the one-third octave band spectra from Microphones A through I at a Mach number of 0.82 for each altitude (3,000 ft; 20,000 ft; 30,000 ft). The resonant peaks in the spectra are evident and appear most strongly at the lowest altitude. It is also evident that dynamic pressure scaling with altitude does not account for the total spread in the data for all microphone locations. Certain positions in the cavity scale reasonably well while others fail by as much as 20 dB. Figure 26 illustrates this failure by presenting the data from Microphones C and D for 3,000 and 30,000 ft altitudes at the 0.82 Mach number. In the figure these data are referenced to the dynamic pressure (q). Position C scales quite well over the entire spectrum. Position D fails to scale by approximately 10 dB. The only positions that scaled reasonably well were $X/L = 0$ and $X/L = 0.5$. An explanation for this lack of scaling is a tendency in flight for the standing wave patterns (explained later in the report) to shift node locations with a change in altitude. If this occurs it would result in a change in the observed SPL that would not be accounted for by dynamic pressure scaling. Previous investigators (Reference 2) have shown that for wind

tunnel results q scaling accounted for all significant changes in the SPL with pressure altitude for a fixed Mach number. Fixed wind tunnel conditions would probably result in a fixed standing wave pattern, thus scaling would appear to be valid throughout the cavity.

In an attempt to verify the mode shapes that were observed in the tunnel tests (Reference 2), the longitudinal variation in the normalized amplitudes of the resonant frequencies, taken from Figures 17 - 25, were plotted in Figures 27 through 29. The mode 1 frequency 1/3 octave band peaks are presented in Figure 27 and the mode 2 in Figure 28. The data are for all three altitudes at a Mach number of 0.82. Figure 29 presents the mode 3 frequency 1/3 octave band peaks for the same conditions. All of the microphones were mounted in the floor of the cavity except at $X/L = 0.75$. At this position a microphone was located on each side wall at 1/2 the depth of the cavity as shown in Figure 5. The SPL at 1/2 the depth was assumed to apply on the floor at $X/L = 0.75$. The amount of error introduced with this assumption is unknown. Comparisons of the microphones on the fore and aft wall at the midpoint position with the ones located in the corner on the floor (See Figure 5) show that there could be a difference as great as 9 dB between the two positions. However, at an altitude of 3,000 feet there was essentially no difference in the two amplitudes. Also, at this position ($X/L = 0.75$) an average of the two SPLs from the microphones on the side walls was used. The difference between the two levels was as high as about 10 dB but typically was near 4 dB. A possible explanation of this fairly large difference is that the cavity was mounted on an ejection rack and the rack was mounted on the aircraft pylon, thus the yaw of the pod may not have been zero as desired. A small yaw angle would alter the flow over the cavity and result in significant variations from side to side of the SPL. The failure of the data to scale with q is readily apparent in Figures 27 - 29 since it is presented referenced to q .

Reference 2 presented observed mode shapes from the wind tunnel tests for the first three mode frequencies, these are shown in Figure 30.

These mode shapes can be described by ramped sinusoidal functions. In order to define the longitudinal pressure distribution in the flight data, ramped sinusoidal functions of the following form were used:

$$(SPL_n)_{X/L} = (SPL_n)_{X/L=1} - (A_1 + A_2 \left(\frac{X}{L}\right) + A_3 |\cos^{\alpha_n} \frac{X}{L}|)_{n=1,2,3} \quad (3)$$

where $(SPL_n)_{X/L}$ are one-third octave band sound pressure levels for the mode frequencies at nondimensional locations in the cavity.

$(SPL_n)_{X/L=1}$ are the one-third octave band sound pressure levels for the mode frequencies at the rear of the cavity.

A_1 , A_2 , A_3 , and α_n are arbitrary constants to be determined from measured data.

The constants were determined to be:

$$A_1 = 17$$

$$A_2 = 7$$

$$A_3 = -10$$

$$\alpha_1 = 3.5$$

$$\alpha_2 = 6.3$$

$$\alpha_3 = 10$$

With these constants and with the level normalized with q Equation 3 becomes:

$$20 \log \left(\frac{P_n}{q}\right)_{X/L} = 20 \log \left(\frac{P_{n \max}}{q}\right) - 10 (1.7 - 0.7X/L - |\cos^{\alpha_n} X/L|) \quad (4)$$

$n=1,2,3$

This equation is plotted in Figure 31 along with the measured data. Very good agreement is obtained for these conditions at nearly all locations in the cavity. The largest discrepancy occurs at $X/L = .75$ where the microphones were not located on the floor as described above. For simplicity, Equation 3, with the constants determined from the measured data for the 3000 foot altitude, will be used to predict the longitudinal distribution for all conditions by assuming dynamic pressure (q) scaling. This assumption will result,

for the higher altitudes, in overpredicting the SPL at those locations where dynamic scaling failed as shown in Figures 27 through 29.

The one-third octave band spectra from Microphone C are presented in Figures 32 - 34 to show Mach number effects. The peak frequencies and amplitudes are seen to increase with Mach number as expected. The amplitude of the resonant frequencies are shown in Figure 35 as a function of Mach number for the 20,000 ft altitude. With a smooth curve faired through each set of points it is evident that the dominant frequency "switches" from mode 3 to mode 2 at approximately a Mach number of 0.7. The other two altitudes displayed similar trends. An explanation for this "switching" is not readily apparent and thus subject for further investigation.

In order to use Equation 3 it is necessary to obtain the maximum amplitude for each mode frequency that occurred during the tests. The worst case prediction curve offered in Reference 2 used the same value for each frequency even though the data shows significant differences between them. The curve in Figure 36 represents the amplitude prediction method of Reference 2. The peak one-third octave band levels obtained from all the flight tests were within the shaded area of Figure 36. Also given in the figure is a curve which encompasses all the flight data which was determined by the method of least squares. This curve is defined by:

$$20 \log \frac{P_{\max}}{q} = -4 + 20 \log (-M^2 + 2M - 0.7) \quad (5)$$

The shaded area in Figure 36 represents a change in SPL of nearly 30 dB. Consequently if a worst case prediction is used for all frequencies and locations in the cavity it is possible to overestimate the environment by this amount. The approach taken above to describe the longitudinal distribution of the fluctuating pressures will greatly reduce this error. It can be further reduced by defining the maximum SPL for each mode frequency. Consideration of all the flight test data showed that in nearly every case the maximum measured level corresponded to the mode two frequency (e.g., Figure 35). This indicates that the normalized level for the mode 2

frequency can be determined from Equation 4. The mode 1 and mode 3 levels were below this value by 14 and 11 dB respectively for Mach numbers above about 0.7. Thus, the normalized level of these two mode frequencies can be expressed by:

$$20 \log \left(\frac{P_{1 \max}}{q} \right) = 20 \log \left(\frac{P_{2 \max}}{q} \right) - 14 \quad (6)$$

$$20 \log \left(\frac{P_{3 \max}}{q} \right) = \begin{cases} 20 \log \left(\frac{P_{2 \max}}{q} \right) - 11 & M > 0.7 \\ 20 \log \left(\frac{P_{2 \max}}{q} \right) & M \leq 0.7 \end{cases} \quad (7)$$

where $P_{2 \max}$ is determined from Equation 5.

$$20 \log \left(\frac{P_{2 \max}}{q} \right) = -4 + 20 \log (-M^2 + 2M - 0.7) \quad (8)$$

The use of Equations 4 through 8 will permit the determination of the one-third octave band levels corresponding to the first three mode frequencies at each location in the cavity. The procedures used will result in predicted levels which are not nearly so conservative as those obtained from the methods of Reference 2.

When predicting the aero-acoustic environment that will result in a cavity exposed to fluid flow, the broadband as well as the narrowband part of the spectrum must be considered. An approximate prediction method for the broadband levels was presented in Reference 2. It was concluded that the maximum normalized broadband level decreased with increasing Mach number and shifted to a higher Strouhal frequency. The current data tends to show an opposite effect, that is, the normalized broadband levels increase with increasing Mach number. This is illustrated in Figure 37 by the one-third octave band data from Microphone C for various Mach numbers. If a smooth curve is drawn through each spectrum, omitting the discrete frequencies, the maximum normalized broadband level increases with an increase in Mach number.

There is a tendency for the maximum to shift to a higher Strouhal frequency as observed in Reference 2.

Figure 38 shows the one-third octave band spectra at locations along the cavity for an altitude of 3,000 ft and Mach number of 0.82. Disregarding the peaks, the data show a tendency for the broadband noise levels to increase from the front to the rear of the cavity. The only position that does not follow the trend is D. However, for prediction purposes it will be assumed that the maximum broadband level linearly increased 10 dB from the fore end to the aft end of the cavity.

The maximum broadband level appears in Figure 38 to be 15 dB below the level of the mode 2 frequency at the rear of the cavity. The maximum one-third octave band level of the broadband noise and the longitudinal variation can therefore be described by:

$$20 \log \left(\frac{P_b}{q} \right)_{X/L} = 20 \log \left(\frac{P_{2 \max}}{q} \right) - 15 - 10 \left(1 - \frac{X}{L} \right) \quad (9)$$

where P_b is the rms pressure in the peak one-third octave band of the broadband spectrum.

A suggested shape of the broadband spectrum is given in Figure 39 relative to the maximum third octave band level defined by Equation 8. The one-third octave band spectrum is assumed to peak at a nondimensional Strouhal frequency of about 0.8.

Resonant Frequencies

To identify the discrete resonant frequencies in the recorded data narrowband (2 Hz) frequency spectra were obtained from various microphone locations and each altitude. Typical narrowband spectra are shown in Figures 40 - 45 for Microphone C at all three altitudes and various Mach numbers. The nondimensional resonant frequencies or Strouhal number ($S = fL/V$) were calculated for each observed resonant frequency f . The free-stream velocity was calculated from the free-stream static temperature. Only those resonant frequencies that were 5 dB or more above the broadband level were used to

calculate the nondimensional frequencies. The resulting frequencies are summarized in Figure 46 along with the results from wind tunnel tests (Reference 2) for a cavity with an L/D ratio equal to 4. The curves represent Rossiter's semiempirical equation. This equation

$$f = \frac{V}{L} \frac{m-\alpha}{M^{-1/K_v}} \quad m = 1, 2, 3 \quad (10)$$

assumes the cavity temperature approaches the free-stream static temperature. The values of the empirical constants, α and K_v used were 0.25 and 0.57, respectively. It should be noted that this equation deviates from the data at the higher Mach numbers. The reason for this difference is the assumption that the cavity temperature approached the free-stream static temperature. Heller (Reference 2) modified this equation by assuming the cavity temperature approached the free-stream stagnation temperature. The modified form

$$f_m = \frac{V}{L} \frac{m - 0.25}{\frac{M}{(1 + \frac{K-1}{2} M^2)^{1/2}}} + 1.75 \quad m = 1, 2, 3 \quad (11)$$

is seen in Figure 47 to fit the data better and is recommended for predicting resonant frequencies.

Vibration Levels

The vibration levels were measured by an accelerometer mounted on the floor of the cavity at 3/4 of the cavity length from the leading edge (See Figure 5). Data were recorded continuously by the same instrumentation as that used with the microphones and one-third octave band analyses were performed for all three altitudes at about every 0.1 Mach number.

Figures 48 and 49 show typical acceleration one-third octave band spectra referenced to 1g. Variation of the acceleration level with respect to altitude is displayed in Figure 48 while the variation with respect to Mach number is

shown in Figure 49. It is seen that the vibration amplitude increases with increasing Mach number; decreases for higher altitudes; and there are pre-dominate resonant frequencies present. These same trends were noted from the microphone data. It is evident that there is some coupling effect between the acoustic oscillations within the cavity and the vibration of the cavity walls. Thus, it remains to be determined whether or not the vibration amplitude is of sufficient magnitude to significantly affect the microphone readings.

The vibratory sensitivity of the microphones used was 90 dB/1g, i.e., 1g of acceleration of the microphone would produce not more than a 90 dB reading. Figure 50 shows the SPL for Microphone E (the nearest one to the accelerometer, see Figure 5) along with the corresponding SPL that a microphone would show due to the measured acceleration for $h = 3,000$ ft and a Mach number of 0.82. There is a 25 dB or more difference between the two curves at all frequencies, therefore, it can be assumed that the vibration effect on the microphones was insignificant. It was also assumed throughout the report that the acoustic energy input to the system from the vibration of the walls was negligible.

Prediction Method for Fluctuating Pressures

The results presented above can be used to predict the characteristics of the fluctuating pressures which will occur in open rectangular cavities. The step by step procedures required to obtain the one-third octave band spectra at various locations in the cavity are given below:

STEP 1 - Determine the first three resonant frequencies from the modified Rossiter equation from:

$$f_m = \frac{V}{L} \frac{m - 0.25}{M} \frac{1}{(1 + \frac{K-1}{2} M^2)^{1/2}} + 1.75 \quad m = 1, 2, 3 \quad (11)$$

STEP 2 - Determine the maximum normalized one-third octave band amplitude for each frequency from:

$$20 \log \left(\frac{P_2 \text{ max}}{q} \right) = -4 + 20 \log (-M^2 + 2M - 0.7) \quad (8)$$

$$20 \log \left(\frac{P_1 \text{ max}}{q} \right) = 20 \log \left(\frac{P_2 \text{ max}}{q} \right) - 14 \quad (6)$$

$$20 \log \left(\frac{P_3 \text{ max}}{q} \right) = \begin{cases} 20 \log \left(\frac{P_2 \text{ max}}{q} \right) - 11 & M > 0.7 \\ 20 \log \left(\frac{P_2 \text{ max}}{q} \right) & M \leq 0.7 \end{cases} \quad (7)$$

STEP 3 - Determine the longitudinal variation of the one-third octave amplitude for each mode frequency from:

$$20 \log \left(\frac{P_n}{q} \right)_{X/L} = 20 \log \left(\frac{P_n \text{ max}}{q} \right) - 10 \left(1.7 - 0.7 \frac{X}{L} - \left| \cos \alpha_n \frac{X}{L} \right| \right) \quad (4)$$

$$n = 1.2.3$$

STEP 4 - Determine the peak normalized one-third octave band levels of the broadband spectrum at the location in the cavity from:

$$20 \log \left(\frac{P_b}{q} \right)_{X/L} = 20 \log \left(\frac{P_2 \text{ max}}{q} \right) - 15 - 10 \left(1 - \frac{X}{L} \right) \quad (9)$$

STEP 5 - Determine the normalized broadband spectrum from Figure 39.

The prediction method given above is empirical and applies to a rectangular cavity with a L/D of 4 and a Mach number range from 0.6 to 1.3. Additional flight data are being analyzed to extend those methods to other L/D ratios.

Working Example

For clarity an example is presented illustrating the use of the prediction method and a comparison is made of results of this method to those

obtained from Reference 2.

Consider the case of an aircraft flying at Mach 0.9 near sea level with an open nearly rectangular cavity 20 feet long and 5 feet deep. It is desired to predict the aero-acoustic environment at the center and at the rear of the cavity. The solution is obtained as follows:

From Step 1 (Equation 11) the first 3 mode frequencies are determined to be:

$$f_1 = 15 \text{ Hz}$$

$$f_2 = 34 \text{ Hz}$$

$$f_3 = 54 \text{ Hz}$$

Equations 6, 7, and 8 of Step 2 are used to calculate the maximum normalized amplitude for each mode frequency and results in the following values:

$$20 \log (P_{1\text{max}}/q) = -29 \text{ dB}$$

$$20 \log (P_{2\text{max}}/q) = -15 \text{ dB}$$

$$20 \log (P_{3\text{max}}/q) = -26 \text{ dB}$$

The amplitude of each mode frequency at the center and rear of the cavity are determined from Equation 4. The results, referenced to $20\mu\text{N}/\text{M}^2$, are:

for $X/L = 0.5$

$$\text{SPL}_1 = 148 \text{ dB}$$

$$\text{SPL}_2 = 170 \text{ dB}$$

$$\text{SPL}_3 = 152 \text{ dB}$$

for $X/L = 1.0$

$$\text{SPL}_1 = 160 \text{ dB}$$

$$\text{SPL}_2 = 174 \text{ dB}$$

$$\text{SPL}_3 = 163 \text{ dB}$$

Step 4 (Equation 9) is then used to obtain the peak normalized one-third octave band levels of the broadband spectrum at the two locations and are

$$20 \log \left(\frac{P_b}{q} \right)_{X/L = 0.5} = -35$$

$$20 \log \left(\frac{P_b}{q} \right)_{X/L = 1.0} = -30$$

The final step is to determine the broadband spectrum from Figure 39.

The spectra obtained are shown in Figure 51 along with the spectrum one would predict using the scheme offered in Reference 2. The current results show resonant modes 1 and 3 completely attenuated for the center position, this is due to the longitudinal mode shapes. The $X/L = 0.5$ position is seen in Figure 31 to be a node for the mode 1 and 3 frequencies while an antinode for mode 2. Thus, there is almost 30 dB difference between the two prediction schemes at the center of the cavity for modes 1 and 3. However, it should be noted that the prediction schemes agree fairly well for the maximum level predicted at the rear of the cavity for the mode 2 frequency.

APPENDIX C
TABLE AND FIGURES

MACH NR	STATIC PRESSURE P_{∞} (psia)	DYNAMIC PRESSURE q_{∞} (psia)	$20 \text{ LOG } \left(\frac{P_{\text{ref}}}{q_{\infty}} \right)$ (dB)
0.61	4.37	1.12	172
	6.76	1.73	175
	13.17	3.37	181
0.71	4.37	1.56	174
	6.76	2.41	178
	13.17	4.69	184
0.82	4.37	2.06	177
	6.76	3.19	181
	13.17	6.21	186
0.93	4.37	2.66	179
	6.76	4.11	183
	13.17	8.01	189
1.05	4.37	3.35	181
	6.76	5.19	185
	13.17	10.11	191
1.17	4.37	4.18	183
	6.76	6.47	187
	13.17	12.60	193
1.30	4.37	5.17	185
	6.76	8.00	189
	13.17	15.58	194

TABLE I PRESSURE REFERENCE DATA

AIR FORCE

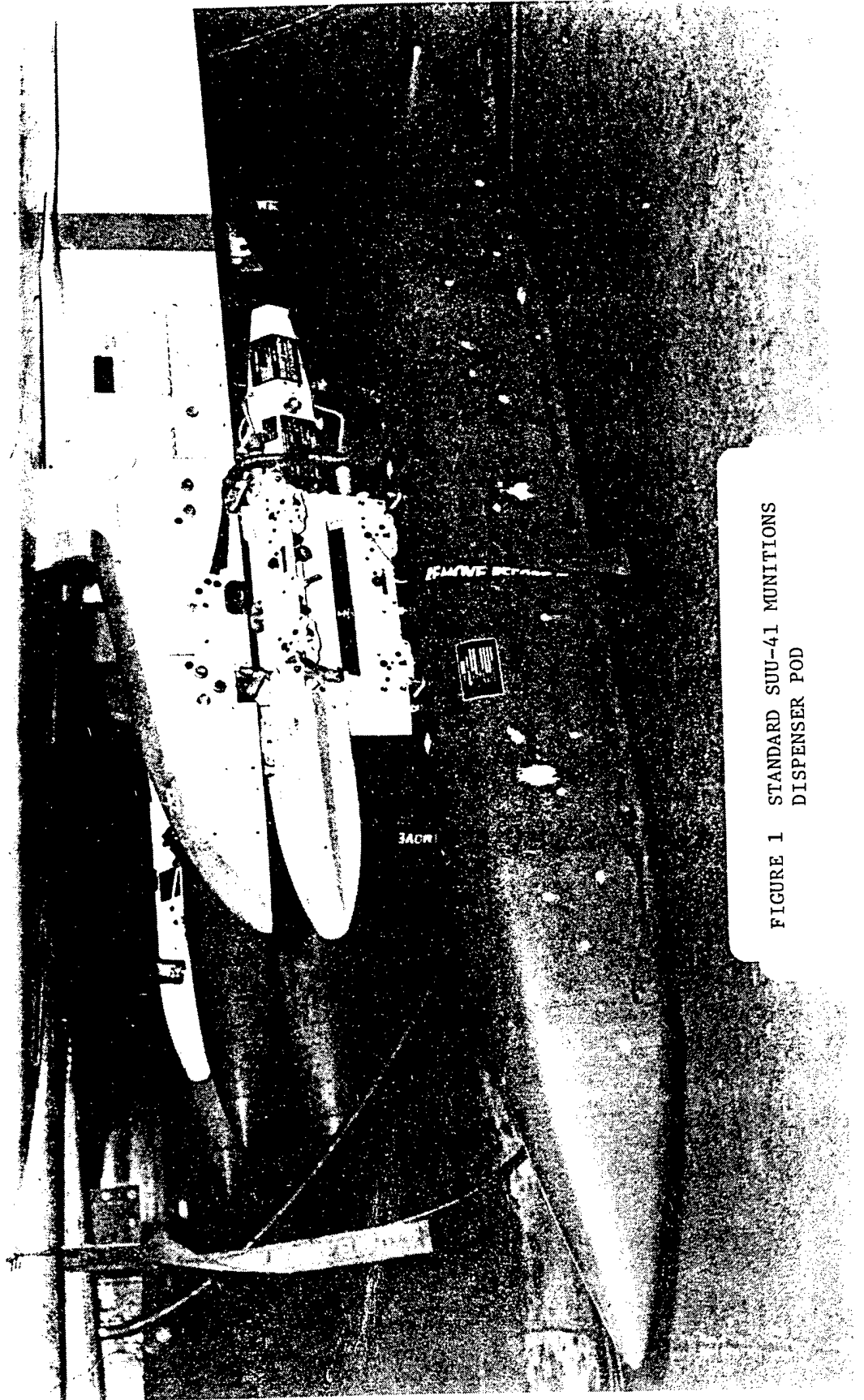


FIGURE 1 STANDARD SUU-41 MUNITIONS
DISPENSER POD

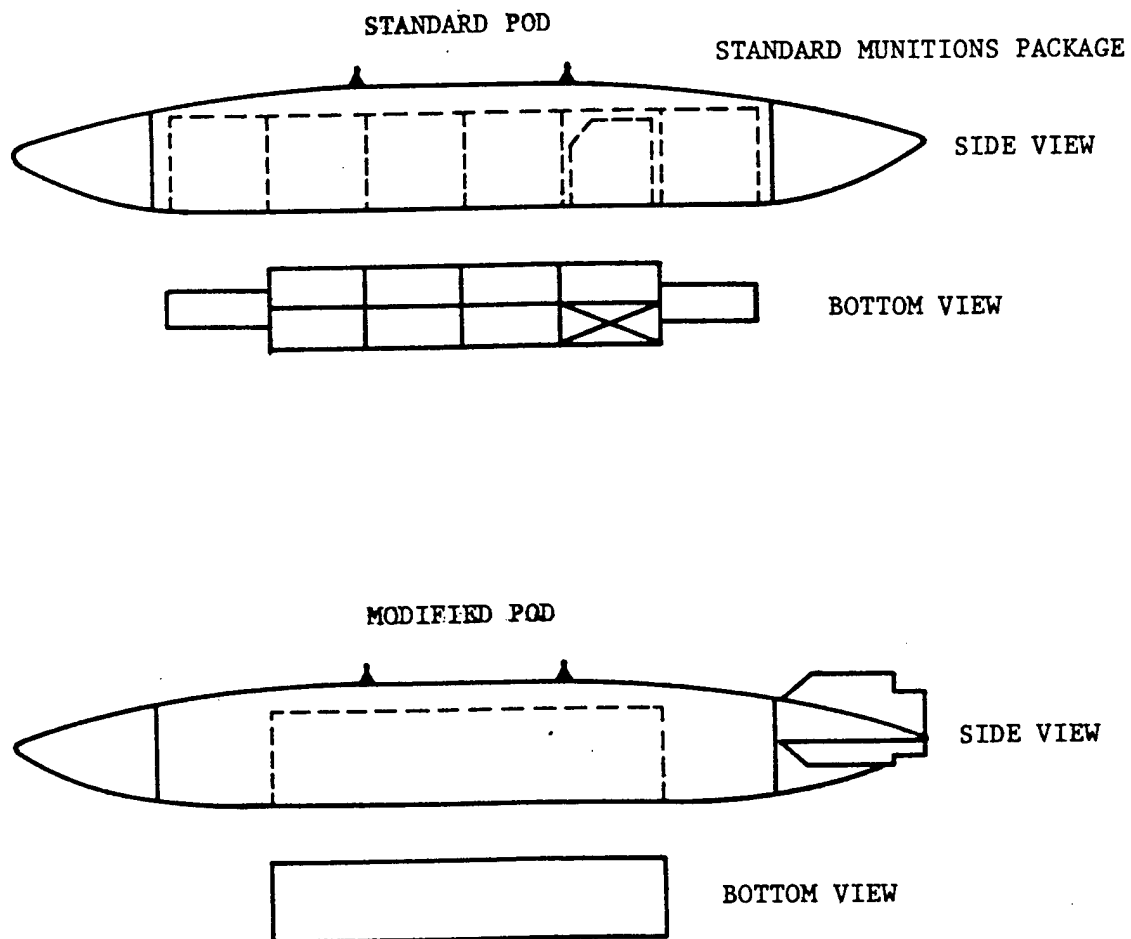


FIGURE 2 MODIFICATIONS TO THE STANDARD SUU-41 DISPENSER POD

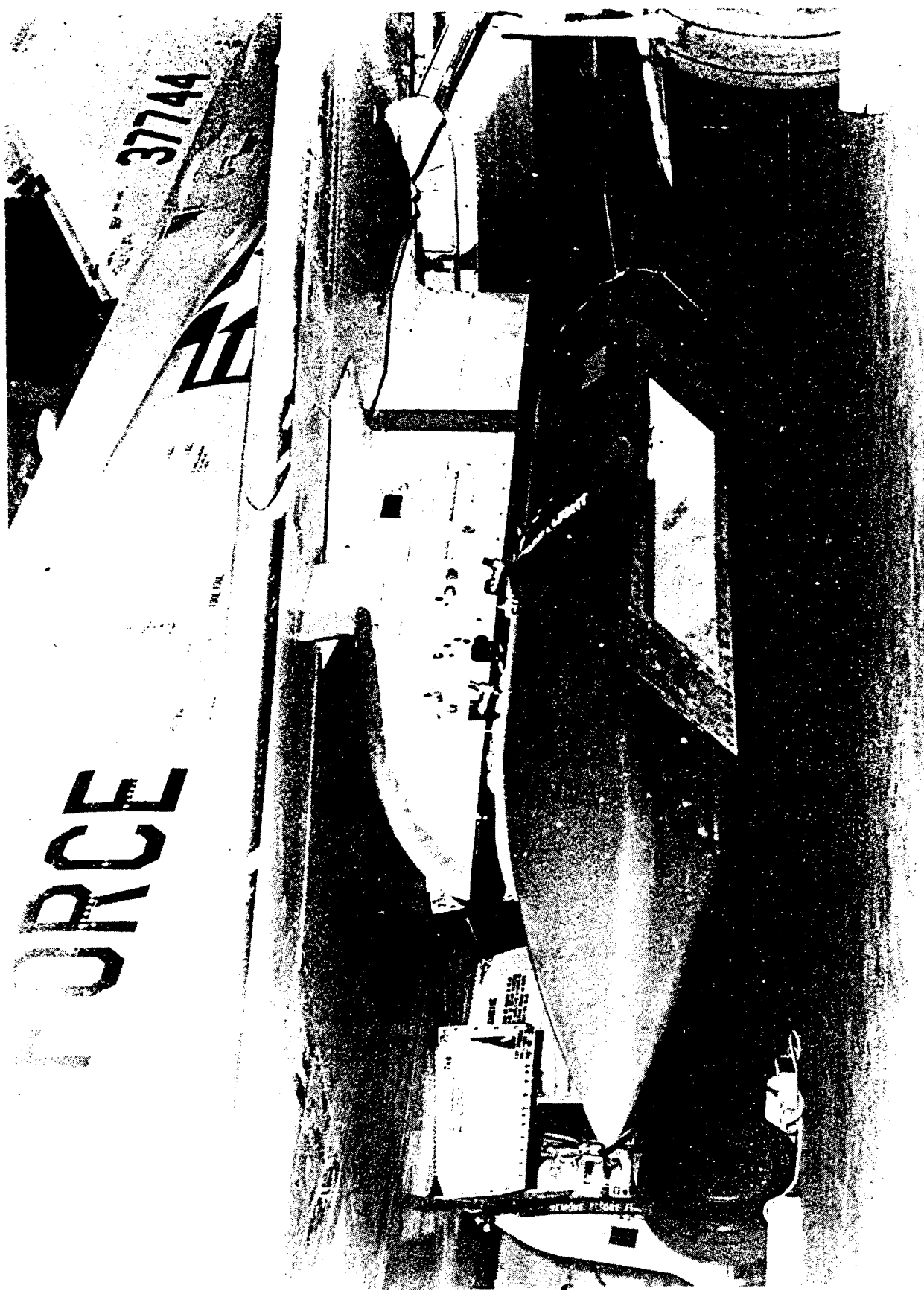
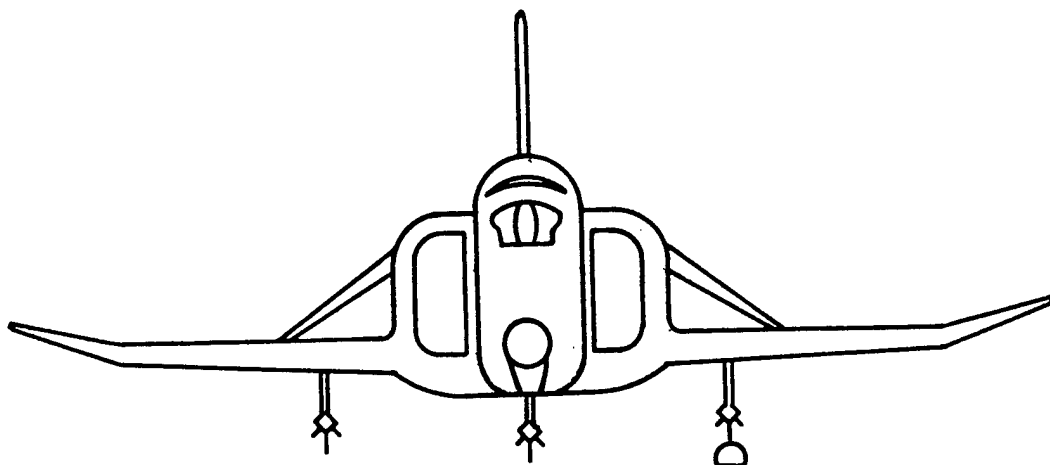


FIGURE 3 TEN INCH CAVITY (L/D=4)
MOUNTED IN MODIFIED
SUU-41 POD

RF-4C AIRCRAFT



POD ON TER OF LEFT INBOARD PYLON

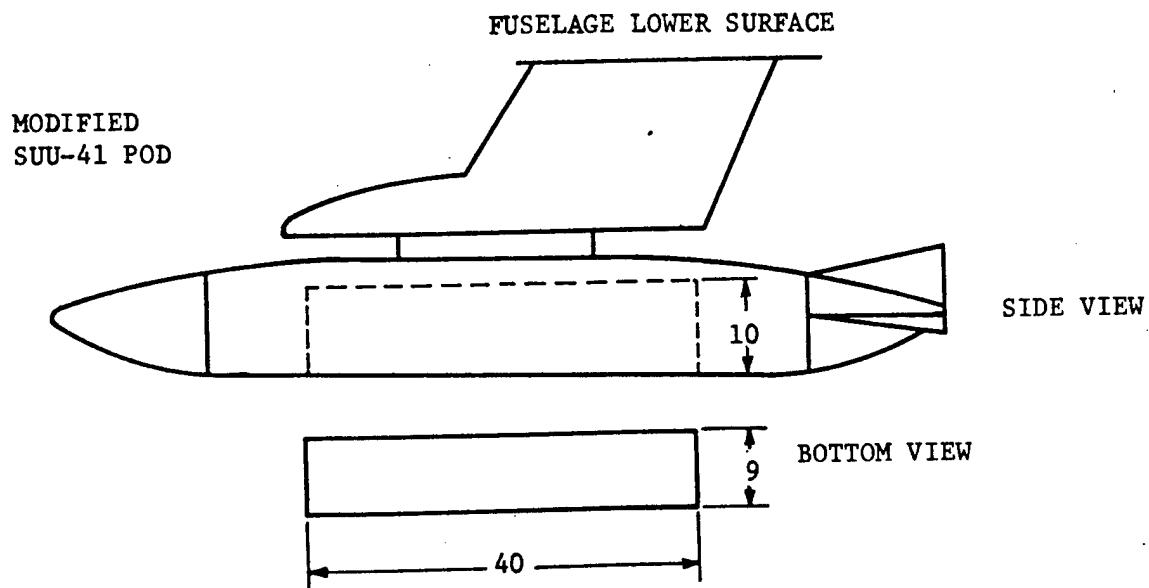
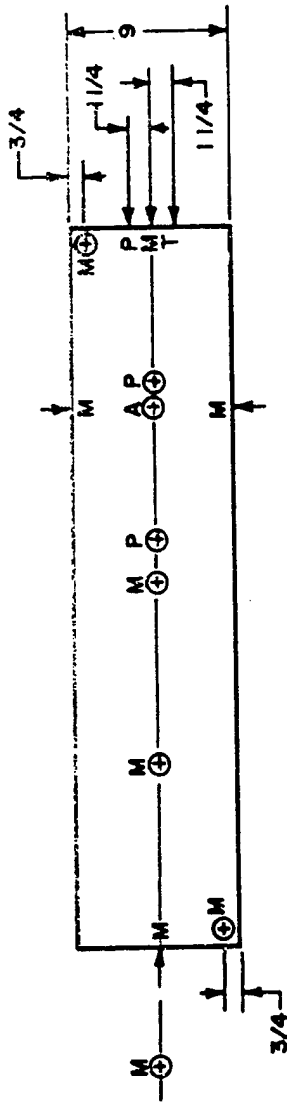
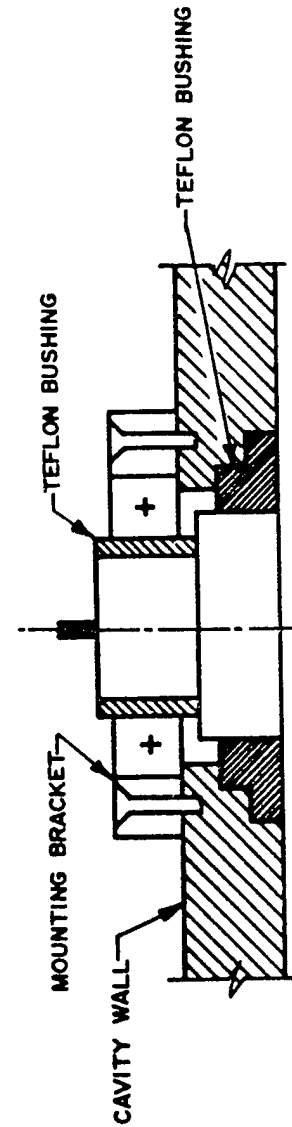
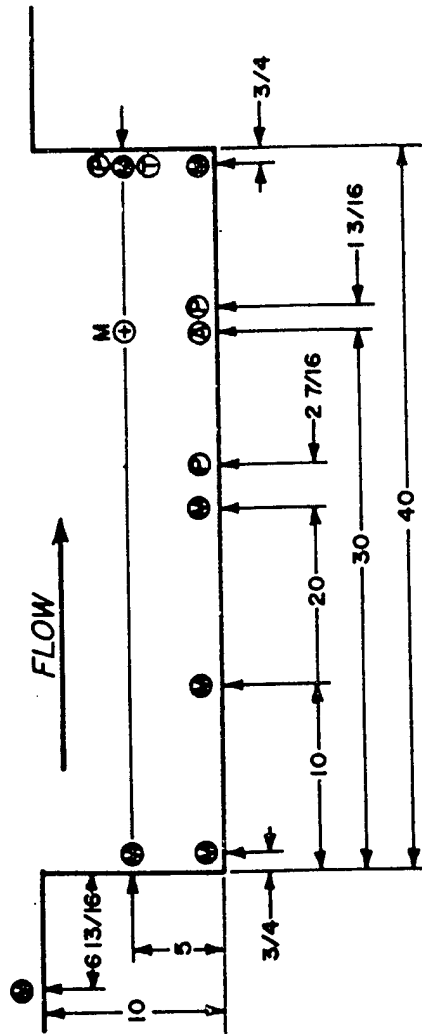


FIGURE 4 MODIFIED SUU-41 POD MOUNTED ON RF-4C TEST AIRCRAFT



M - MICROPHONE
 T - THERMOCOUPLE
 A - ACCELEROMETER
 P - STATIC PRESSURE TAP



TYPICAL MICROPHONE MOUNTING

FIGURE 5, OPEN CAVITY INSTRUMENTATION LOCATION

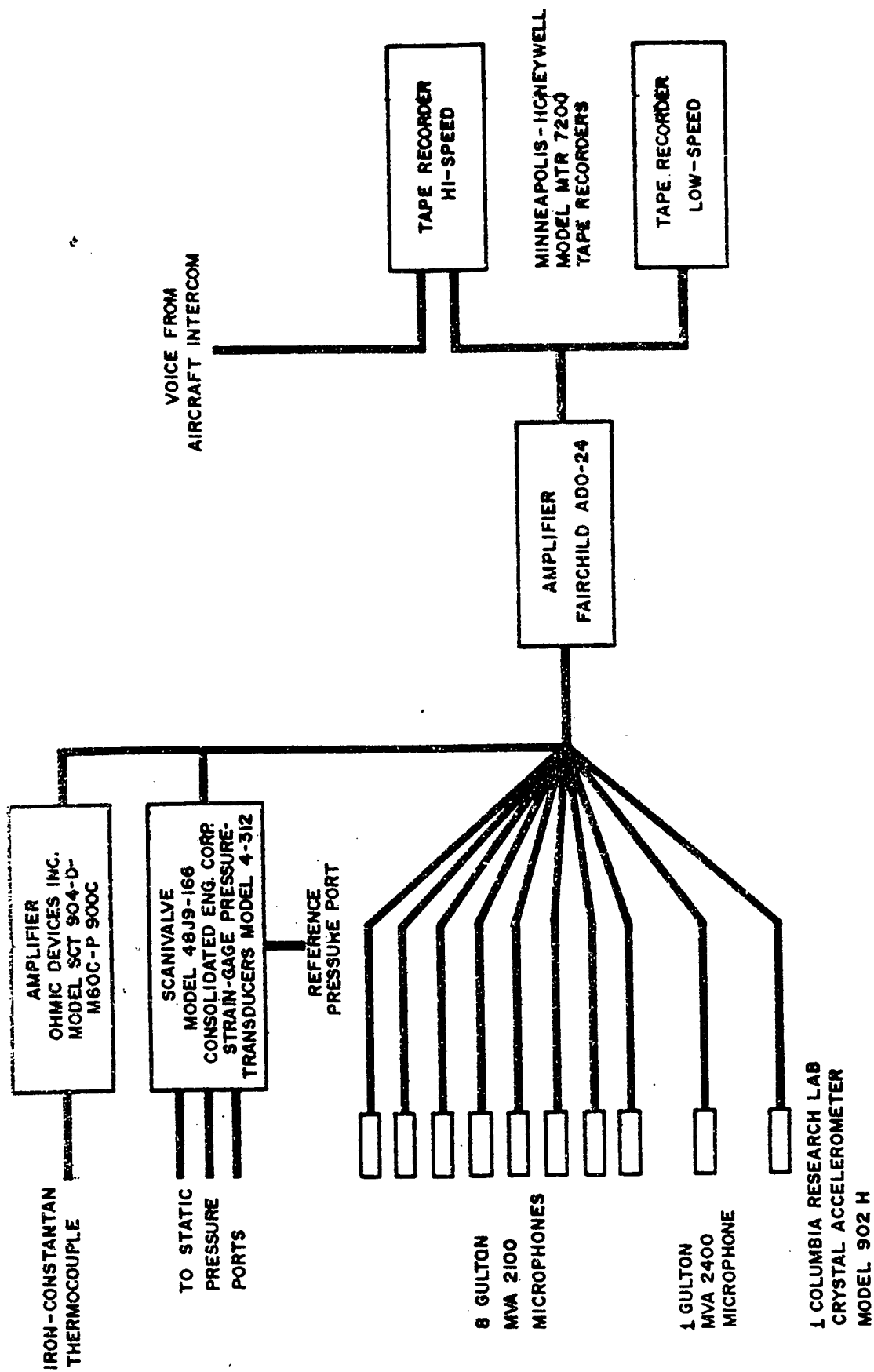


FIGURE 7, BLOCK DIAGRAM OF DATA ACQUISITION INSTRUMENTATION.

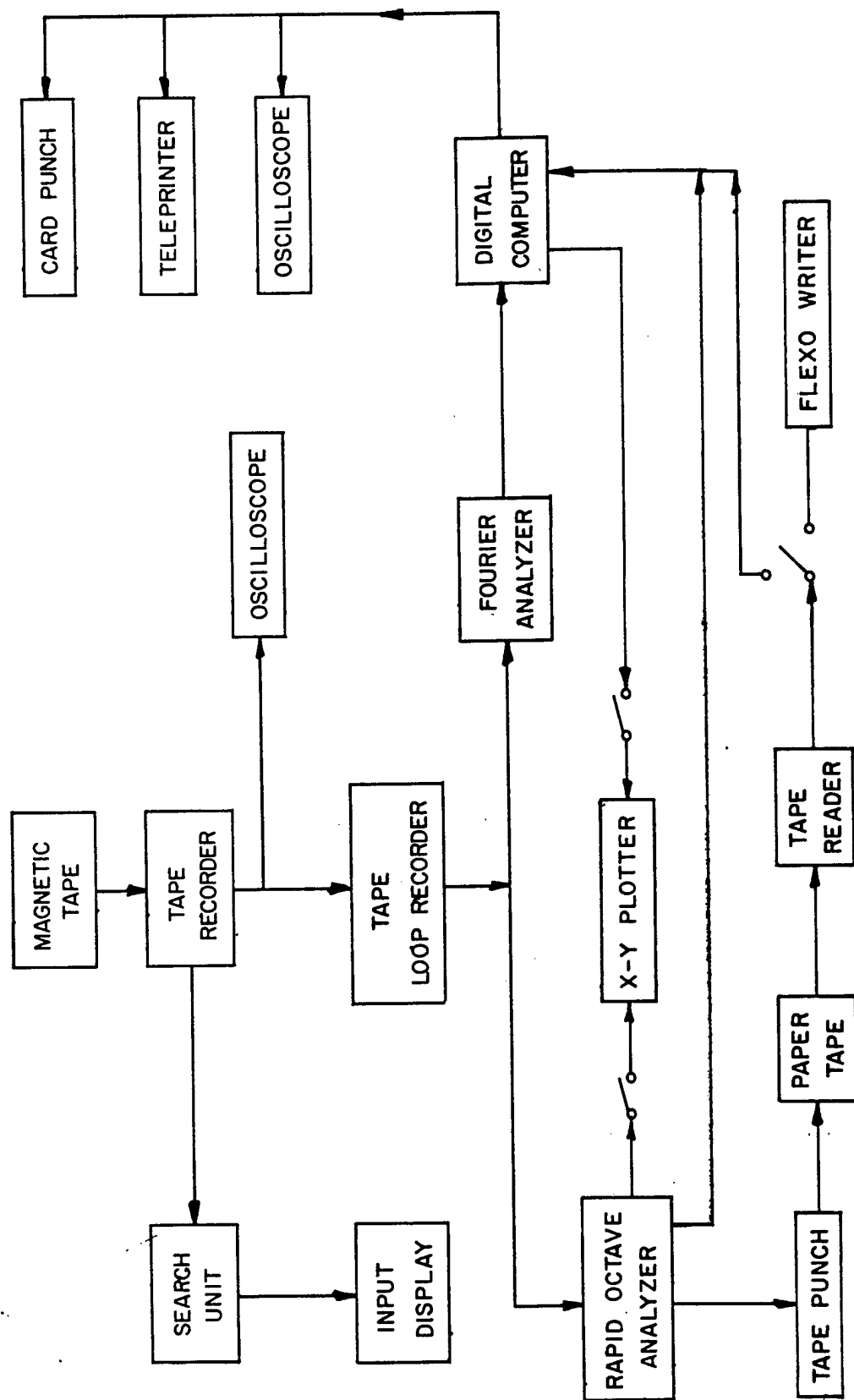
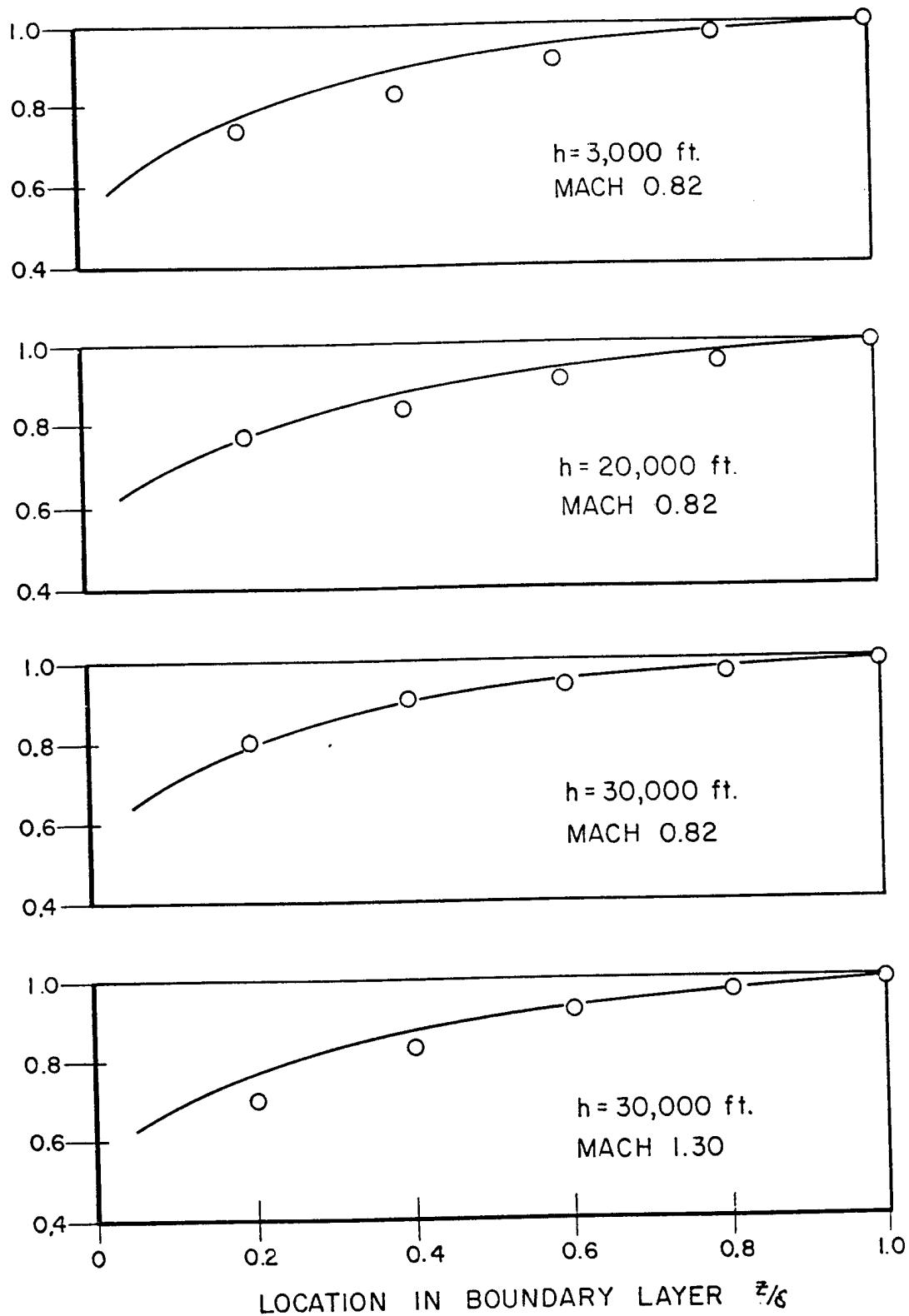


FIGURE 8, DATA REDUCTION SYSTEM

VELOCITY RATIO V/V_∞



— = 1/7 POWER LAW

○ = EXPERIMENTAL

FIGURE 9 BOUNDARY LAYER PROFILES FROM THE MODIFIED SUU-41 POD

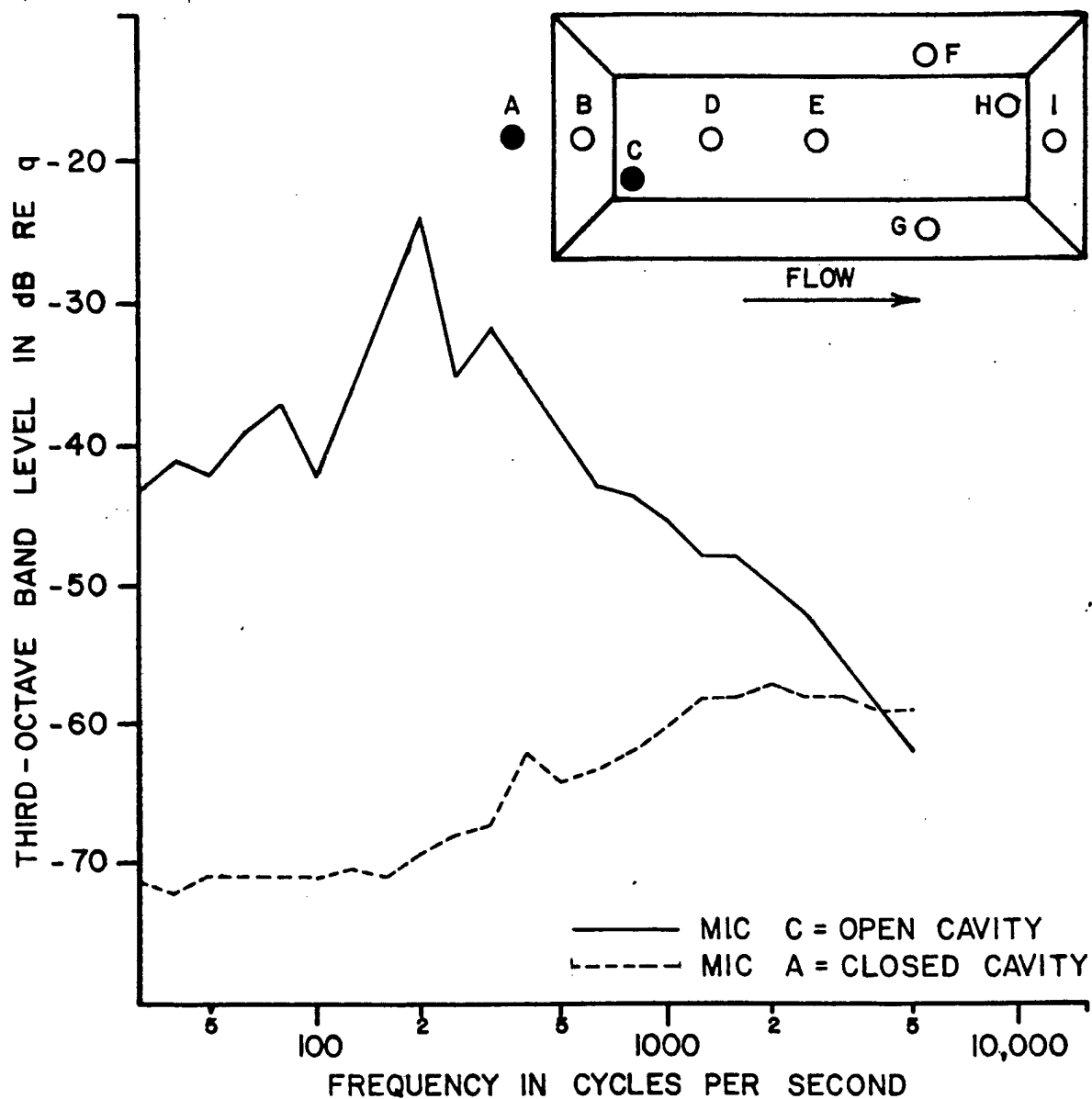


FIGURE 10 ONE-THIRD OCTAVE BAND SPECTRA FROM THE 10 INCH DEEP MODIFIED SUU-41 POD FOR 3,000 FOOT ALTITUDE AND MACH 0.82

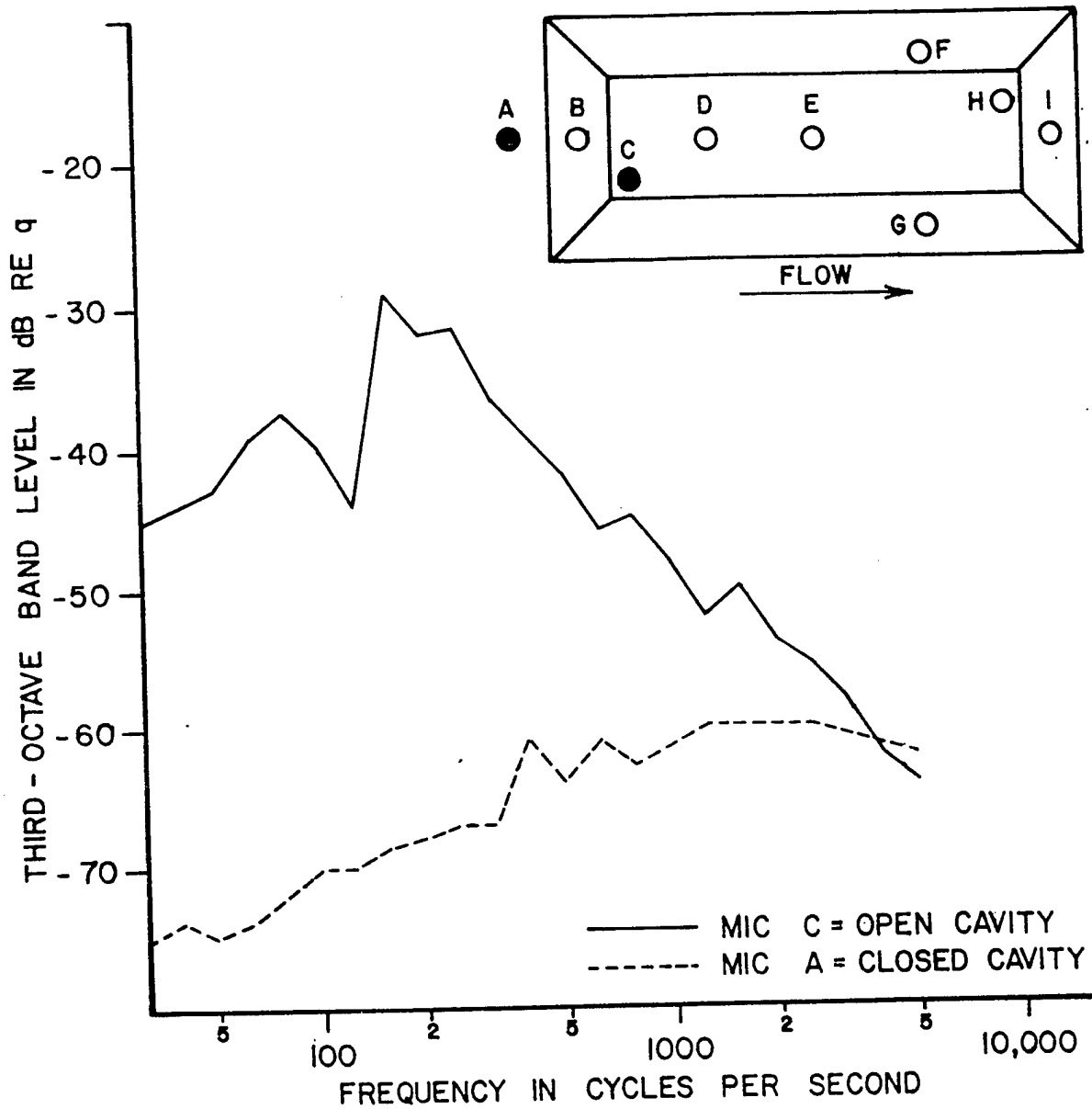


FIGURE 11 ONE-THIRD OCTAVE BAND SPECTRA FROM THE 10 INCH DEEP MODIFIED SUU-41 POD FOR 20,000 FOOT ALTITUDE AND MACH 0.82

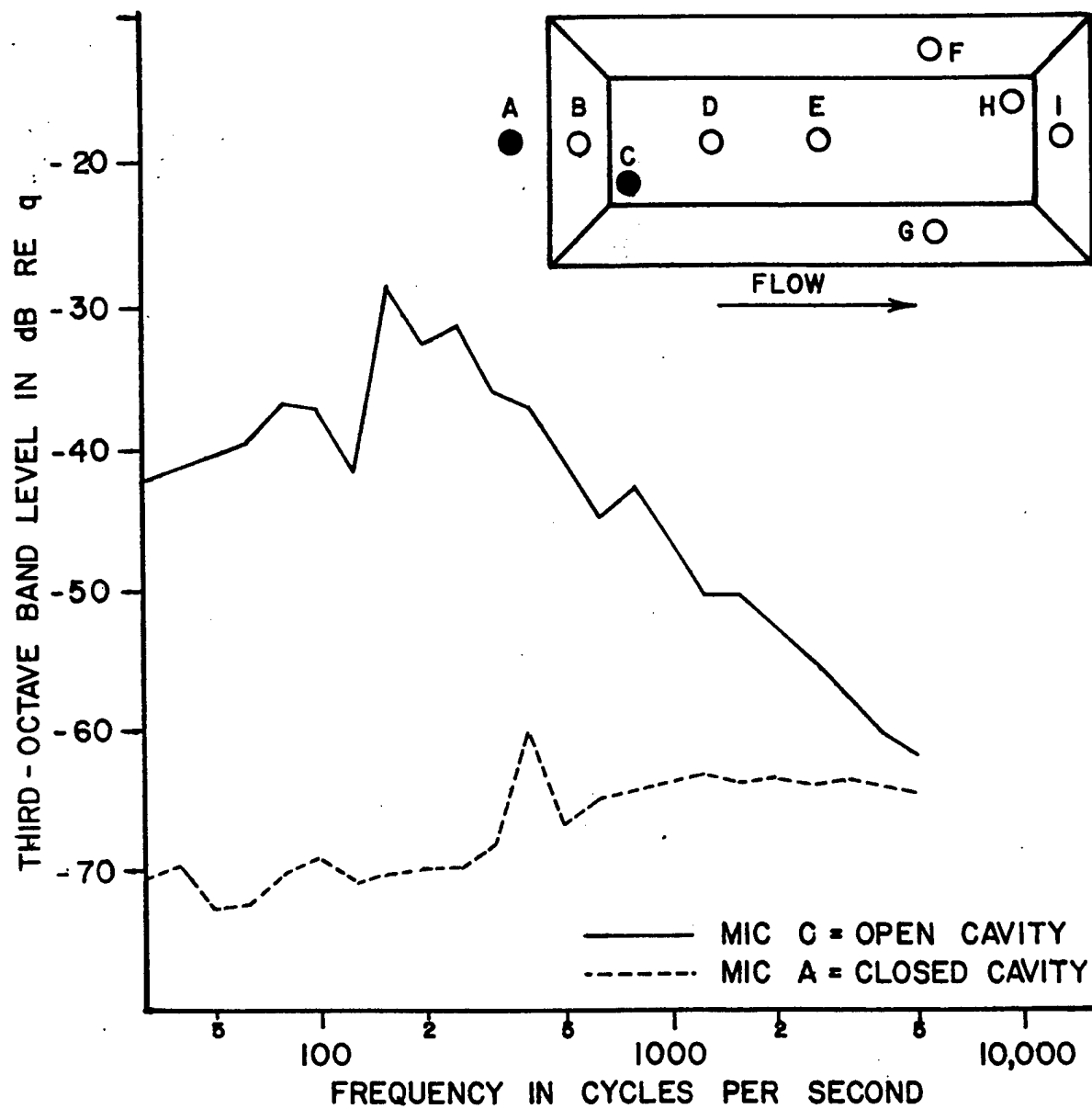


FIGURE 12 ONE-THIRD OCTAVE BAND SPECTRA FROM THE 10 INCH DEEP MODIFIED SUU-41 POD FOR 30,000 FOOT ALTITUDE AND MACH NUMBER 0.82

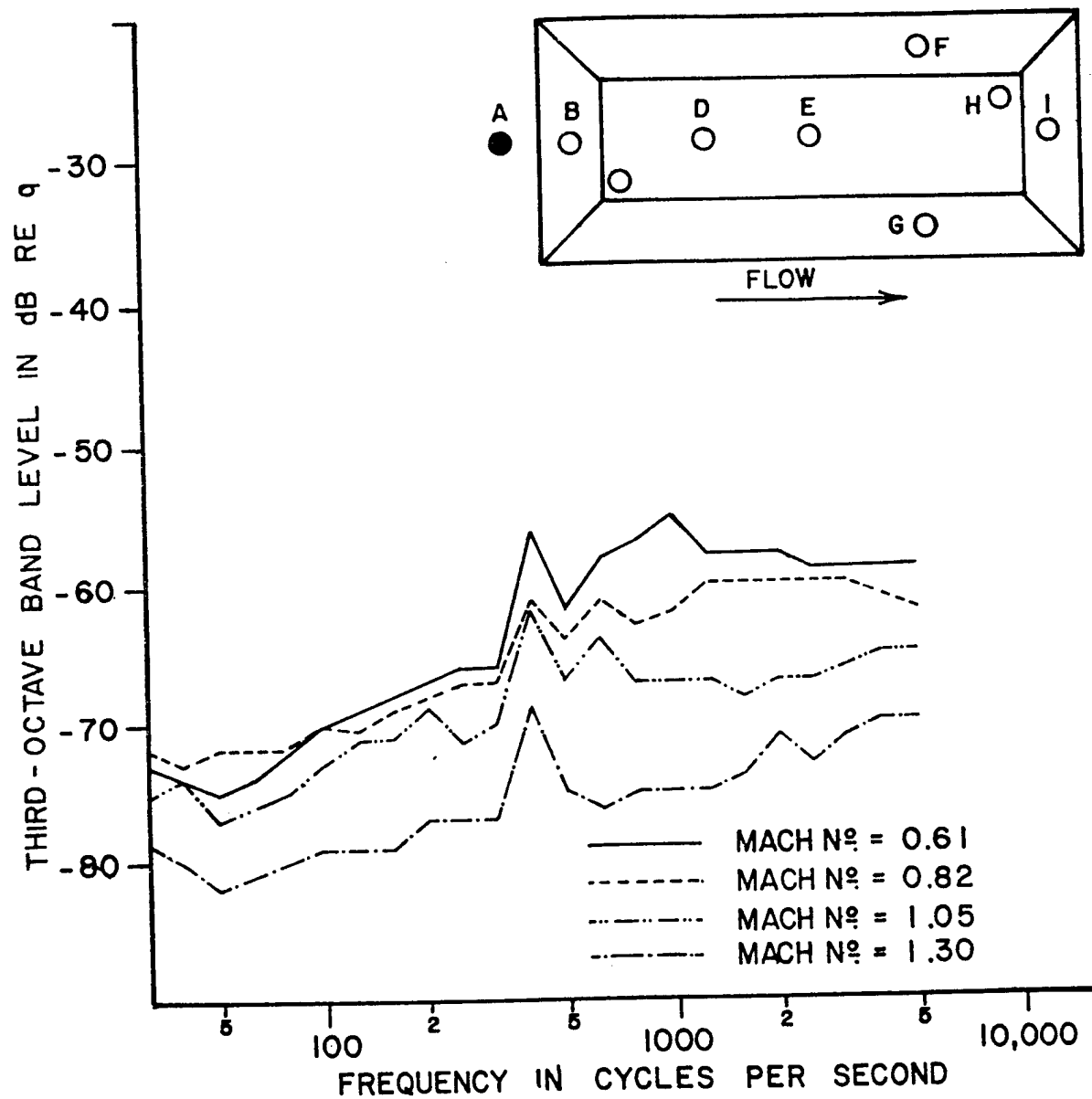


FIGURE 13 ONE-THIRD OCTAVE BAND SPECTRA FROM MICROPHONE A OF THE CLOSED CAVITY FOR 20,000 FOOT ALTITUDE

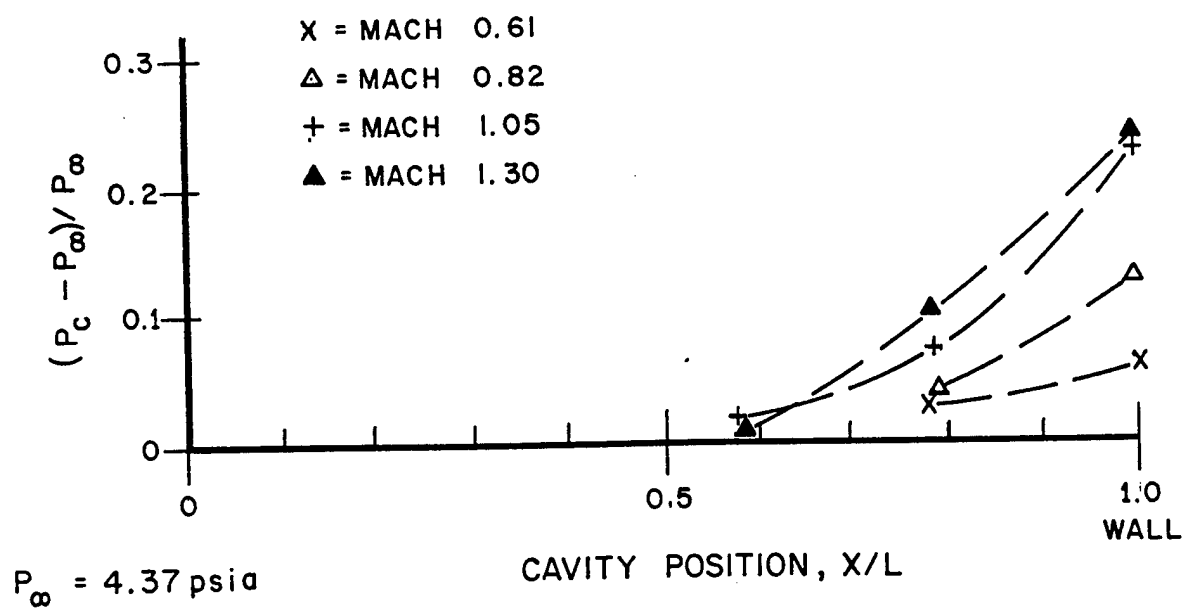


FIGURE 14 LONGITUDINAL VARIATION OF STATIC PRESSURE ALONG CAVITY FLOOR FOR THE MODIFIED SUU-41 POD

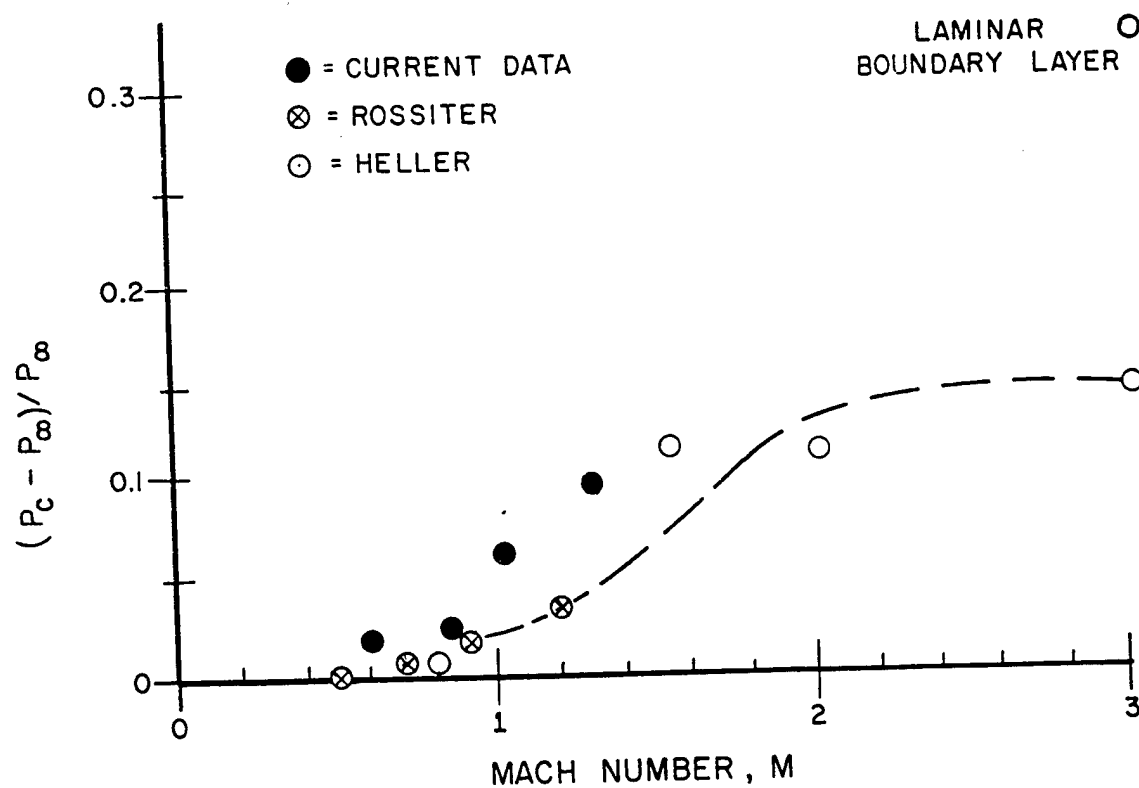


FIGURE 15 MACH NUMBER VARIATION OF THE NORMALIZED STATIC PRESSURE

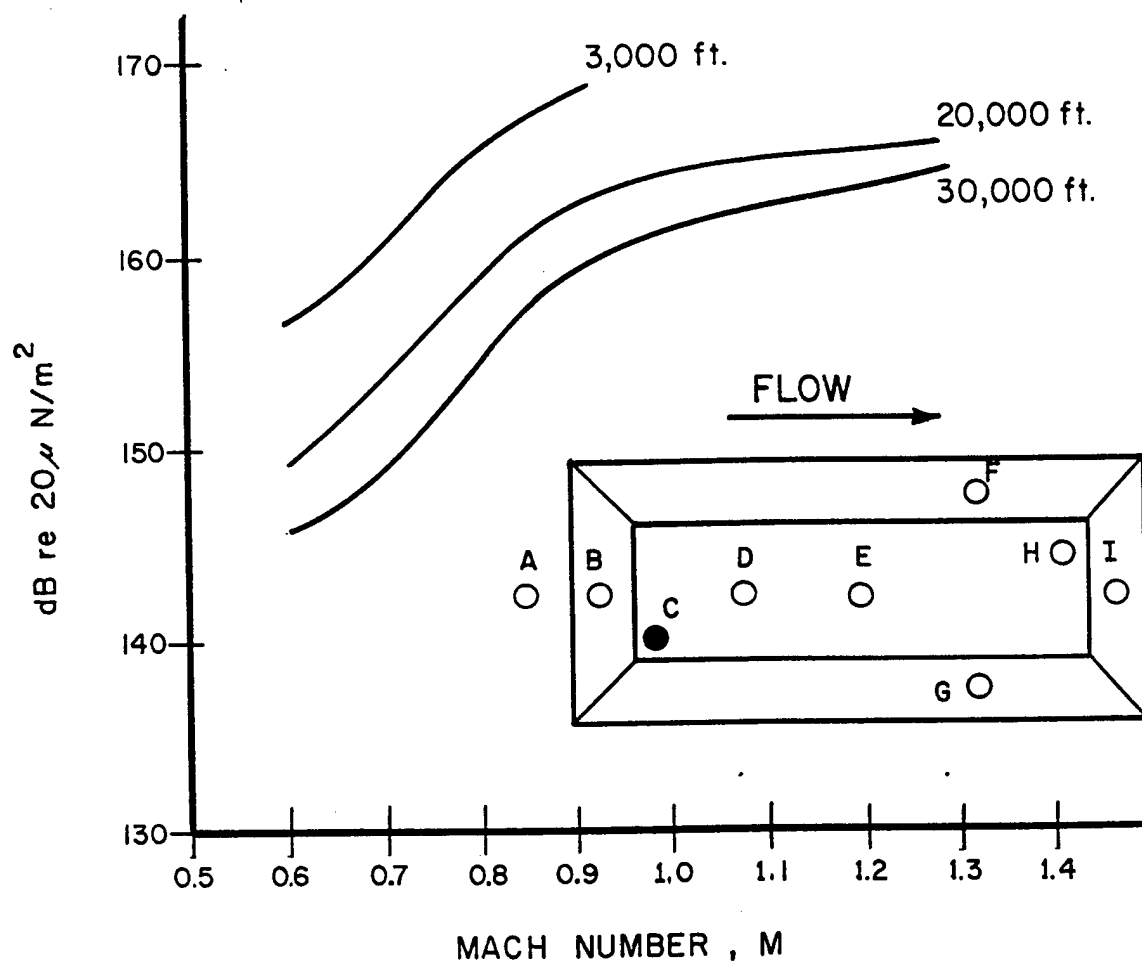


FIGURE 16 OVERALL FLUCTUATING PRESSURE TIME HISTORIES FROM MICROPHONE C FOR THE 10 INCH DEEP MODIFIED SUU-41 POD

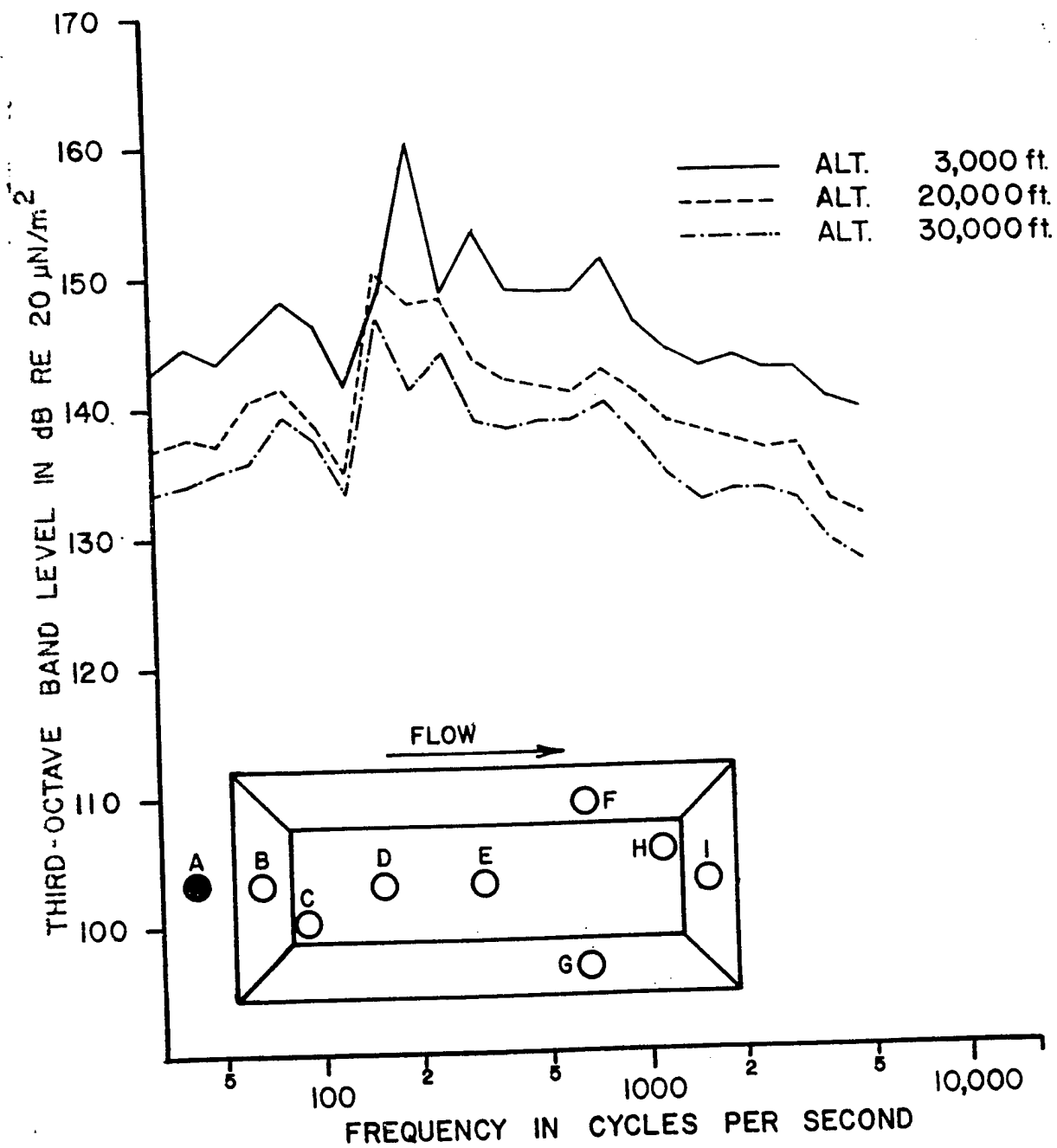


FIGURE 17 ONE-THIRD OCTAVE BAND SPECTRA FROM MICROPHONE A FOR A MACH NUMBER OF 0.82

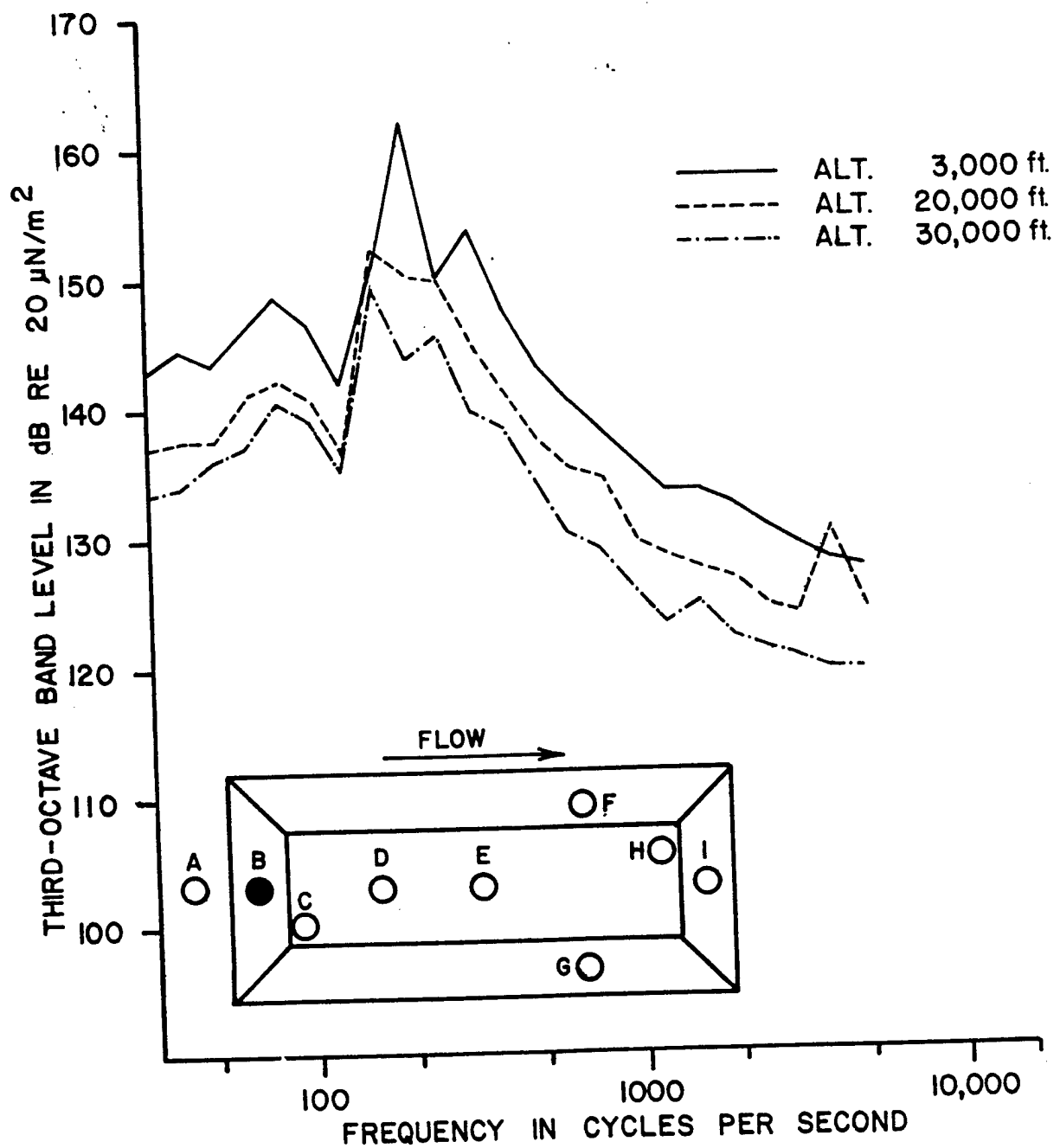


FIGURE 18 ONE-THIRD OCTAVE BAND SPECTRA FROM MICROPHONE B FOR A MACH NUMBER OF 0.82

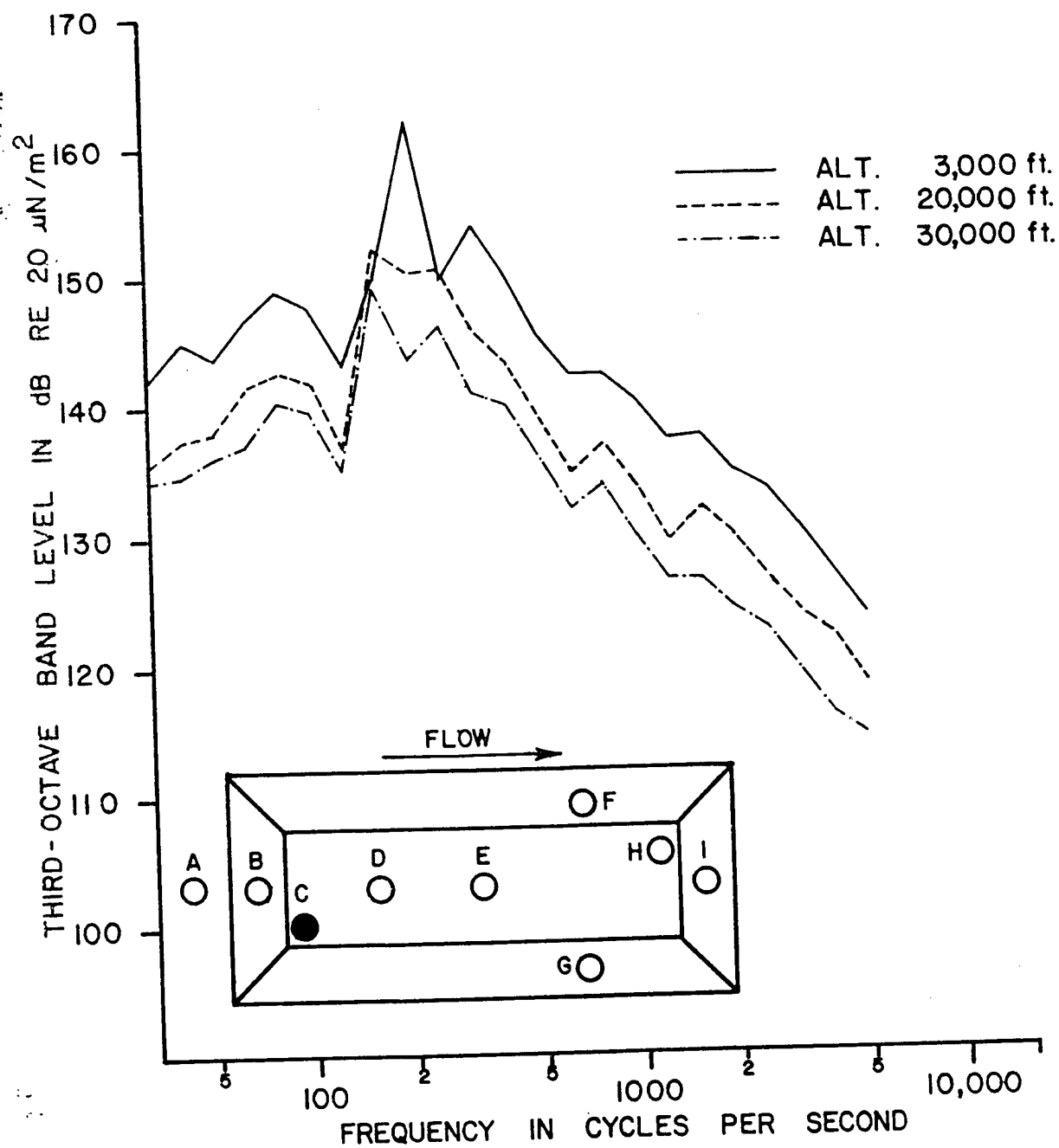


FIGURE 19 ONE-THIRD OCTAVE BAND SPECTRA FROM MICROPHONE C FOR A MACH NUMBER OF 0.82

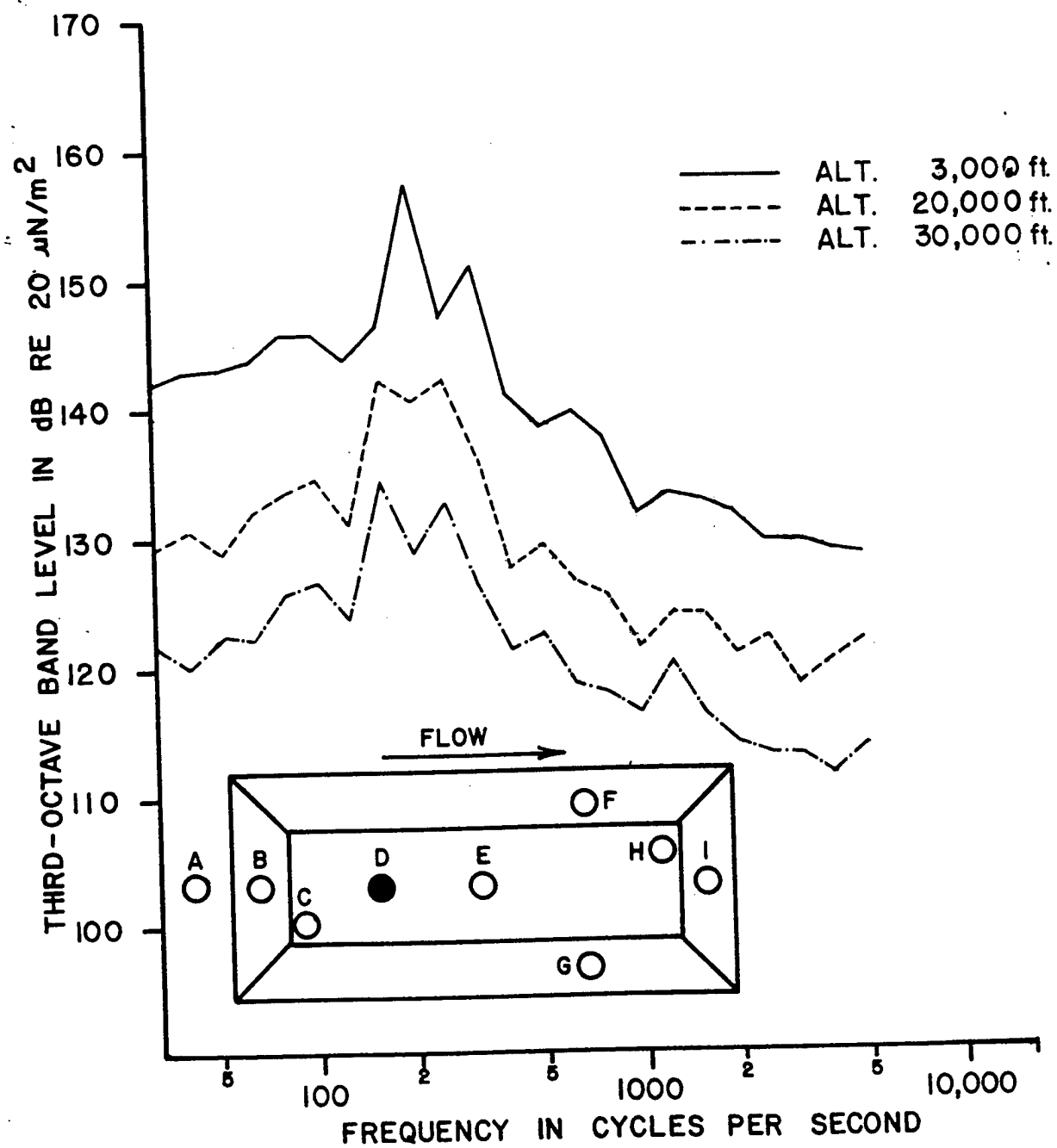


FIGURE 20 ONE-THIRD OCTAVE BAND SPECTRA FROM MICROPHONE D FOR A MACH NUMBER OF 0.82

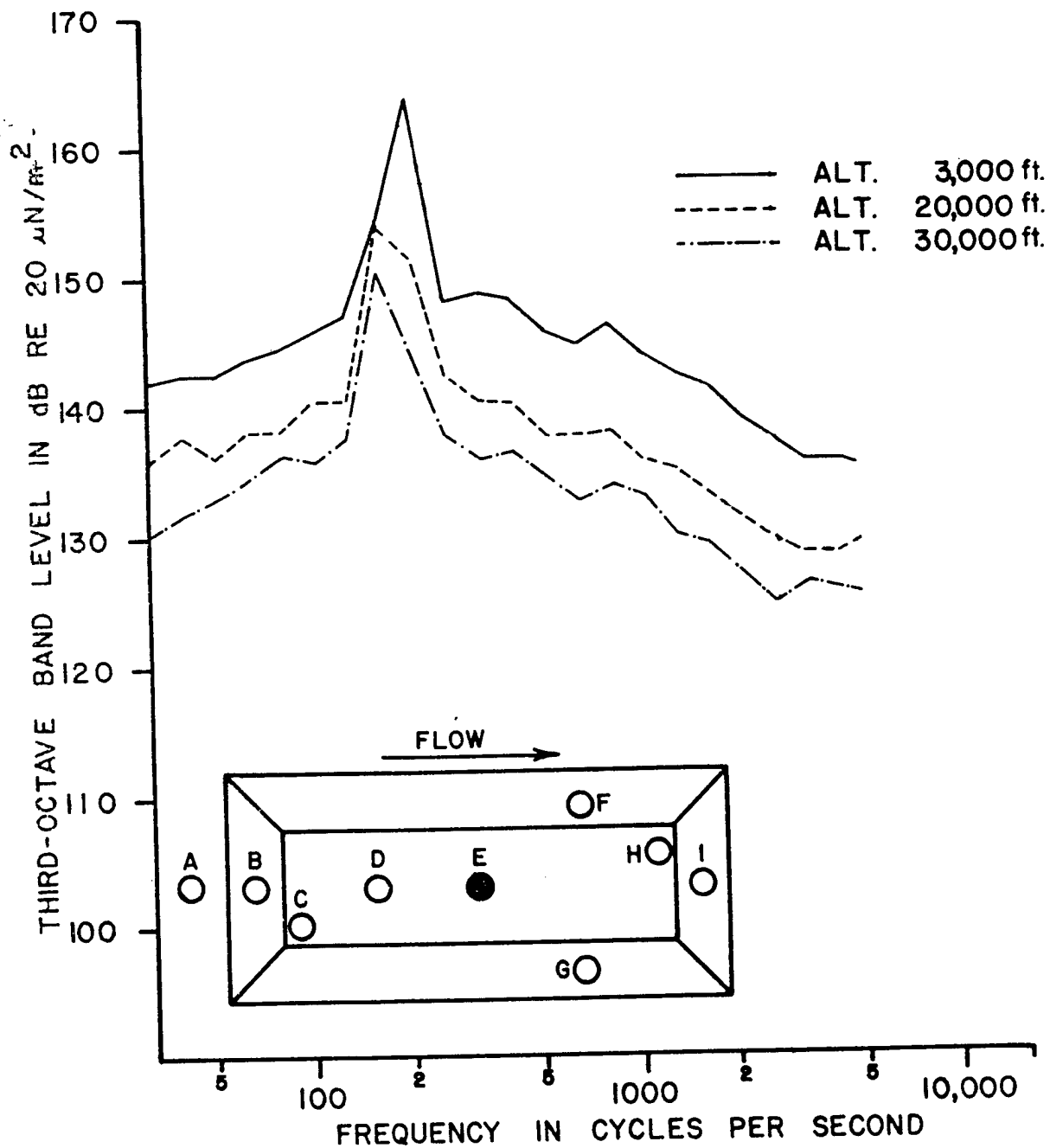


FIGURE 21 ONE-THIRD OCTAVE BAND SPECTRA FROM MICROPHONE E FOR A MACH NUMBER OF 0.82

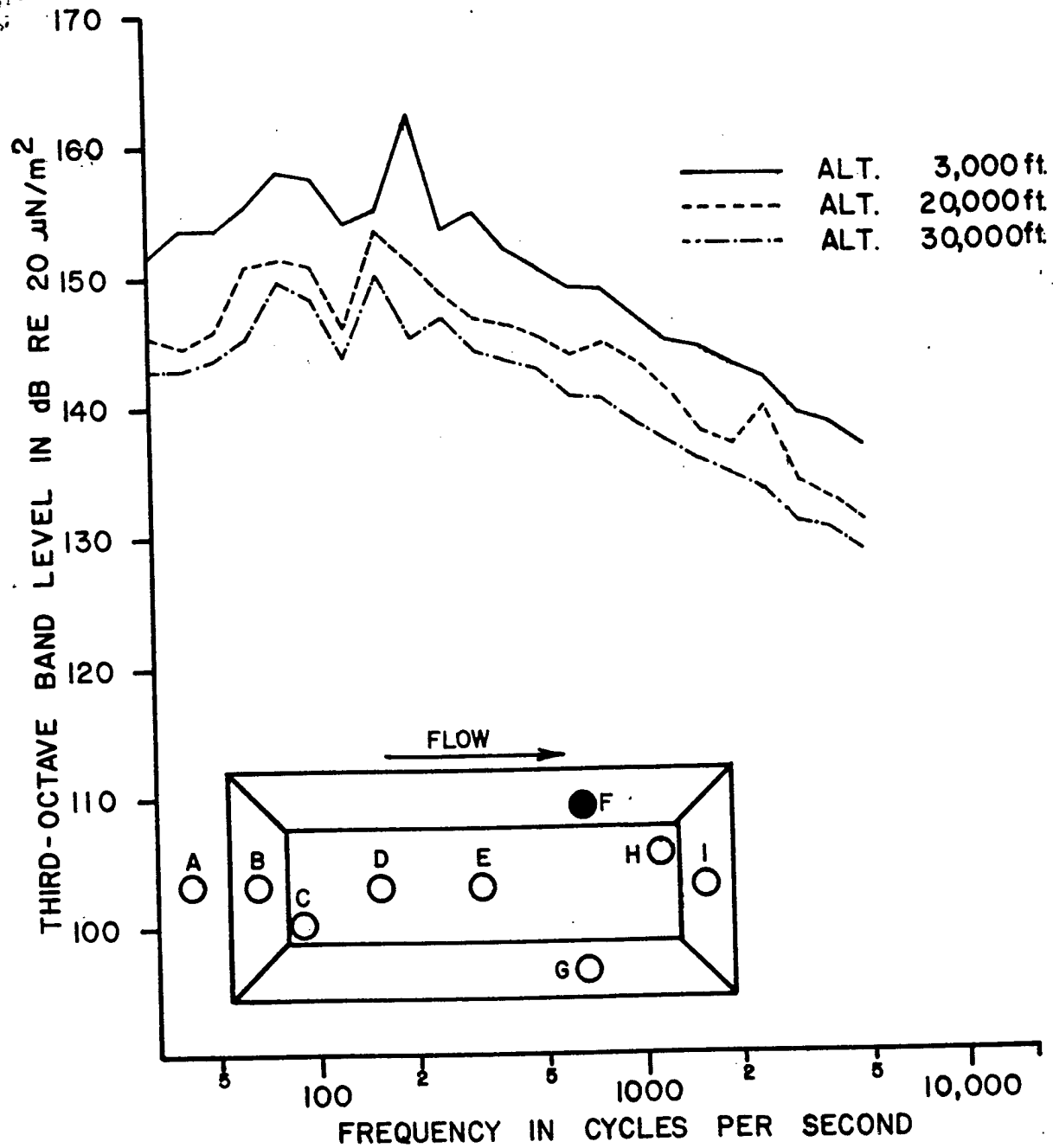


FIGURE 22 ONE-THIRD OCTAVE BAND SPECTRA FROM MICROPHONE F FOR A MACH NUMBER OF 0.82

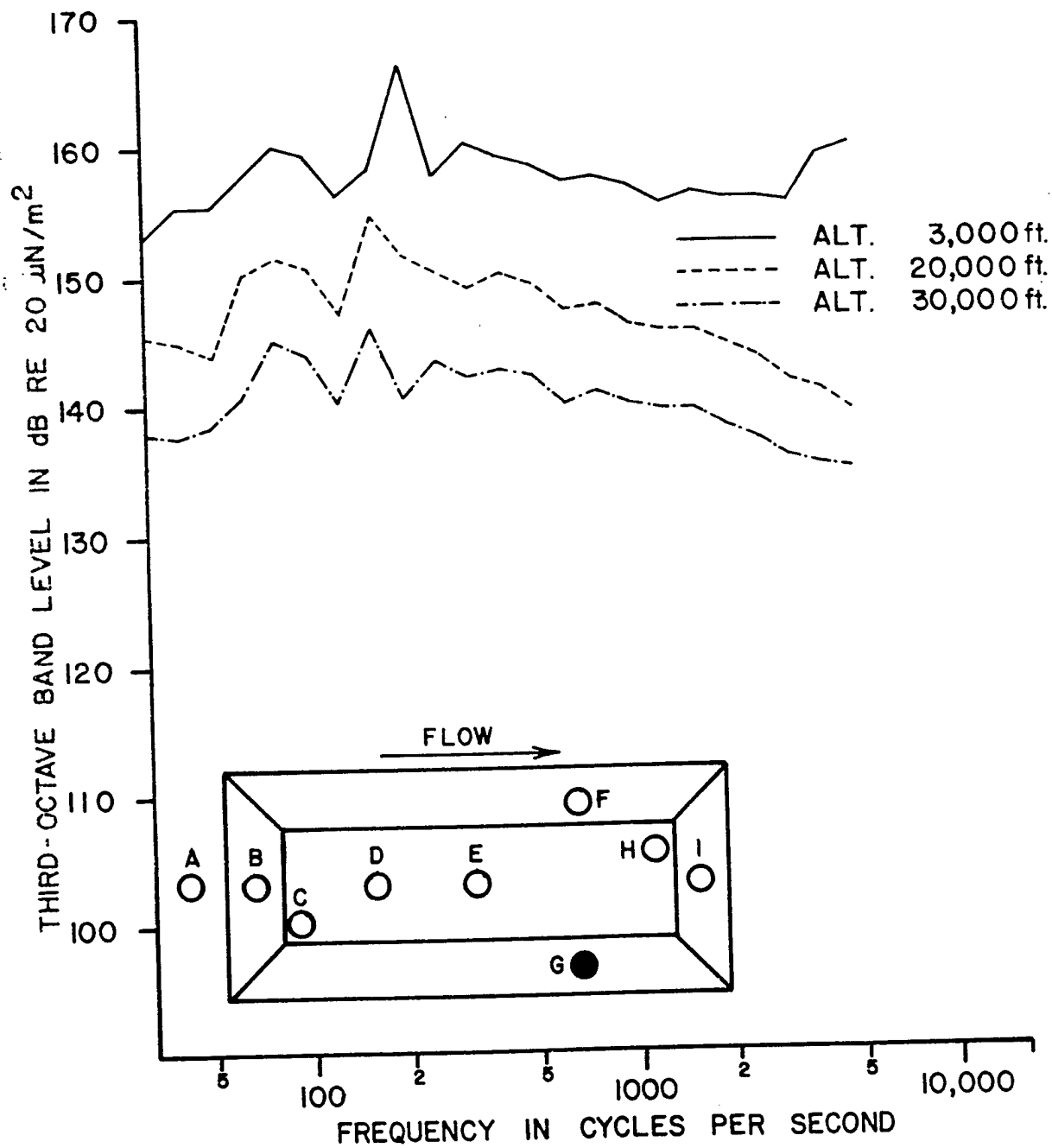


FIGURE 23 ONE-THIRD OCTAVE BAND SPECTRA FROM MICROPHONE G FOR A MACH NUMBER OF 0.82

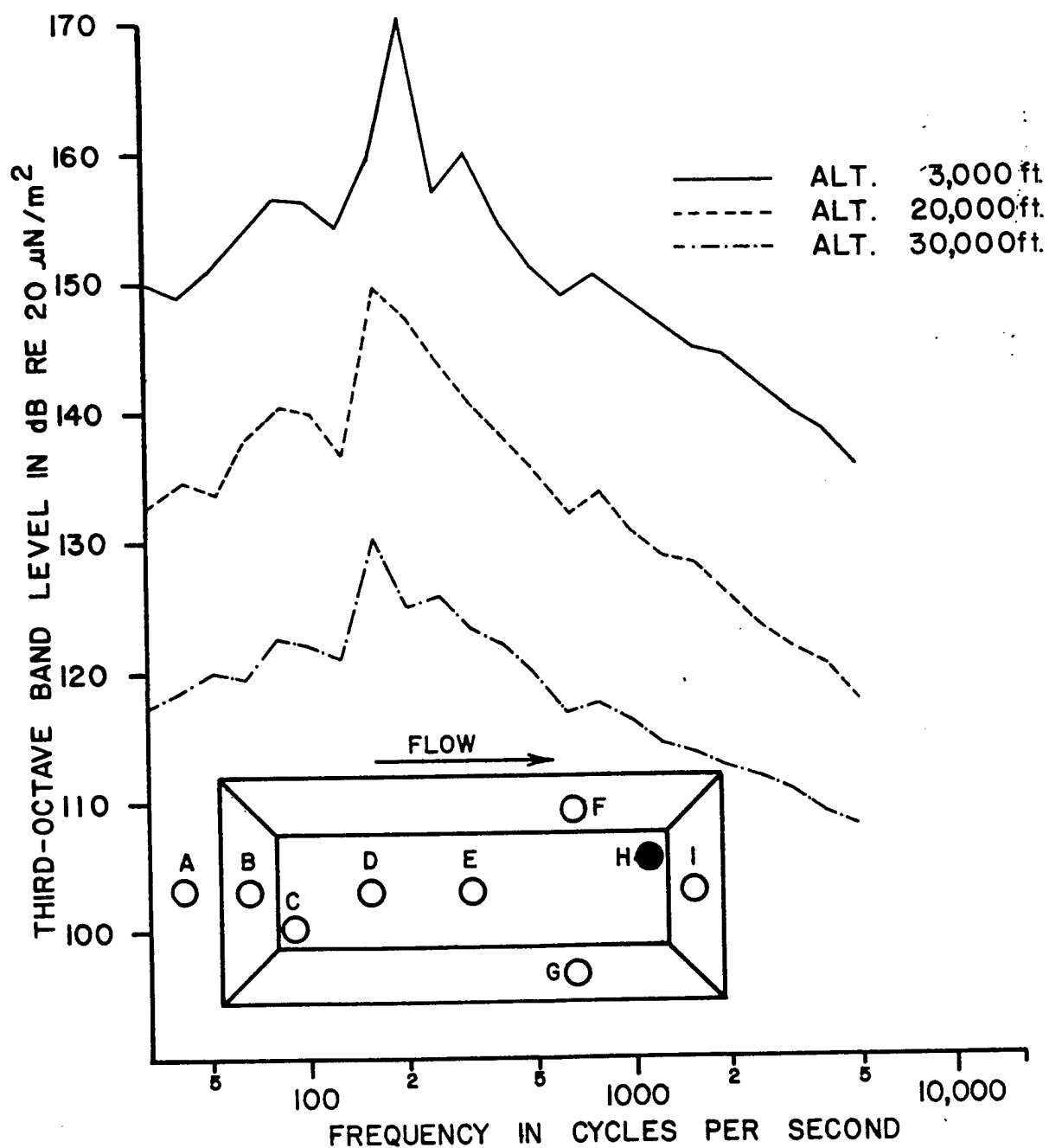


FIGURE 24 ONE-THIRD OCTAVE BAND SPECTRA FROM MICROPHONE H FOR A MACH NUMBER OF 0.82

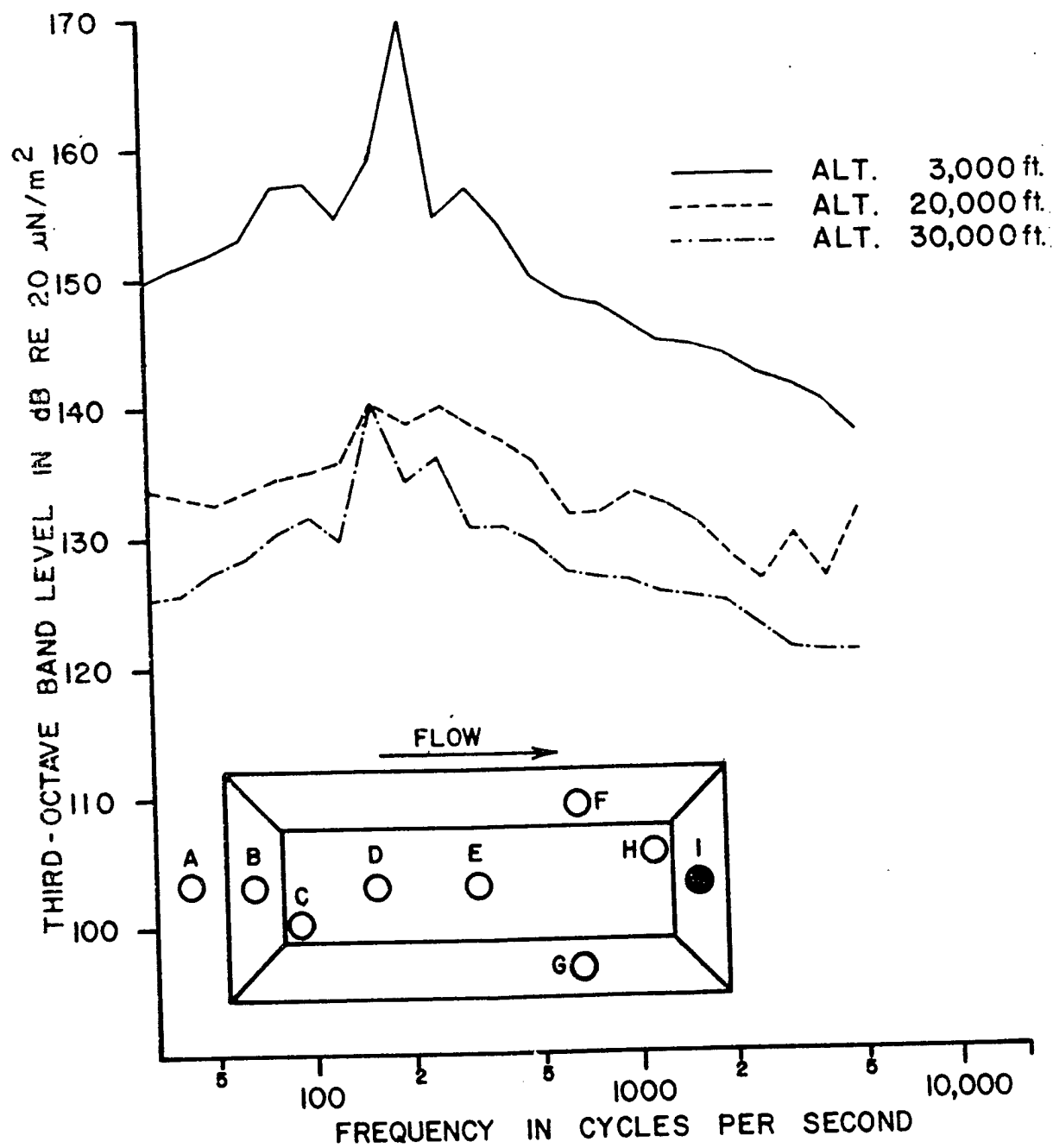


FIGURE 25 ONE-THIRD OCTAVE BAND SPECTRA FROM MICROPHONE I FOR A MACH NUMBER OF 0.82

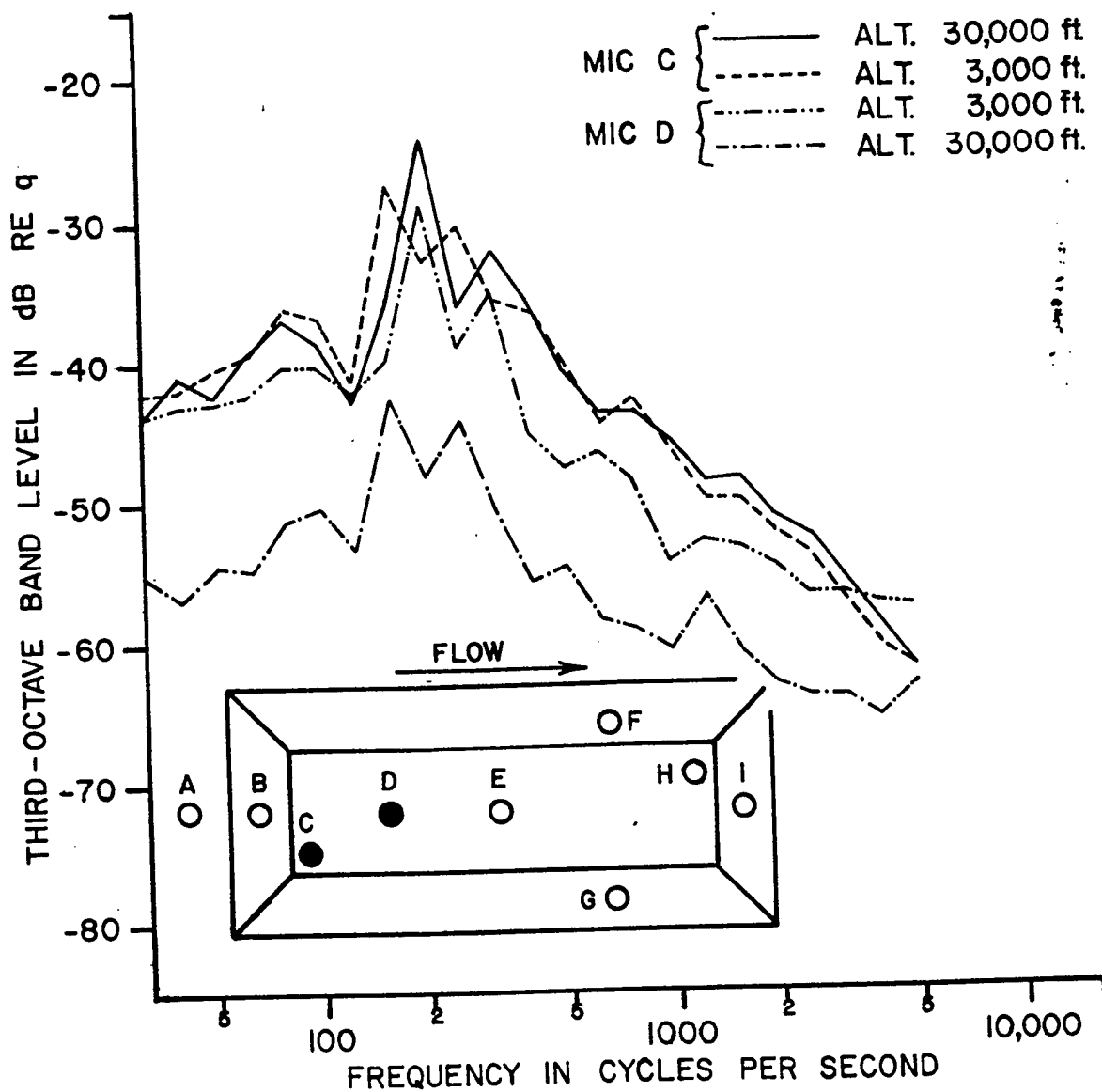


FIGURE 26 ONE-THIRD OCTAVE BAND SPECTRA FOR MACH NUMBER 0.82 DEPICTING FAILURE OF DYNAMIC PRESSURE SCALING

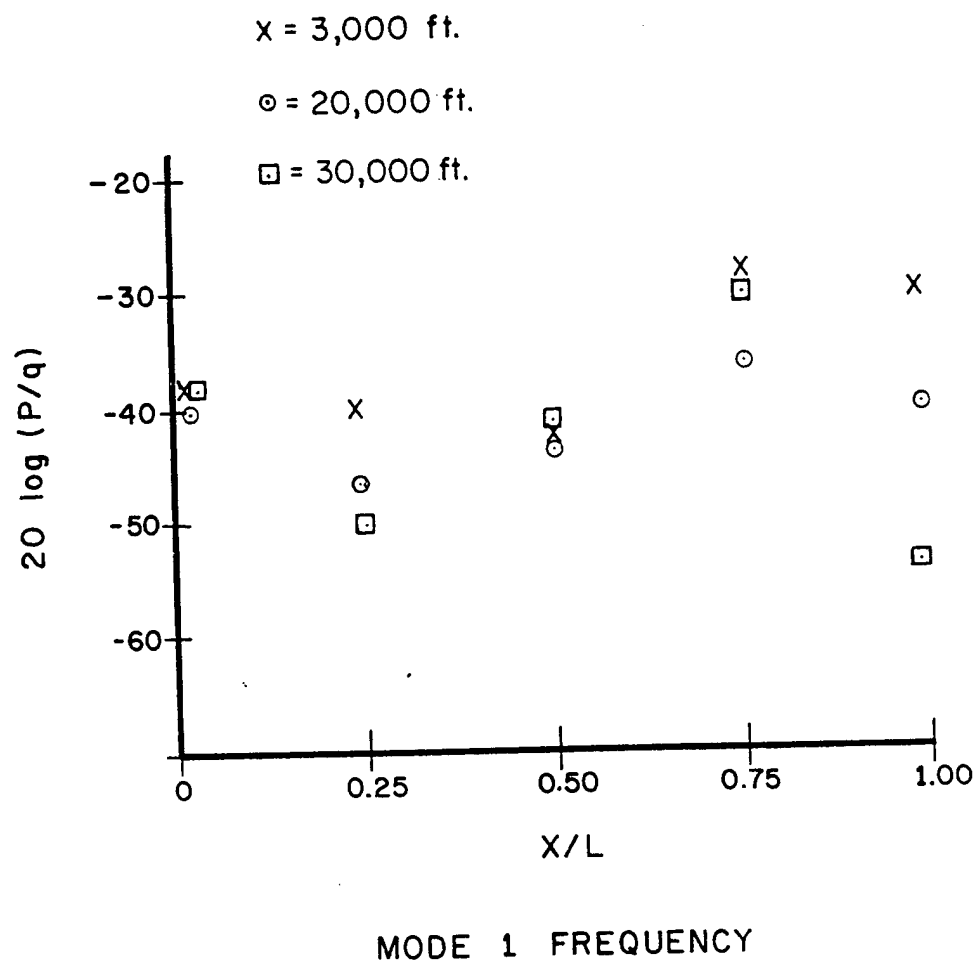


FIGURE 27 LONGITUDINAL VARIATION OF PEAK ONE-THIRD OCTAVE BAND REFERENCED TO FREE-STREAM DYNAMIC PRESSURE DICTATING MODE SHAPES FOR MACH NUMBER 0.82

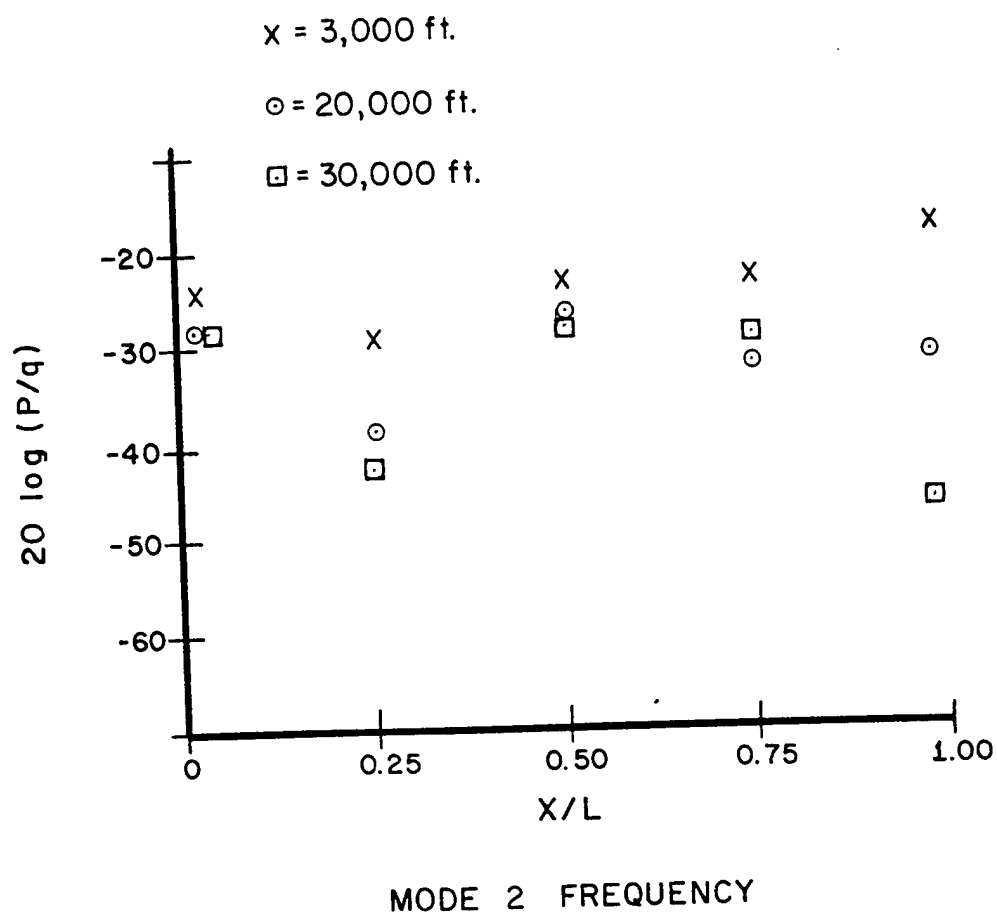


FIGURE 28 LONGITUDINAL VARIATION OF PEAK ONE-THIRD OCTAVE BAND REFERENCED
 TO FREE-STREAM DYNAMIC PRESSURE DEPICTING MODE SHAPES FOR MACH
 NUMBER 0.82

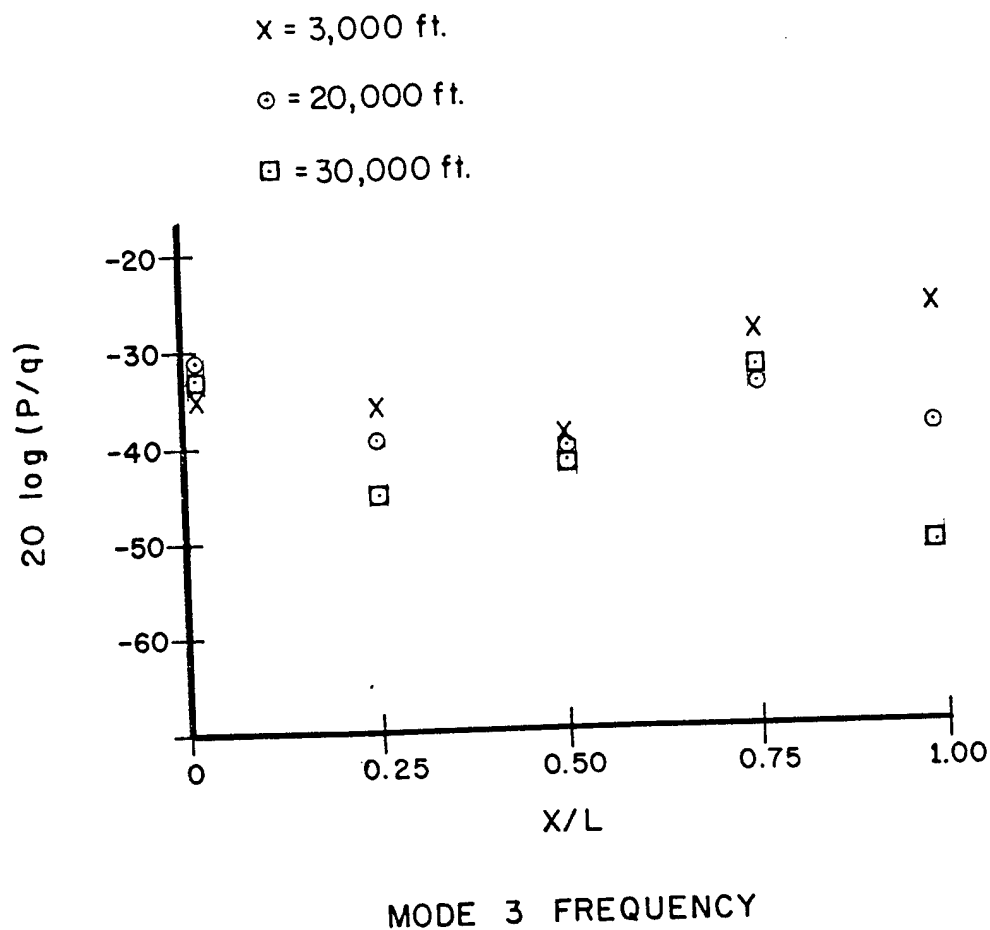


FIGURE 29 LONGITUDINAL VARIATION OF PEAK ONE-THIRD OCTAVE BAND REFERENCED TO FREE-STREAM DYNAMIC PRESSURE DEPICTING MODE SHAPES FOR MACH NUMBER 0.82

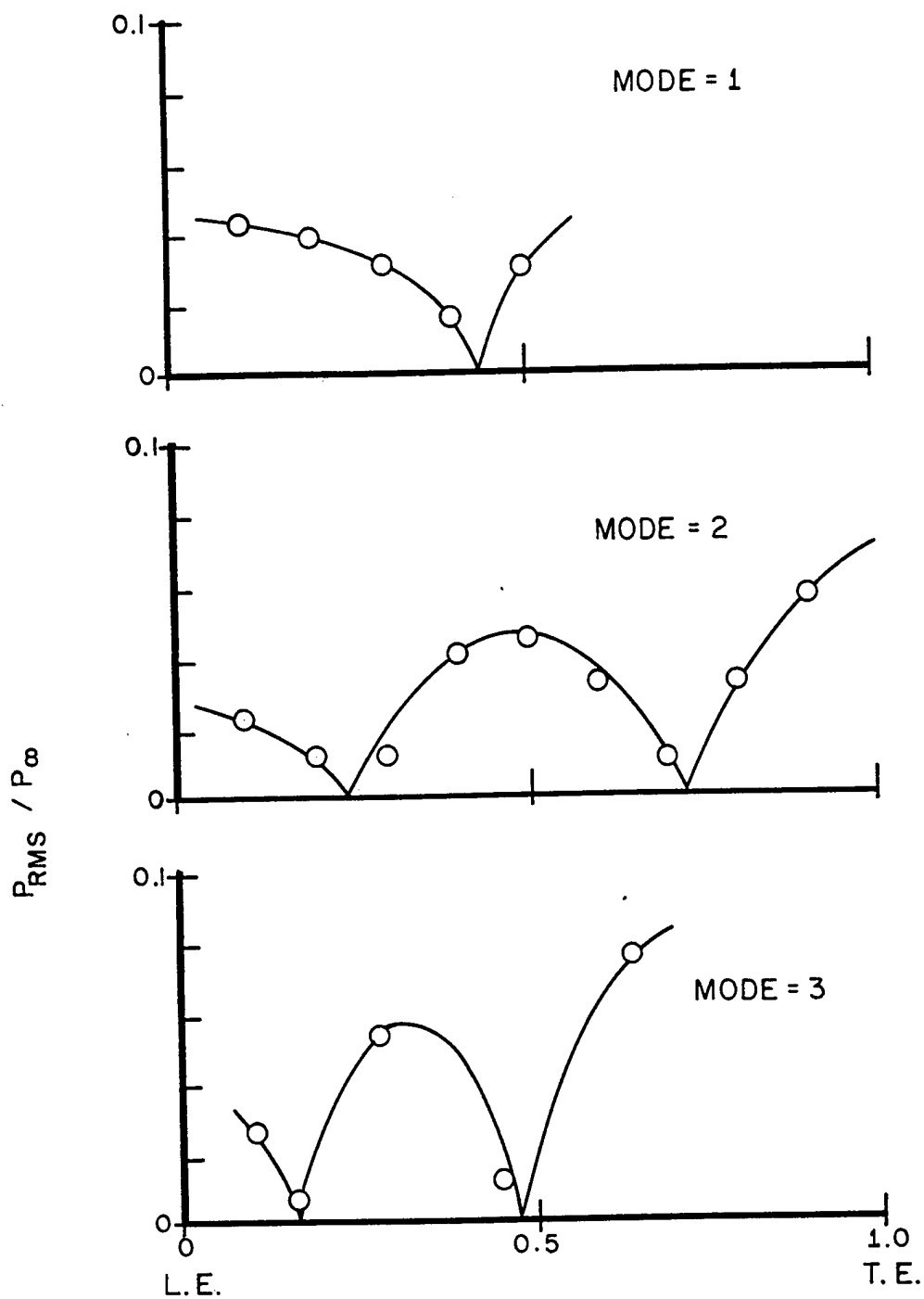


FIGURE 30 SUGGESTED SHAPE FOR FIRST, SECOND AND THIRD ORDER MODES FROM REFERENCE 2

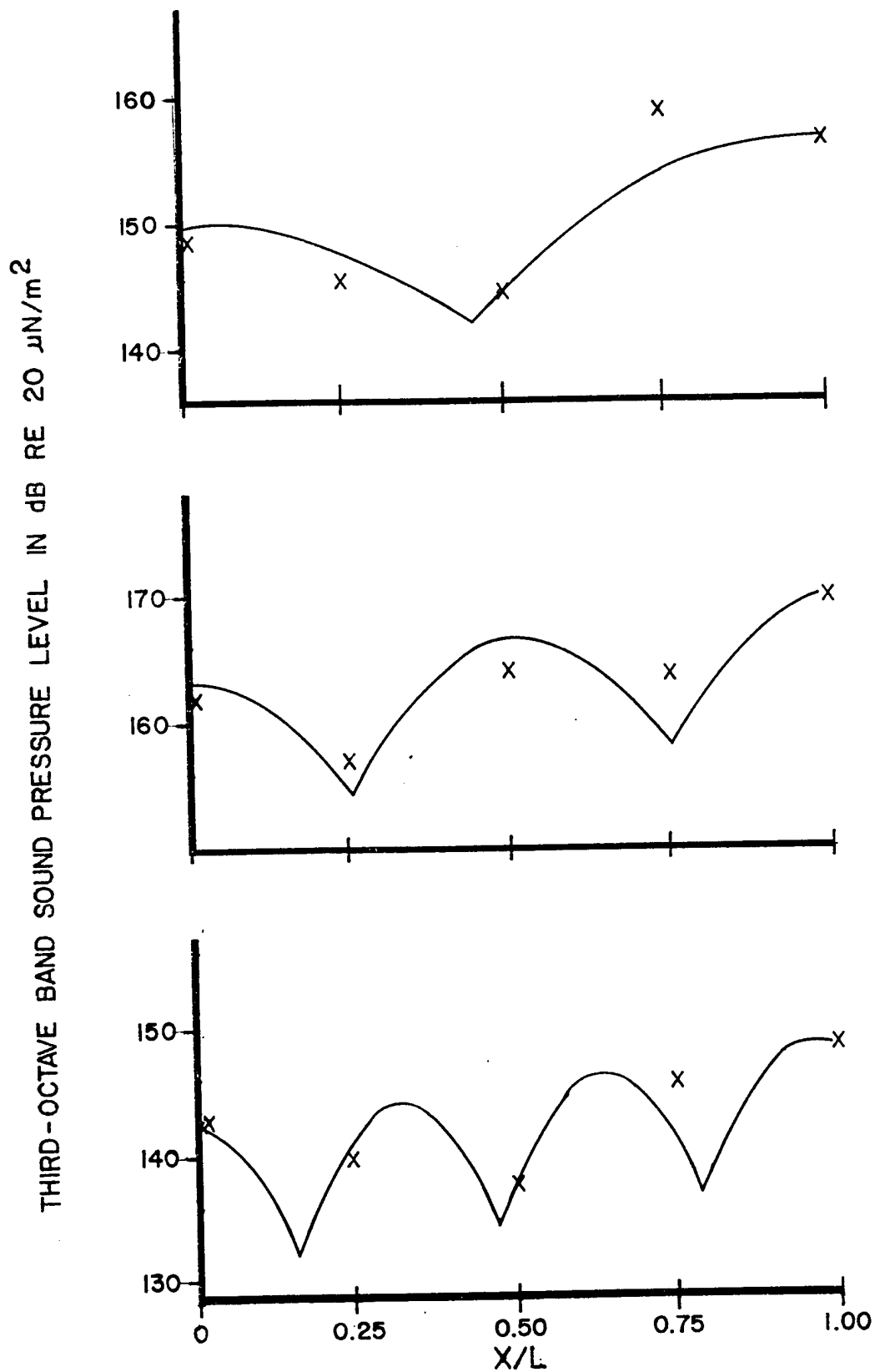


FIGURE 31 LONGITUDINAL VARIATION OF PEAK ONE-THIRD OCTAVE BAND DEPICTING MODE SHAPES FOR AN ALTITUDE OF 3,000 FEET AND MACH NUMBER 0.82

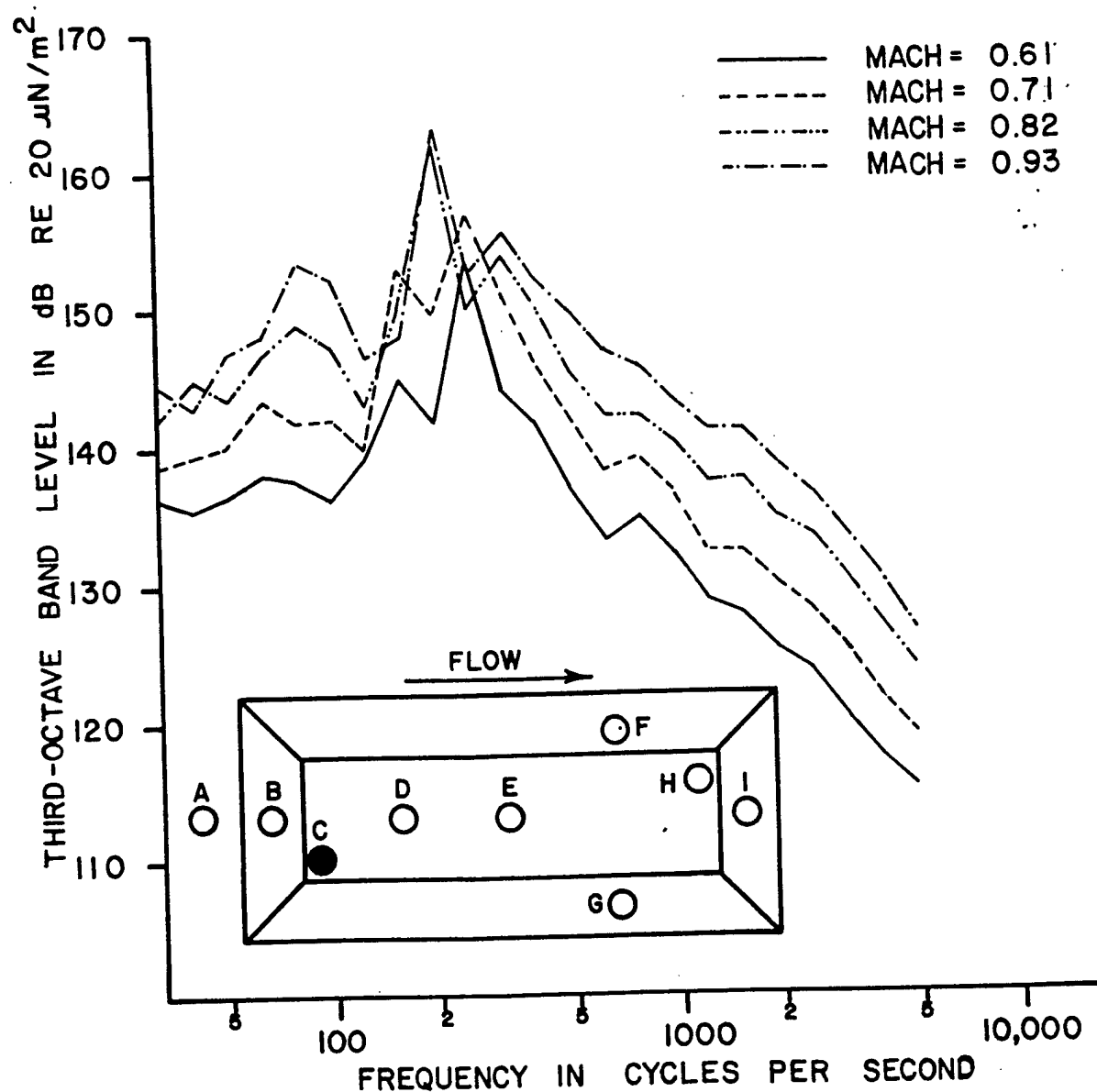


FIGURE 32 ONE-THIRD OCTAVE BAND SPECTRA FROM MICROPHONE C FOR AN ALTITUDE OF 3,000 FT

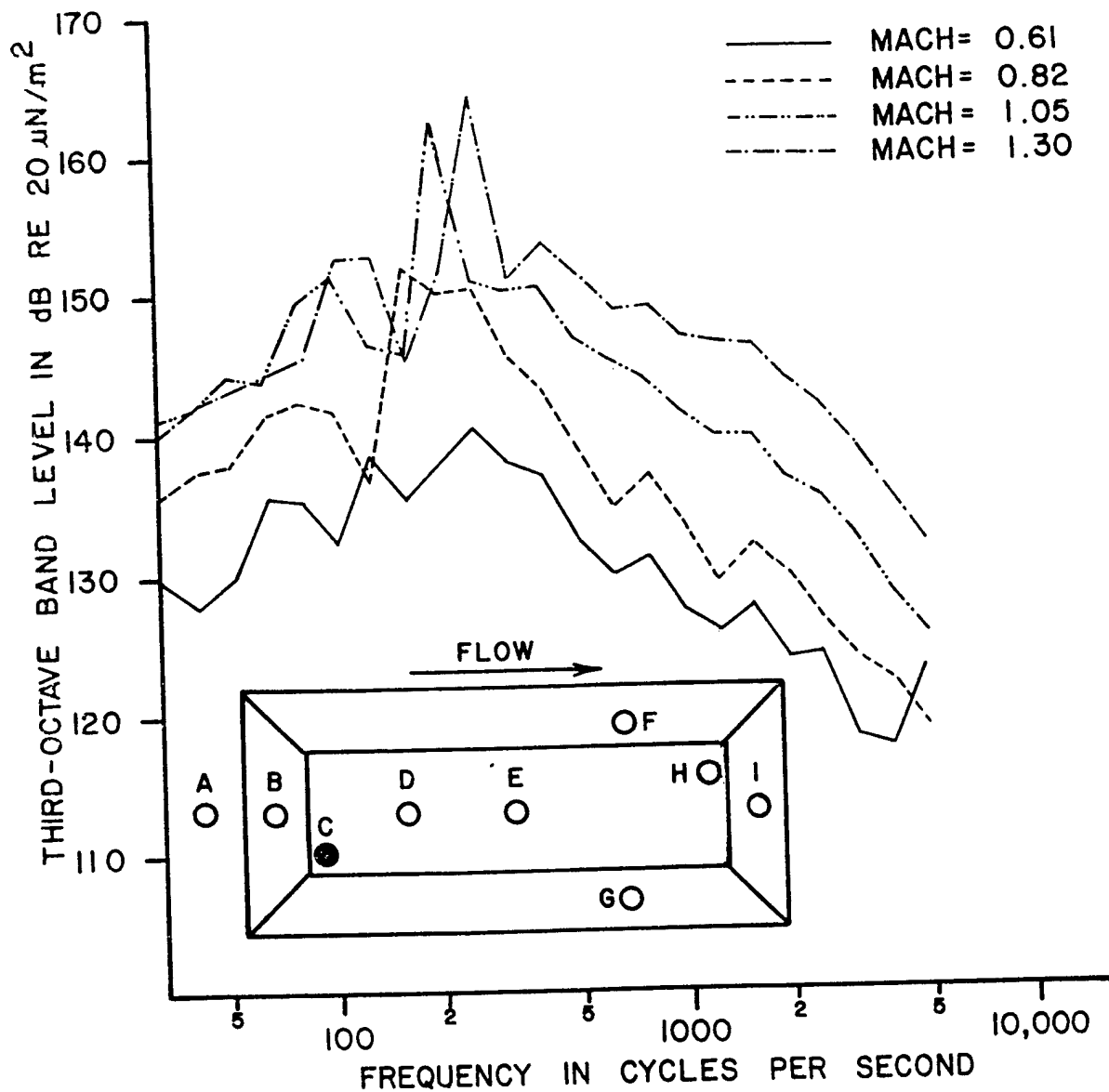


FIGURE 33 ONE-THIRD OCTAVE BAND SPECTRA FROM MICROPHONE C FOR AN ALTITUDE OF 20,000 FT

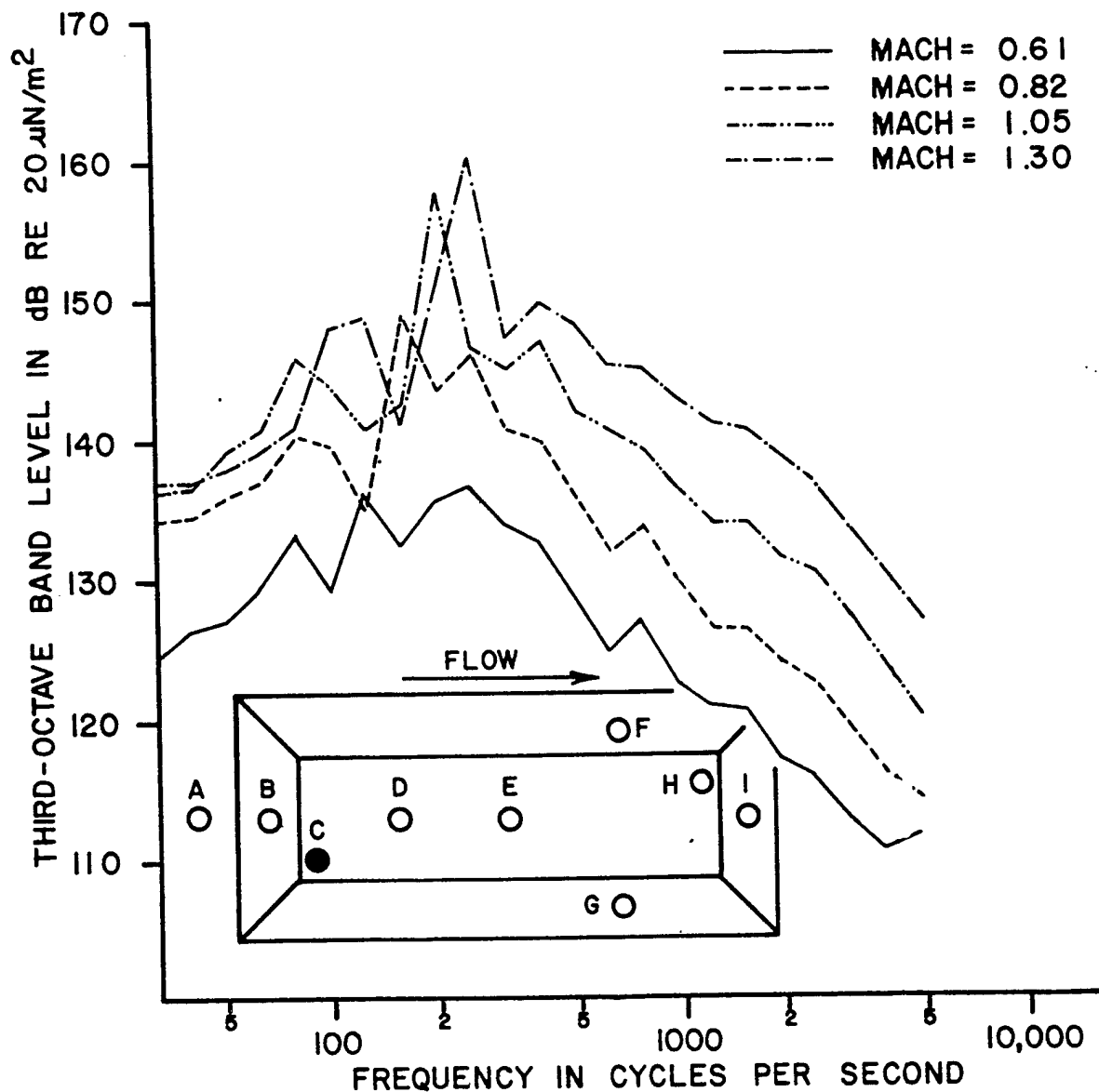


FIGURE 34 ONE-THIRD OCTAVE BAND SPECTRA FROM MICROPHONE C FOR AN ALTITUDE OF 30,000 FT

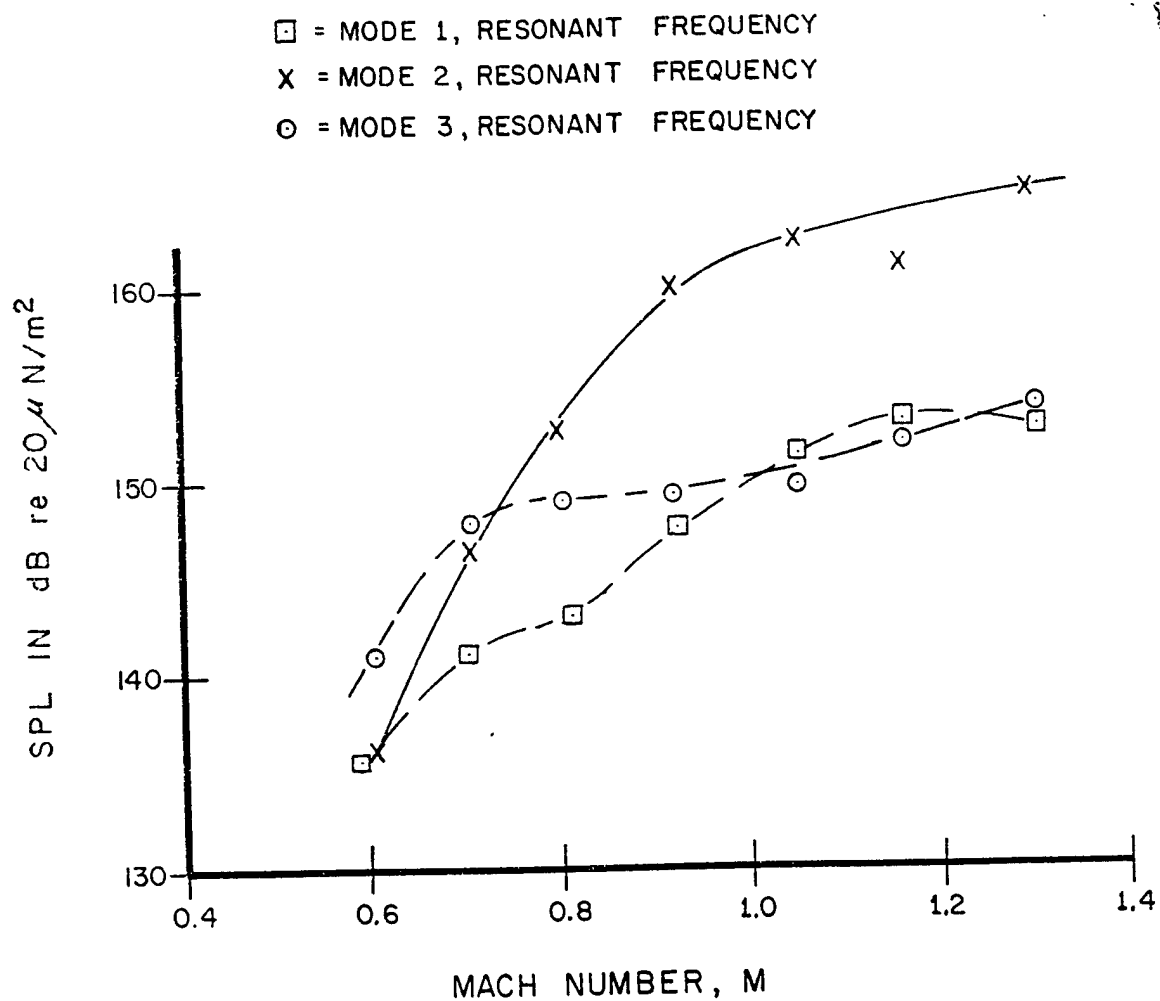


FIGURE 35 ONE-THIRD OCTAVE BAND PEAKS FROM MICROPHONE C FOR THE 10 INCH
 DEEP MODIFIED SUU-41 POD AT 20,000 FOOT ALTITUDE

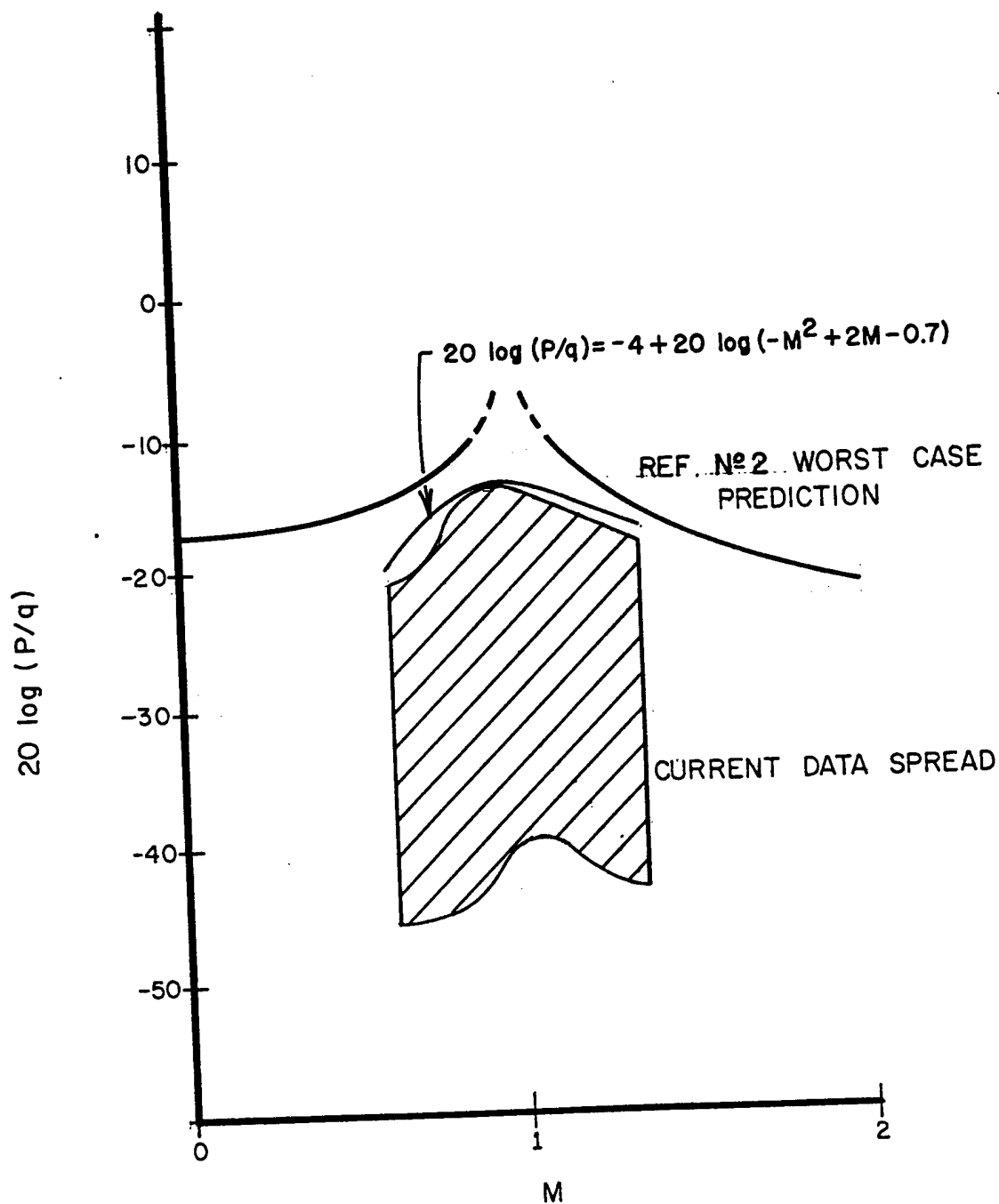


FIGURE 36 PEAK ONE-THIRD OCTAVE BAND SPL AS A FUNCTION OF MACH NUMBER FOR ALL MICROPHONE LOCATIONS AND ALTITUDES

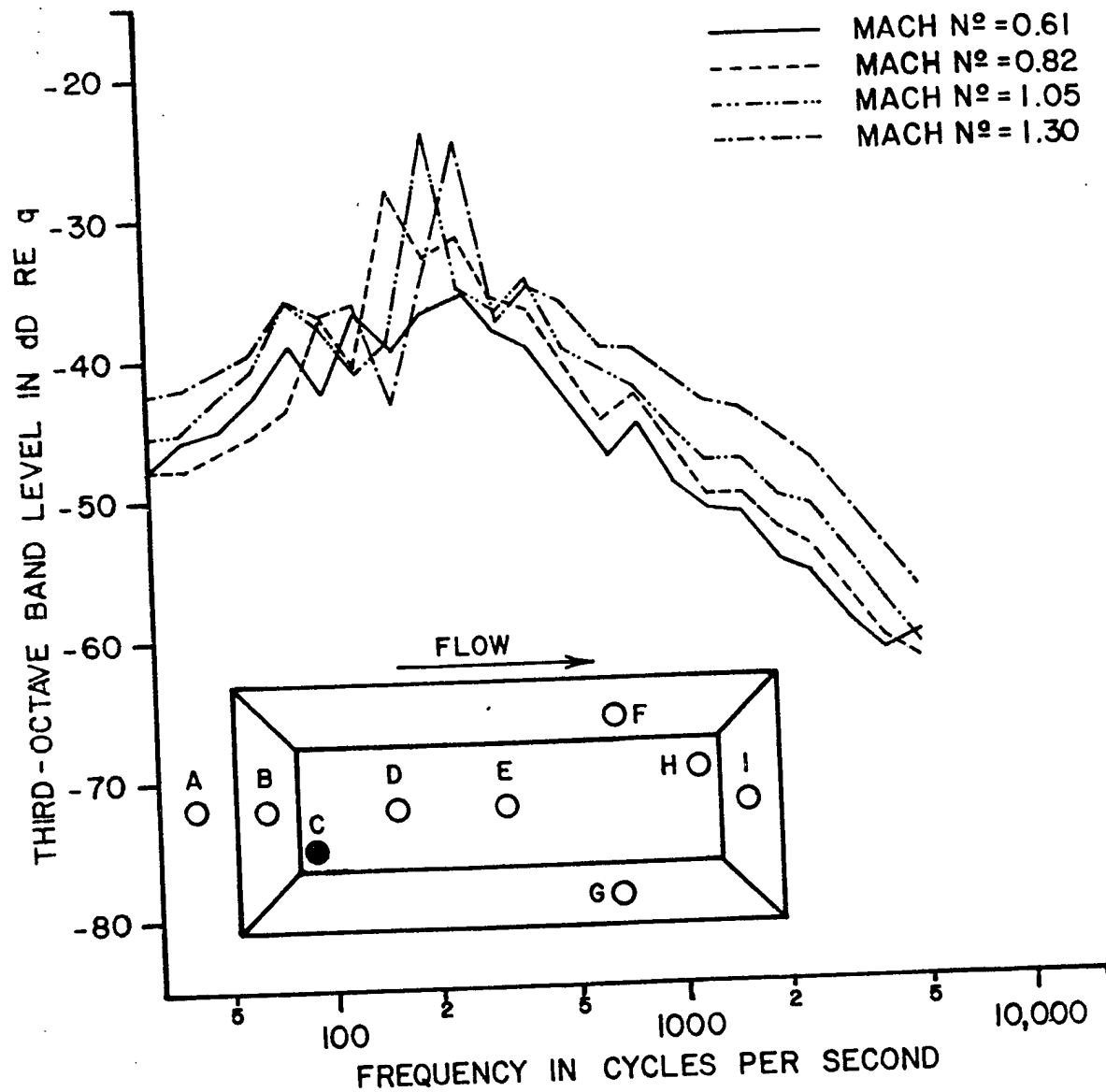


FIGURE 37 ONE-THIRD OCTAVE BAND SPECTRA FROM THE FRONT OF THE CAVITY AT 30,000 FOOT ALTITUDE

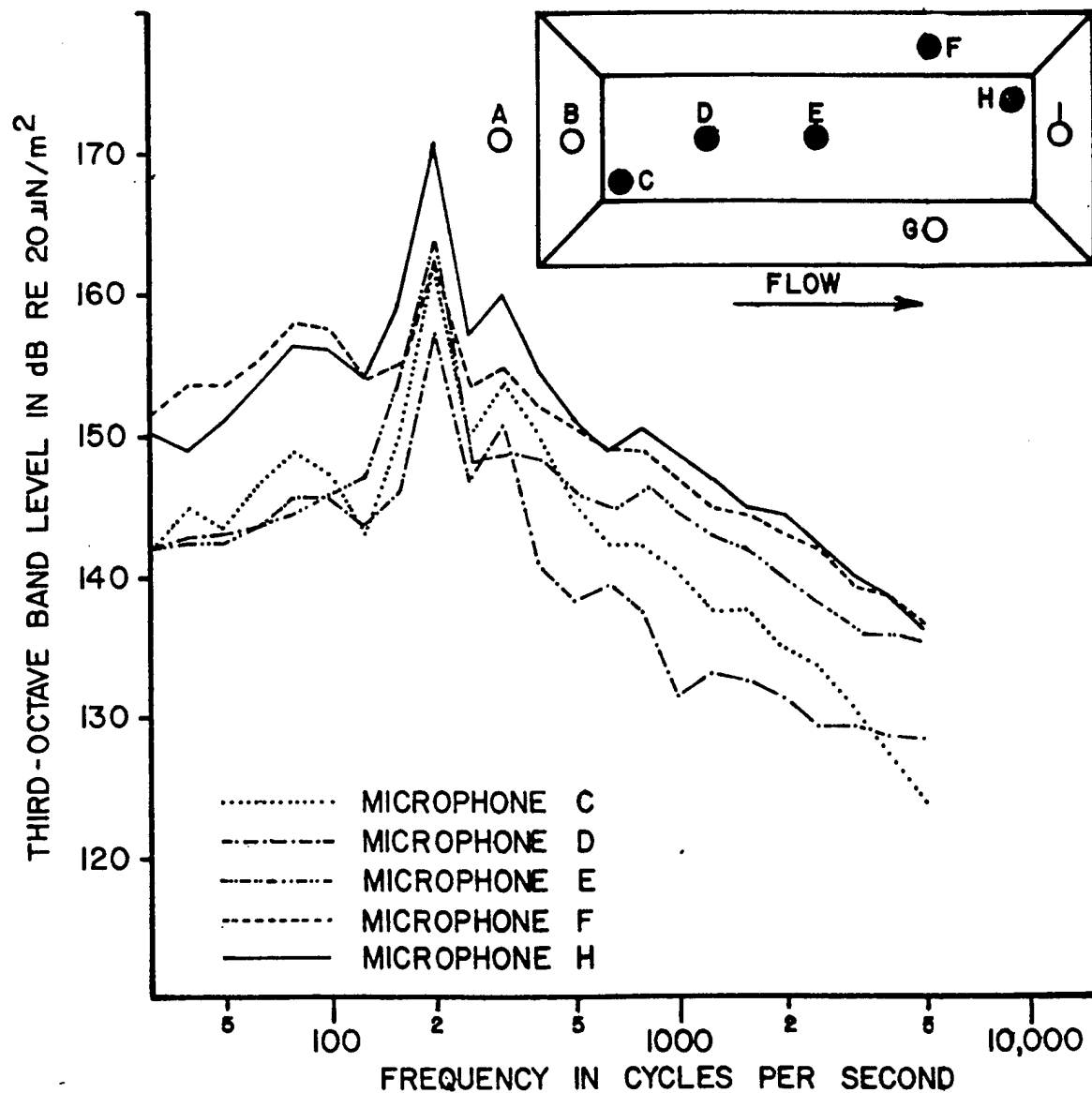


FIGURE 38 ONE-THIRD OCTAVE SPECTRA FOR 3,000 FOOT ALTITUDE AT MACH 0.82
DISPLAYING LONGITUDINAL EFFECT ON BROADBAND LEVEL

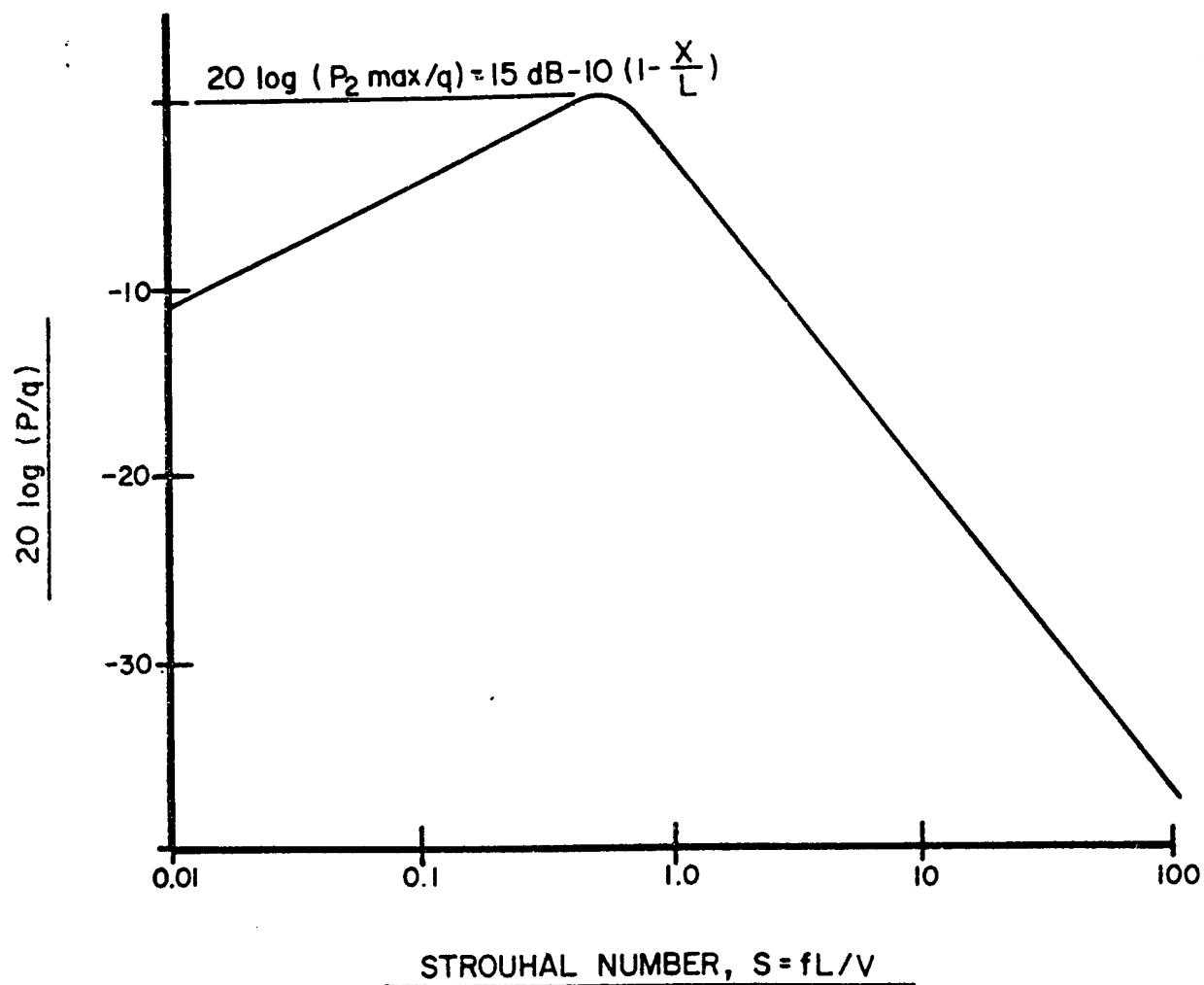


FIGURE 39 BROADBAND LEVEL VERSUS STROUHAL NUMBER

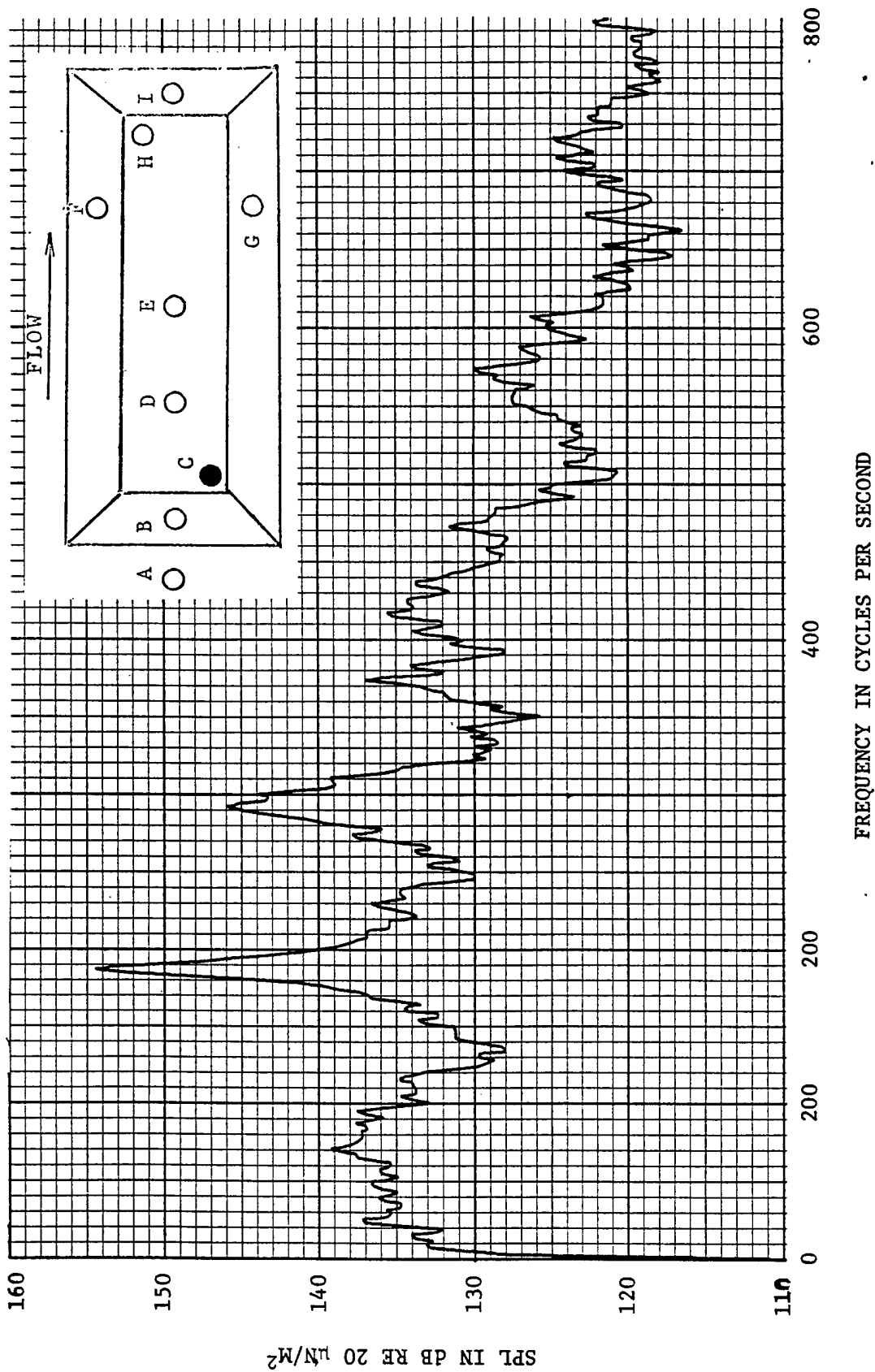
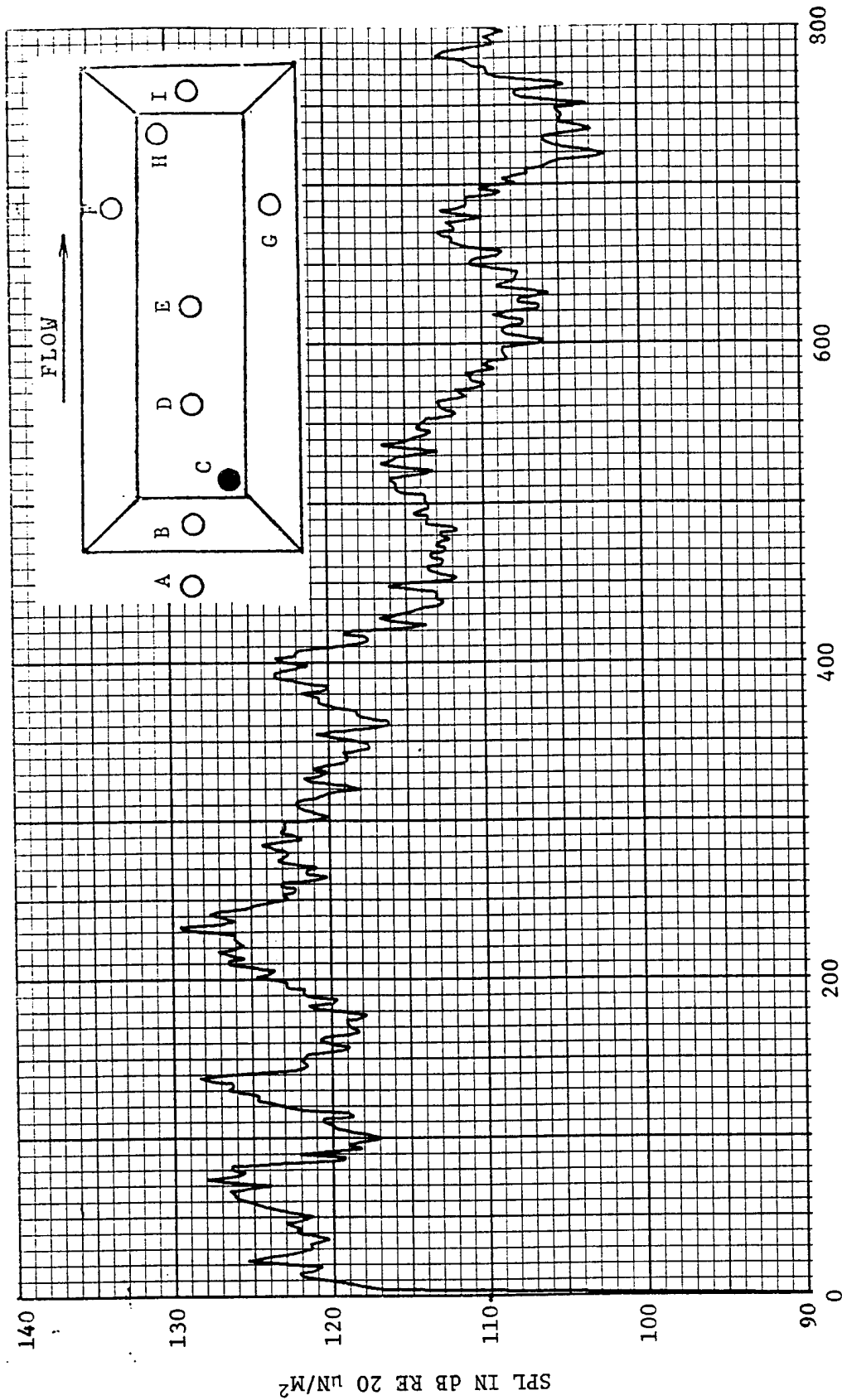


FIGURE 40 2 Hz NARROWBAND SPECTRUM FROM MICROPHONE C FOR THE 10 INCH DEEP MODIFIED SUU-41 POD AT 3000 FOOT ALTITUDE AND AT MACH=0.82



FREQUENCY IN CYCLES PER SECOND

FIGURE 4.1 2 Hz NARROWBAND SPECTRUM FROM MICROPHONE C FOR THE 10 INCH DEEP MODIFIED SUU-41 POD AT 20,000 FOOT ALTITUDE AND AT MACH=0.61

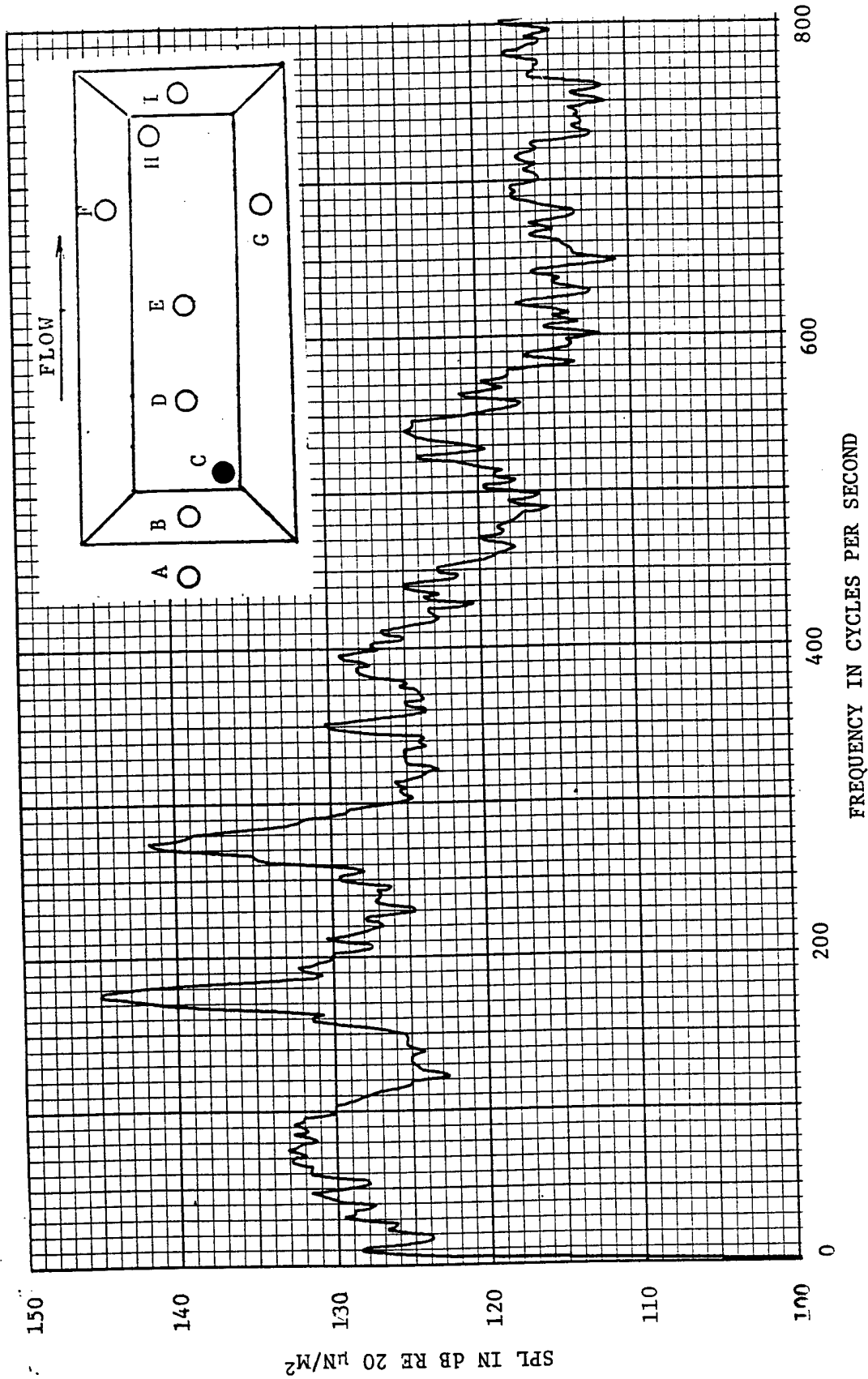


FIGURE 42 2 Hz NARROWBAND SPECTRUM FROM MICROPHONE C FOR THE 10 INCH DEEP MODIFIED
SUU-41 POD AT 20,000 FOOT ALTITUDE AND AT MACH=0.82

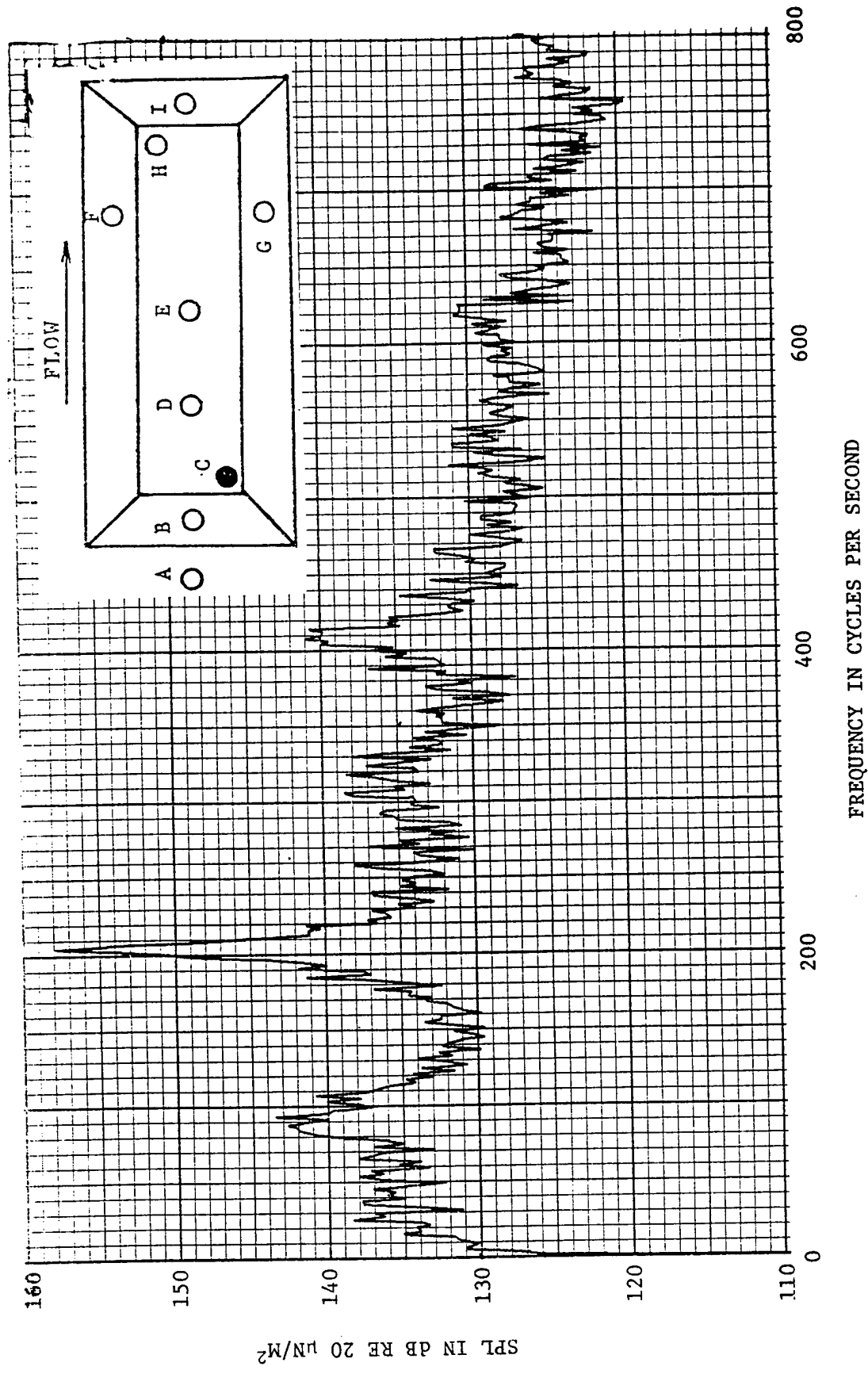


FIGURE 43 2 Hz NARROWBAND SPECTRUM FROM MICROPHONE C FOR THE 10 INCH DEEP MODIFIED SUU-41 POD AT 20,000 FOOT ALTITUDE AND AT MACH=1.05

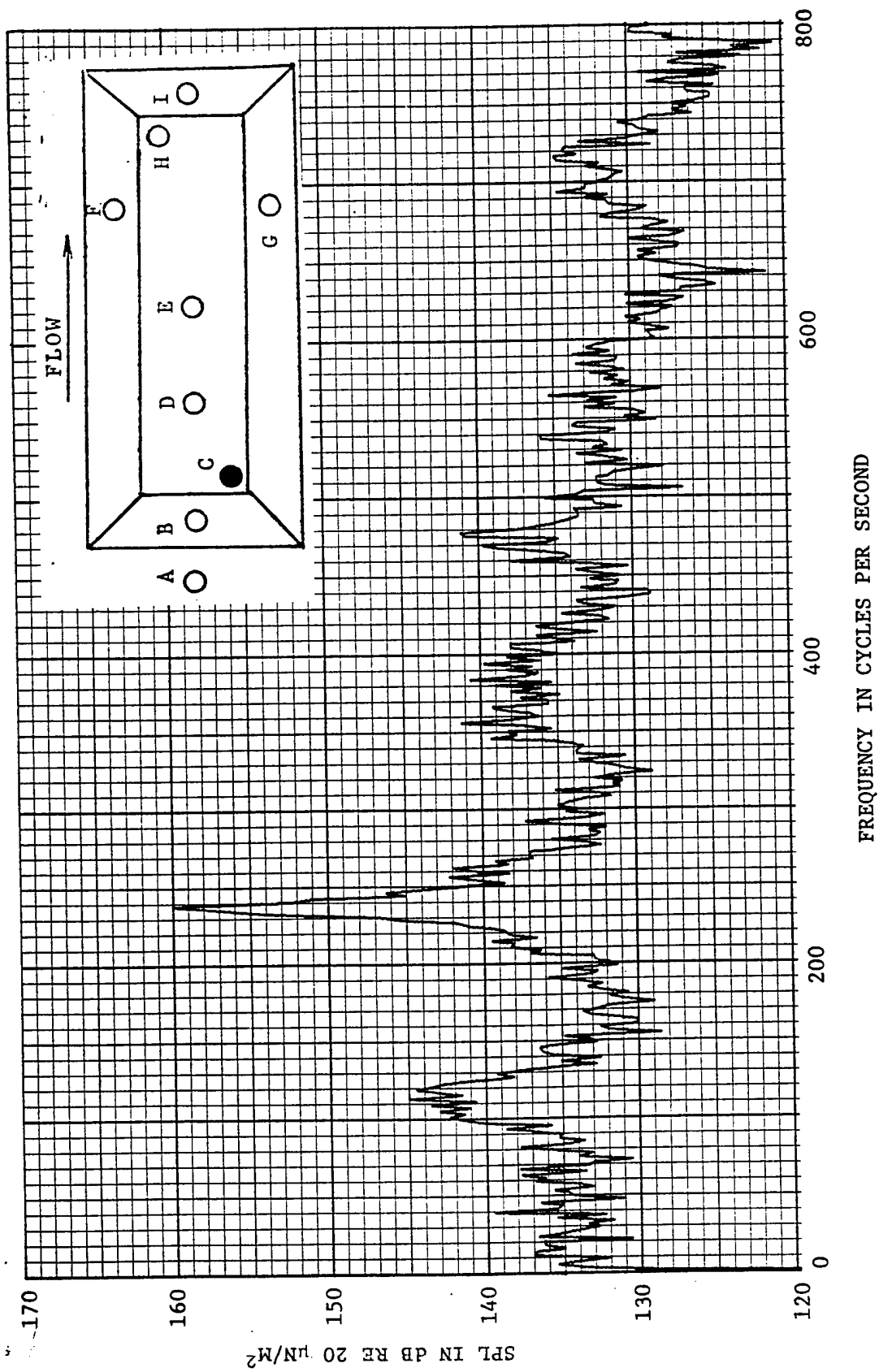


FIGURE 44 2 Hz NARROWBAND SPECTRUM FROM MICROPHONE C FOR THE 10 INCH DEEP MODIFIED
SUII-41 POD AT 20,000 FOOT ALTITUDE AND AT MACH=1.30

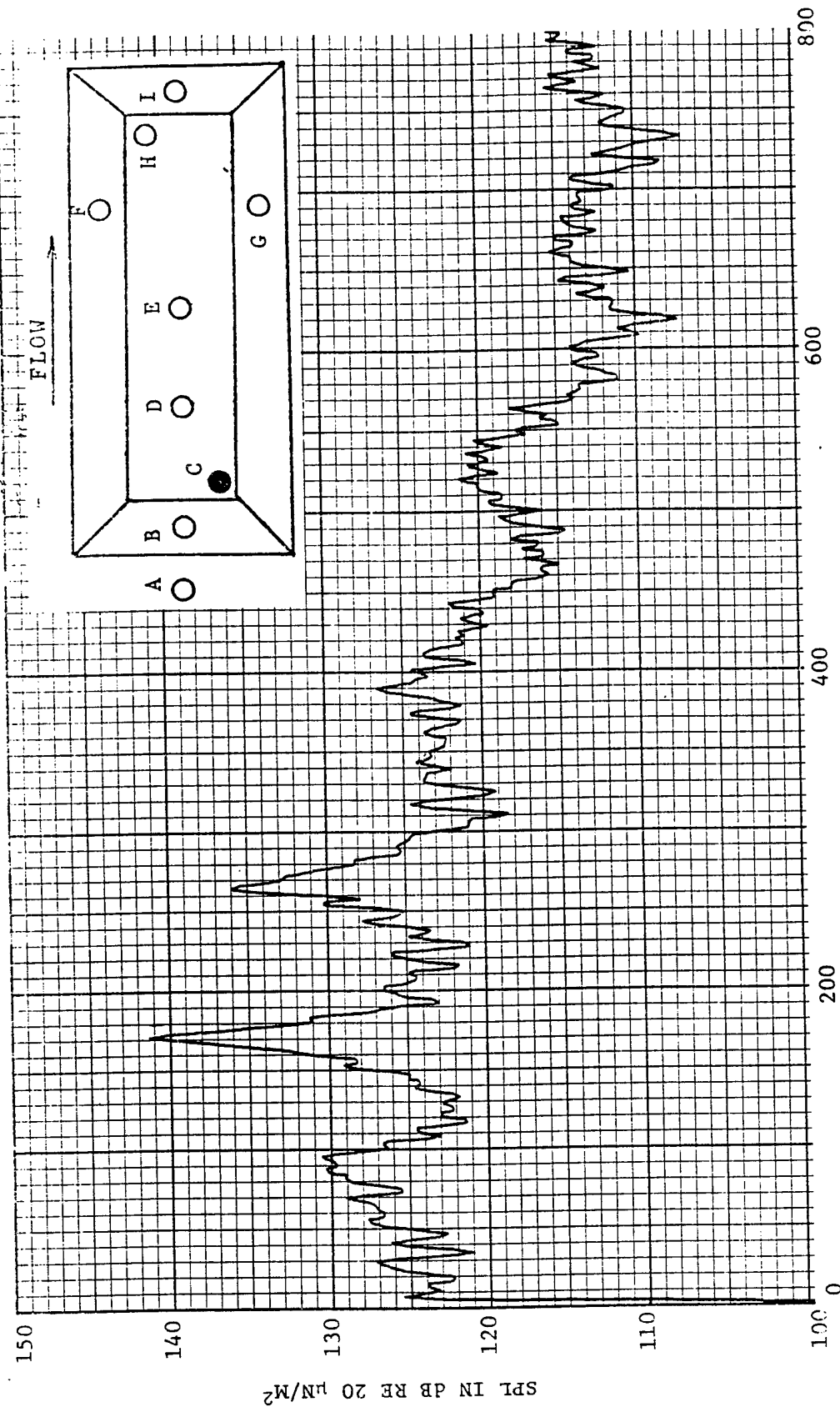


FIGURE 45 2 Hz NARROWBAND SPECTRUM FROM MICROPHONE C FOR THE 10 INCH DEEP MODIFIED SUU-41 POD AT 30,000 FOOT ALTITUDE AND AT MACH=0.82

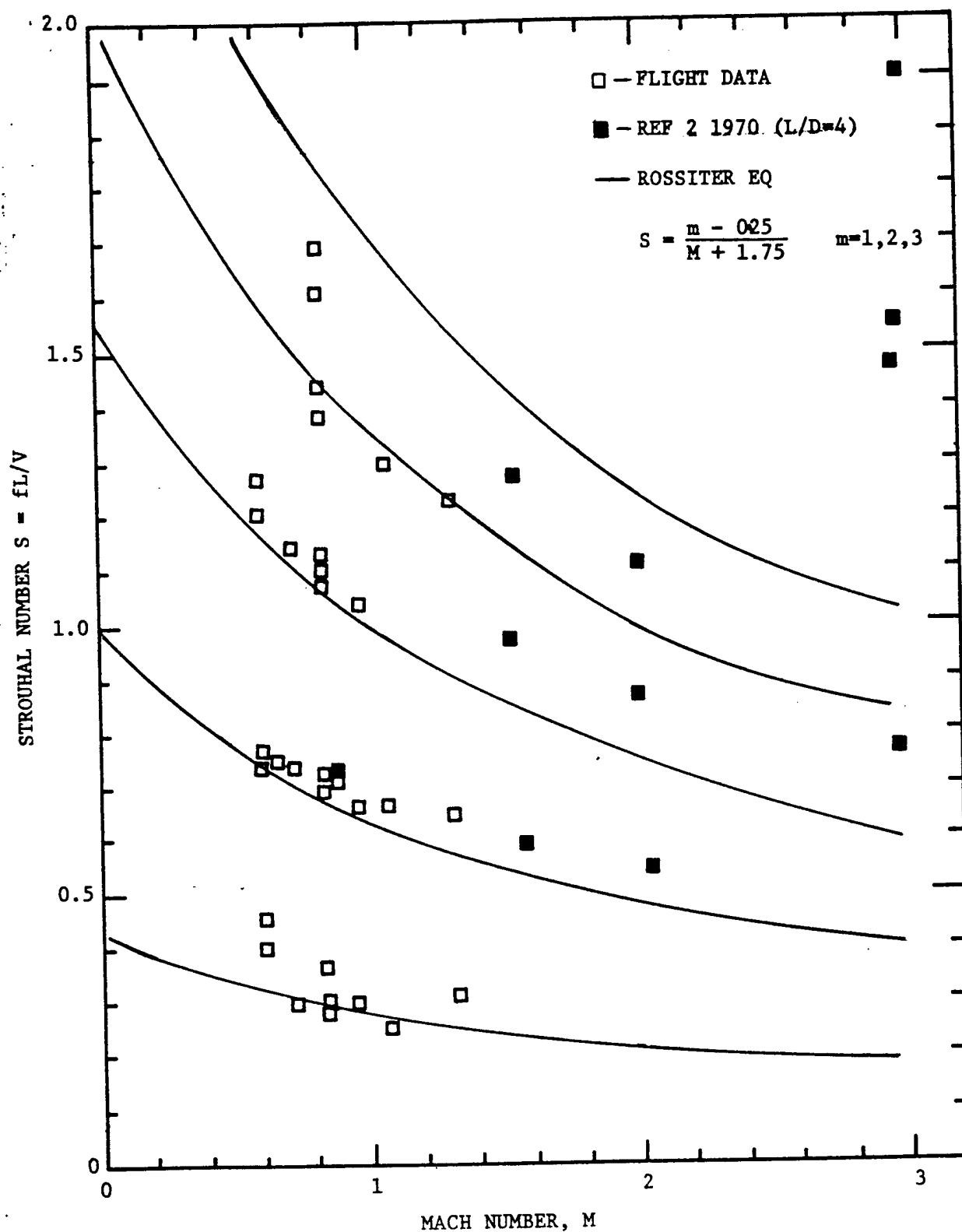


FIGURE 46 NONDIMENSIONAL RESONANT FREQUENCIES FROM THE MODIFIED SUU-41 POD AS A FUNCTION OF MACH NUMBER WITH ROSSITER FORMULA

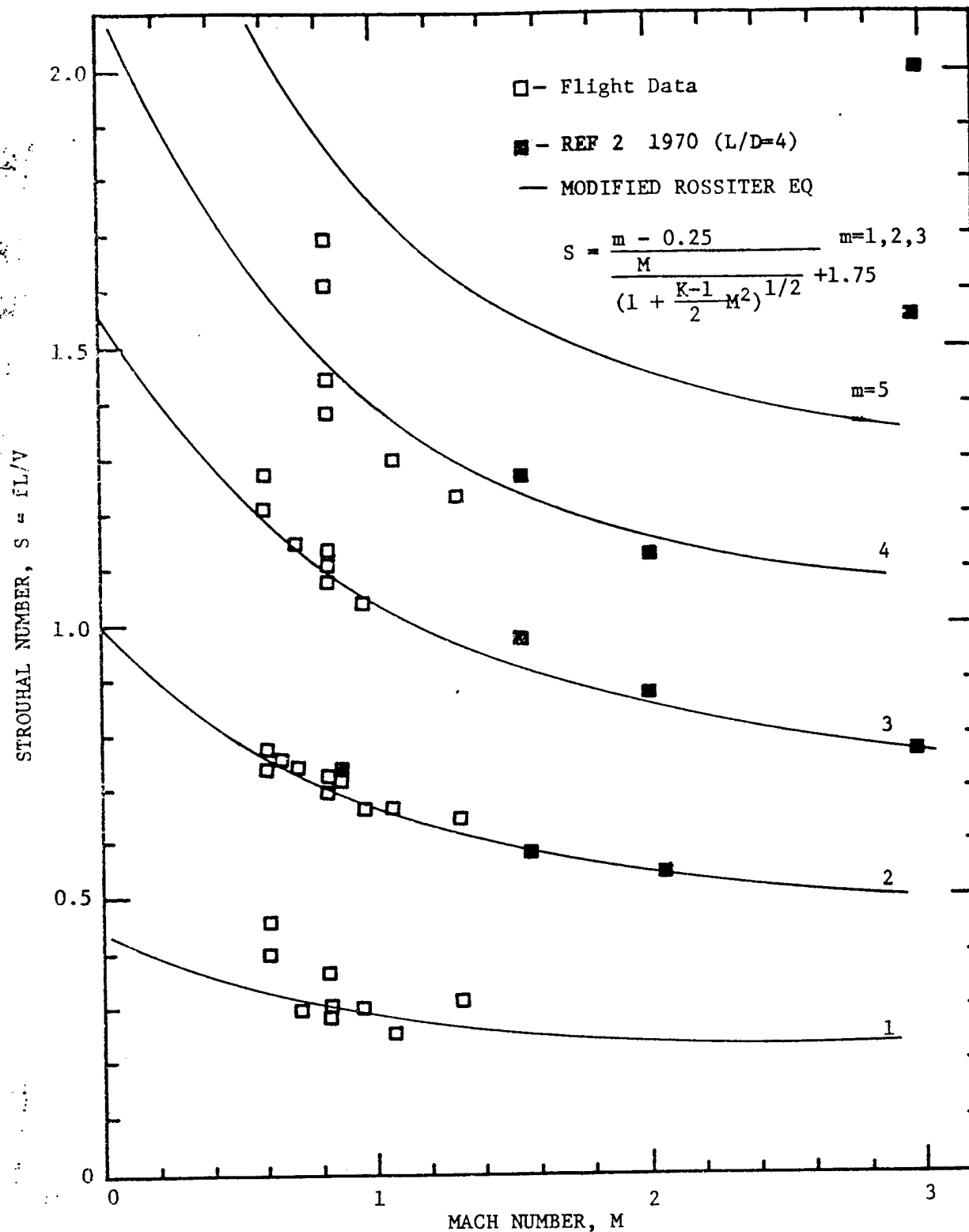


FIGURE 47 NONDIMENSIONAL RESONANT FREQUENCIES FROM THE MODIFIED SUU-41 POD AS A FUNCTION OF MACH NUMBER WITH MODIFIED ROSSITER FORMULA

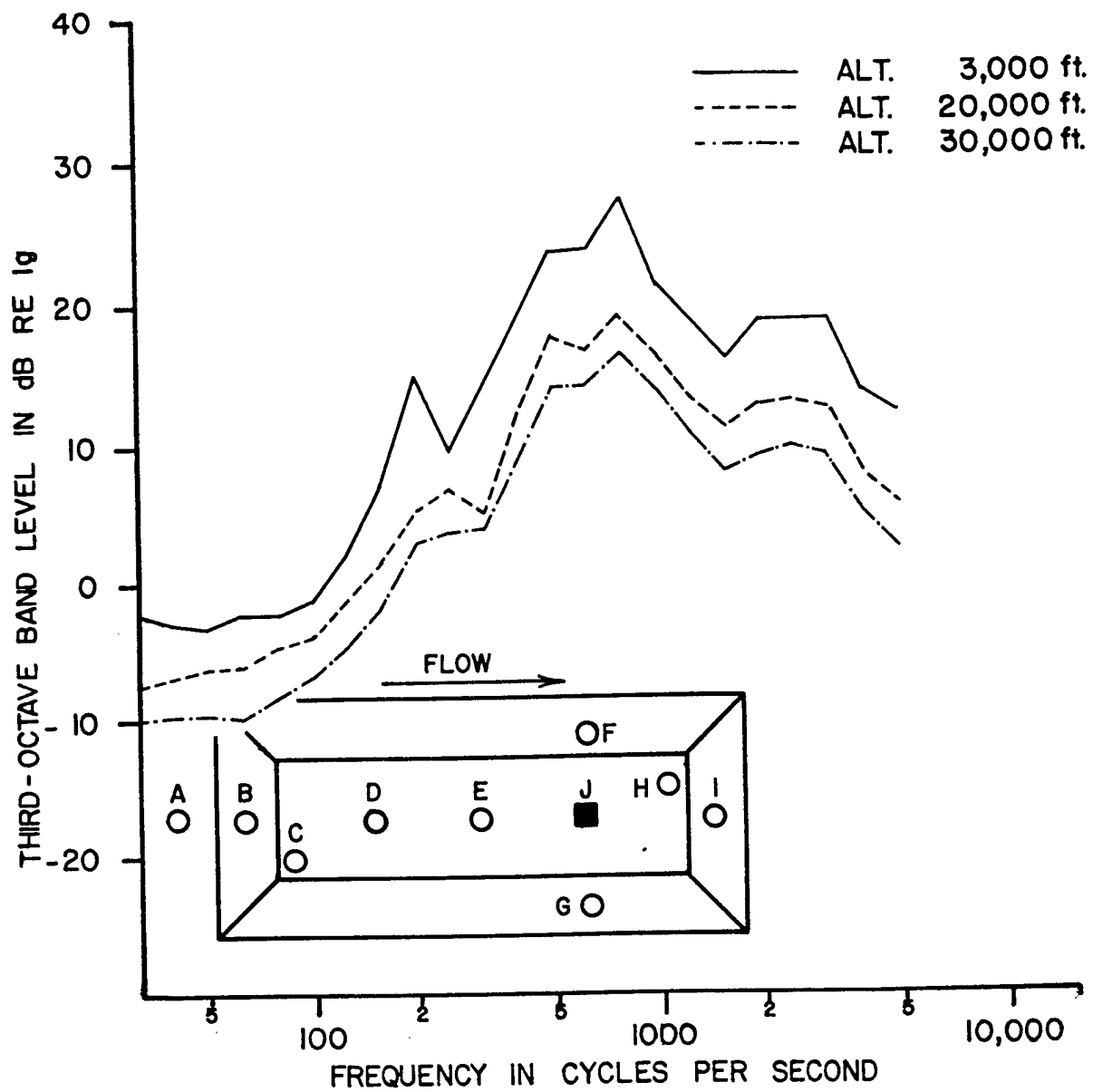


FIGURE 48 ONE-THIRD OCTAVE BAND SPECTRA FROM ACCELEROMETER J FOR THE 10 INCH DEEP MODIFIED SUU-41 POD AT MACH 0.82

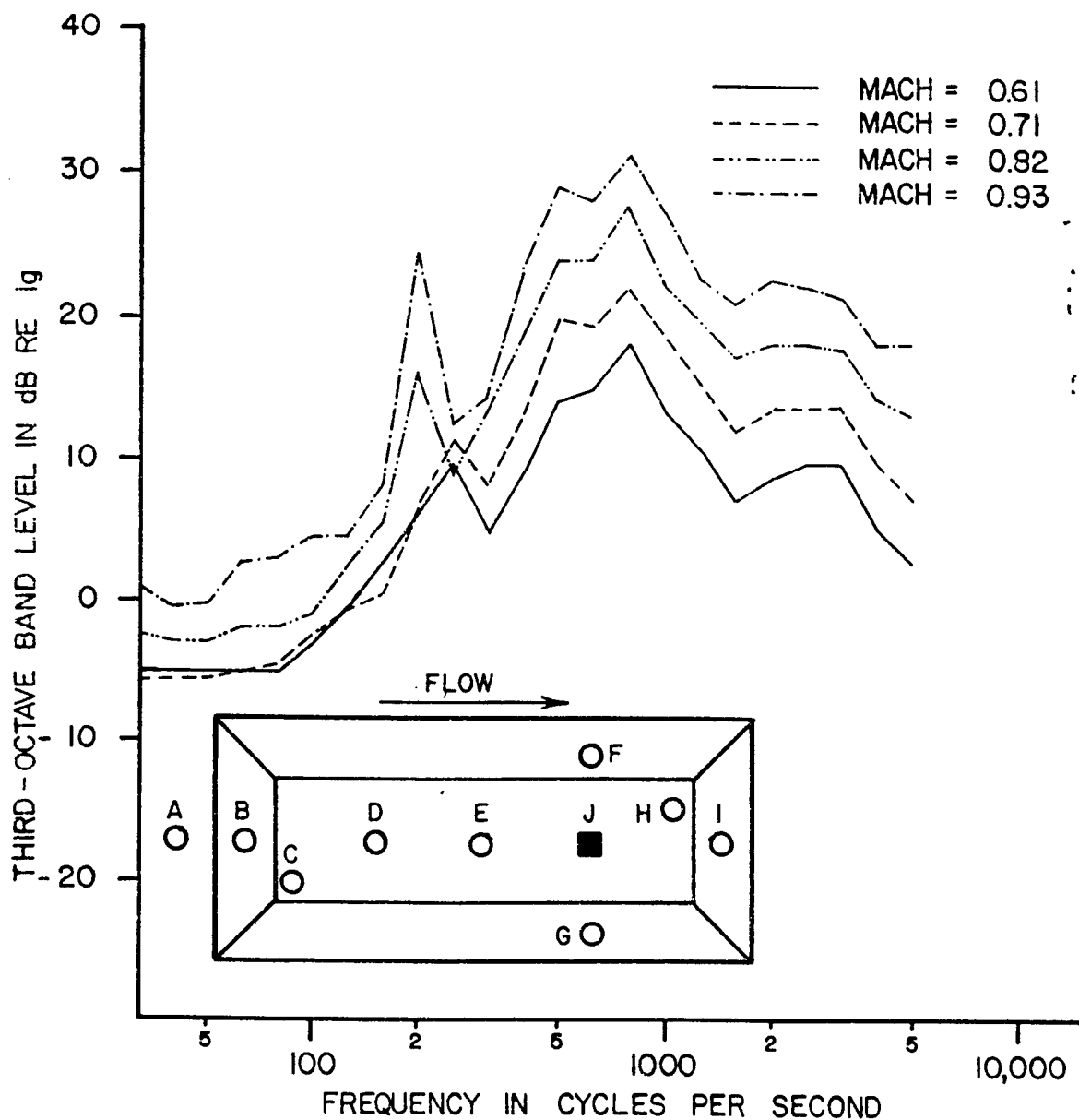


FIGURE 49 ONE-THIRD OCTAVE BAND SPECTRA FROM ACCELEROMETER J FOR THE 10 INCH DEEP MODIFIED SUU-41 POD FOR 3,000 FOOT ALTITUDE

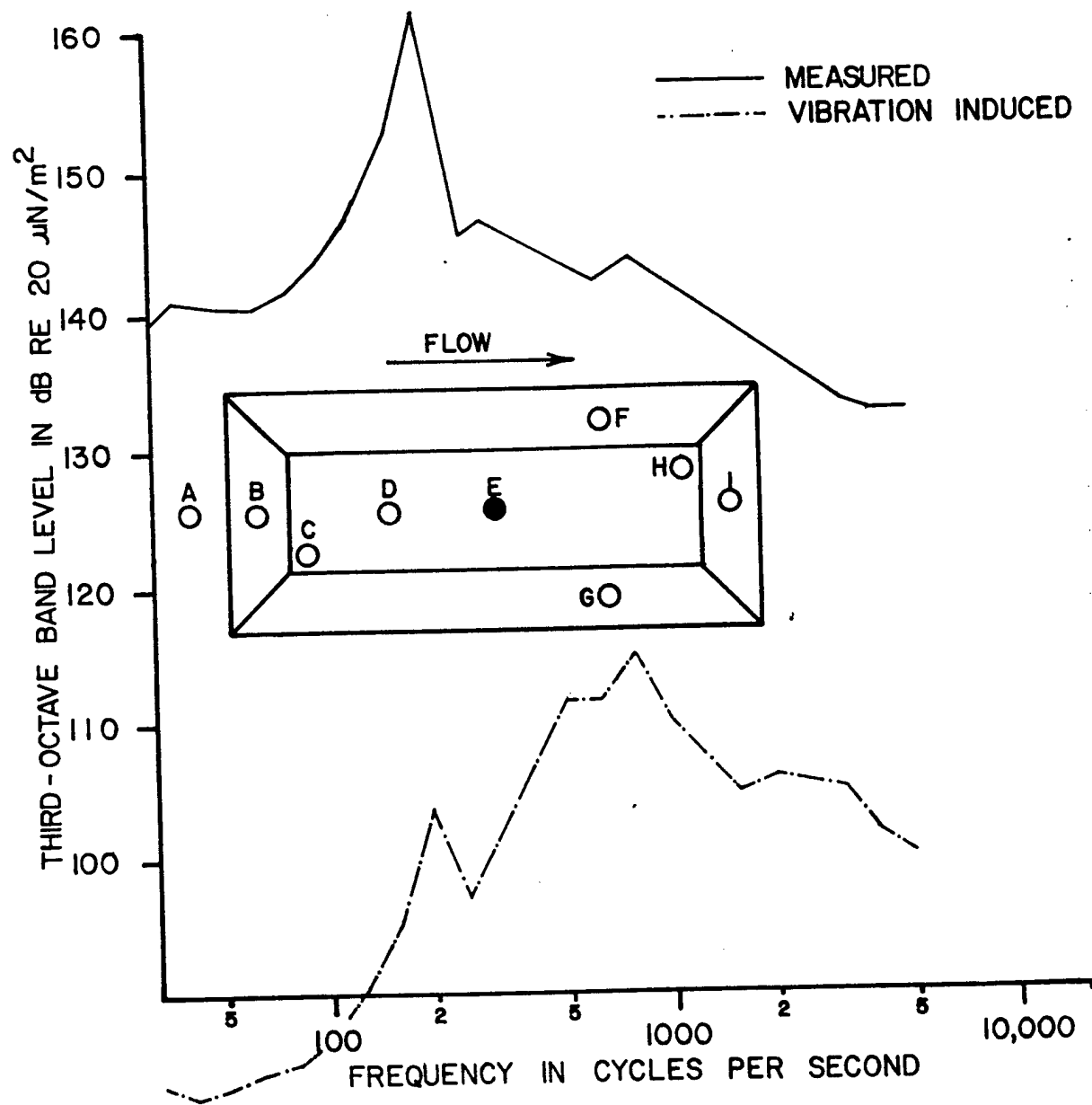


FIGURE 50 ONE-THIRD OCTAVE BAND SPECTRUM FOR MEASURED AND VIBRATION INDUCED SPL FROM MICROPHONE E FOR THE 10 INCH DEEP MODIFIED SUU-41 POD AT MACH 0.82 AND 3,000 FOOT ALTITUDE

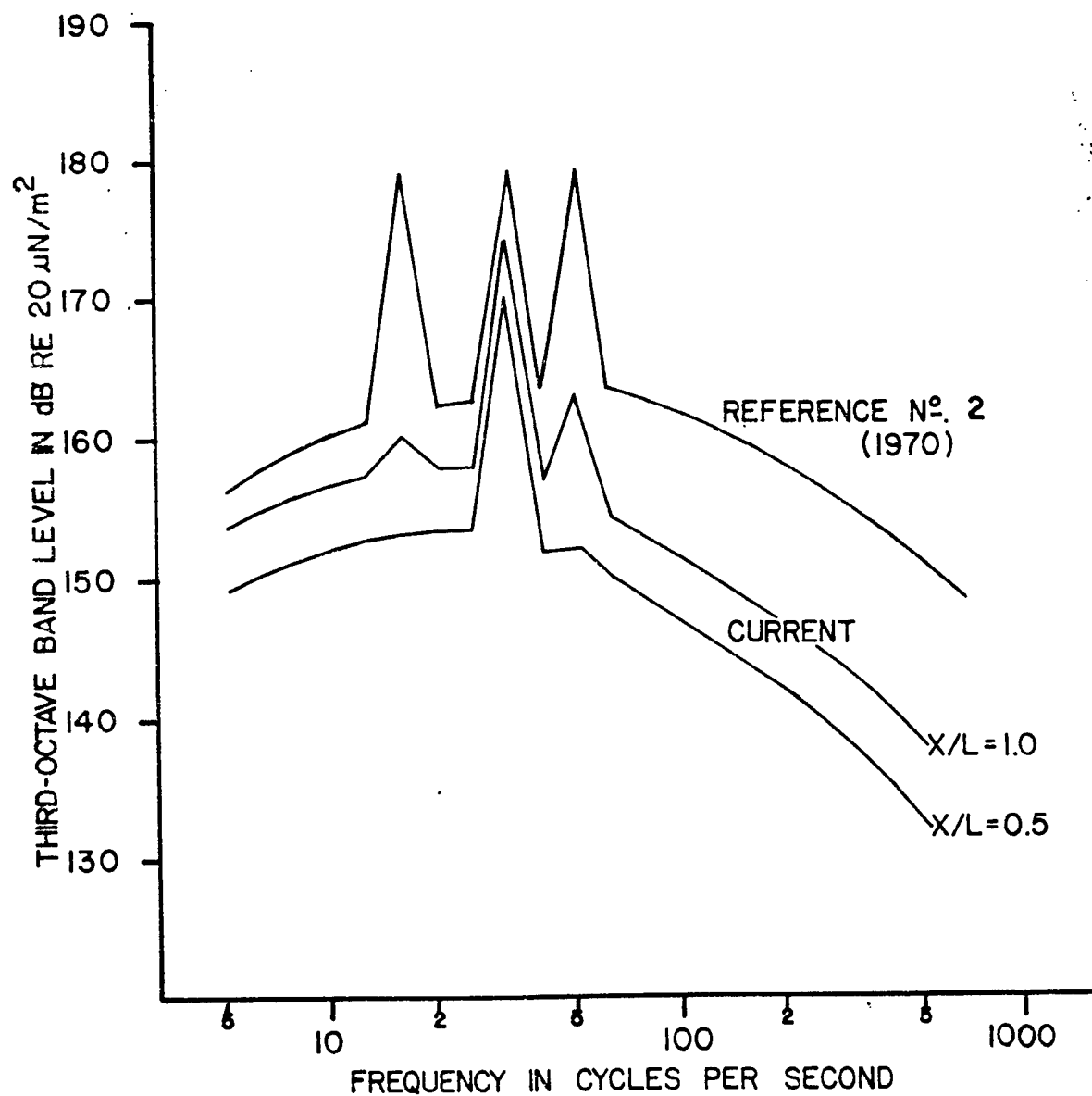


FIGURE 51 COMPARISON OF SPECTRA FROM THE WORKING EXAMPLE FOR THE CURRENT PREDICTION SCHEME AND THE PREDICTION SCHEME FROM REFERENCE 2

REFERENCES

1. East, L.F., "Aerodynamical Induced Resonance in Rectangular Cavities", *Journal of Vibration and Sound*, May 1966.
2. Heller, H.H., Holmes, G. Covert, E.E., "Flow-Induced Pressure Oscillations in Shallow Cavities", AFFDL-TR-70-104, Dec 1970.
3. Krishnamurty, K., "Acoustic Radiation from Two-Dimensional Rectangular Cutouts in Aerodynamic Surfaces", NACA Tech Note 3487, August 1955.
4. Maull, D.J., and East, L.F., "Three-Dimensional Flow in Cavities", *Journal of Fluid Mech* 16, p 620, 1963.
5. Plumblee, H. D., Gibson, J. S., and Lassiter, L. W., "A Theoretical and Experimental Investigation of the Acoustic Response of Cavities in Aerodynamic Flow", WADD-TR-61-75, 1962.
6. Roshko, A., "Some Measurements of Flow in a Rectangular Cutout", NACA Tech Note 3488, 1955.
7. Rossiter, J.E., "Wind Tunnel Experiments on the Flow Over Rectangular Cavities at Subsonic and Transonic Speeds", RAE Rep Nr 64037, R&M Nr 3438, 1966.
8. Chaump, L.E., Martellucci, A., Monfort, A., "Aeroacoustic Loads Associated with High Beta Re-Entry Vehicles", AFFDL-TR-72-138, May 1973.